

Water Dehydrogenation by First-Row Transition
Metal Cations.
A Paradigm for Two-State Reactivity

Doctoral Dissertation

Arantxa Irigoras Balda
April 9, 1999

DOKTOREGO-TESIAREN IRAKURKETARAKO TRAMITEA

**TESIAREN ZUZENDARIAREN ONESPENA BERORREN
AURKEZPENERAKO**

Jesus M. Ugalde Uribe-Etxebarria Doktoreak, Miren Arantzazu Irigoras Balda Doktoregal Andreak Polimeroen Zientzia eta Teknologia Sailean buruturiko "Water Dehydrogenation by First-Row Transition Metal Cations. A Paradigm for Two-State Reactivity" Doktorego-Tesiaren Zuzendari gisa, alpatu Doktorego-Tesiaren aurkezpena baimentzen dut, berorren defentsarako beharrezkoak diren baldintzak betetzen ditu eta.

Donostian, 1999.eko Apirilaren 9an.

TESIAREN ZUZENDARIA

Sinaturik: JESUS M. UGALDE URIBE-ETXEBARRIA

SAILAREN ADOSTASUNA

Sailak, 1999.eko aren (e)an eginiko bileran, jarraian alaturiko lizenburua duen Doktorego-Tesiaren irakurketa tramiterako onartzea erabaki da: "*Water Dehydrogenation by First-Row Transition Metal Cations. A Paradigm for Two-State Reactivity*", Jesus M. Ugalde Uribe-Etxebarria Doktoreak zuzendua eta Miren Arantzazu Irigoras Balda Andreak Sail honen aurrean aurkeztua.

Donostian, 1999.eko aren (e)an.

O.E. SAILAREN ZUZENDARIA SAILAREN IDAZKARIA

Sinaturik:
P.A. Santamaría Ibarburu

Sinaturik:
J.I. Egulazabal Ortiz de Elguea

DOKTORE GRADUKO AKTA
DOKTORE TESIAREN DEFENTSAKO AKTA

DOKTOREGAIA: Miren Arantzazu Irigoras Balda
TESIAREN IZENA: "*Water Dehydrogenation by First-Row Transition Metal Cations. A Paradigm for Two-State Reactivity*"
UPV/EHUko Doktorego Batzordeak epalmahala izendatu zuen goian adierazitako doktore tesia epaltzeko. Epalmahal hori behean aipatzen den egunean bildu da, eta doktoregaiak defentsa burututa, eta aurkeztu zaizkion eragozpen edota proposamenei erantzuna eman ondoren, epalmahalak, honako kalifikazio hau eman dio:



Donostian, 1999.eko aren (e)an.

Epalmahalko burua,

Idazkaria,

Izpta.:

Izpta.:

1.epalmahaikidea

2.epalmahaikidea

3.epalmahaikidea

Izpta.:

Izpta.:

Izpta.:

Doktoregaia,

Izpta.:

*Famili zabal batean hazitzearen zortea izan dudanez,
beraiei eskeini nahi diet nere lan hau. Eta bereziki amari,
aitari eta izeba Maloxi.*

Muxu haundi bat denontzat.

Mila Esker!

Hauze duzue nere azken sei urte hauetako lanaren emaitza. Jesus Ugalde izan da guzti honen zuzendari eta "errudun" nagusia. Bere esku atzerrira joan ahal izan nintzen karreraren laugarren maila ikastera; orduan mundu berri bat ireki zitzaidan parean. Benetan ahaztezinak Kent-eko garai haiek. Handik bueltatu eta segituan bere taldean hasi nintzen "lanean", edo hobeto esanda, tabarra ematen. Kimika kuantikoaren eta ordenadoreen munduan murgiltzen nintzen ehinean nere jakinmina ase ezina bihurtu zen. Zerotik hasi eta pirkanaka-pirkanaka joan nintzen ikasten, laguntza askori esker... Xabi eta Willy: mila esker! Karrera bukatu eta gero tesi hau lantzen hasi nintzen, ikerkuntzaren munduak zeharo liluratua baininduen. Jesusen taldean sortutako giro apartak du gainontzeko erru guztia, ezin ahaztu lanean bi kubatar izatearen eragina, "mi amor eta corazón" hitzak dantzan egun guztian, Elso eta América. Gure napparrak, Txema eta Txoni. Joseph, ameriketatik etorrita hau ere, baina ez Karibetik, baizik eta Georgiatik; azkenengo urte hauetan, ez neri bakarrik, baizik eta lantalde guztiari eskeini dion laguntza izugarriarengatik, mila esker. Guzti hauek osatu dugu Jesusen mintegiko taldea azken urte hauetan, bai lanerako eta bai parrandetarako talde bikaina osatu dugularik. Cecilia, Joxe Mari, eta organikako guztiei, mila esker zuen arretagatik. Gure taldetik jende gehiago igaro da denbora laburrago batez, baina nonbait moztu behar dudanez, azkenengo bi urtetan nerekin egondako bi ikasle aipatu nahi nituzke, Oihana eta Iñaki, mila esker zuei erakutsi nahian erakutsi didazuenengatik.

Tesia aurrera joan ehinean bai Kanadako eta bai Suediako ikerketa talde bitan hiru hilabeteko egonaldiak egiteko aukera izan dut; bertsio ofizialak dioenez, zenbait gauza berri ikastera joan nintzen, baina aho gaiztoek diotenez, etzeko taldearen "lasaitasun" beharrek bultzatuta bidali omen ninduten. Dena dela, bai Dalhousie Unibertsitateko eta bai Estokolmoko Unibertsitateko kimika kuantikoko taldeak aipatu nahi nituen, erakutsitako eskuzabaltasun eta abegikortasunarengatik.

Eusko Jaurlaritza eskertu behar dut ere, beka baten bitartez lan honetan hainbeste denboraz aritzeko modua eman dit eta.

Ikasle garaietan, talde zoragarri bat osatu genuen fakultatean, oraindik ere askotan elkartzen garelarik. Badakizue, sagardotegiren

*bat, San Ferminak, San Alberto (festarik gabe gelditu ginen artean)...
Agur bero bat guztientzat!*

Bainan kimika munduan ez ezik, bestela ere, jende apartaz inguratuta egotearen zortea izan dut.

Nere adiskideak... Guztien gainetik, Nekane eta Nerea bereziki aipatu nahi ditut, nere petralaldiak askotan jasan baitituzte. Maite, lehengusuaz gain lagun aparta zarelako. Pello, laguna baino gehiago... Muzu bana.

Beste irakasle eta lagun bat ere aipatu gura dut, Jozé Manuel, dultzaina jotzen erakusteagatik eta askotan psikologo lanak egiteagatik ere. Dultzainari esker, ondo pasa eta gauza asko ikasi baititut, baita jende aparta ezagutu ere! Andoain-Tolosako dultzainero guztiei eta ibilitako dantza taldeei, bereziki Eskolako musikoei, mila esker igarotako une guztiengatik, eta etorriko direnengatik...

Lan guzti hau familiari eskeini diot hasieran, eta beraiek agurtzen bukatuko nahi nuke ere.

Bejondizuela!

*Arantza Irigoras Balda
Andoainen, 1999.ko Apirilaren 9an.*

Acknowledgments!

This is the result from the work carried out over the last six years. Jesus Ugalde has been the director and the main "culprit" behind all of this. Thanks to his insistence I spent my fourth undergraduate year abroad where a new world opened in front of my eyes. I will never forget that great days at the University of Kent. When I came back, I started "working" in Jesus's lab, I say "working" because I was almost always disturbing. The more I learned about quantum chemistry and computers the more I wanted to learn. I started from zero and very slowly. I realize I have learned much with the help of Xabi and Willy: thanks a lot! Once I finished my undergraduate studies, I found investigation so fascinating that I started with this project. The rest of the "fault" is due to the great environment in Jesus' group. I can not forget the Cubans' influence with their "mi amor" and "corazón", Elso and América; the people from Nafarroa, Txema and Txoni; Joseph, also coming from America, but not from the Caribbean, from Georgia... he has given, not only to me, but to the group in general, much help, huge thanks! All these people have formed the seminar group these last years, a great group for working and partying. Cecilia, Joze Mari and all the people from the "organic" group, many thanks for all your attention. More people have been in our group for a shorter time. Greetings to all of them, but as I do not want to extend this too much, I just would like to name my students, Oihana and Iñaki, thanks for all that you have taught me when I was trying to teach you.

As the thesis was going on I spent a marvelous time, first in Halifax (Canada) and after in Stockholm (Sweden), thanks to the hospitality of Prof. Russ Boyd and Leif Eriksson, respectively. The "official" version says that I went to learn new things that could be important for my thesis, but some say that I was sent because the people from Donostia needed some "rest". Anyway, I would like to thank all the people from Dalhousie and the Physikum, thanks for being so generous and patient!

I also wish to thank the Basque Government for the grant that has given to me the opportunity of stay so long in this work.

While I was a undergraduate I had the good luck of being part of a group of friends that still today meets often for several "celebrations"... Greetings!

I have also the good fortune to be surrounded by good friends away from chemistry.

From my best friends, Nekane and Nerea, a special mention for them since they are the ones that needed more patience with me. Maite, an excellent friend and cousin. Pello, he is more than a friend... Kisses!

I would like to mention also another professor and friend, Jozé Manuel, he taught me how to play the "dultzaina". Thanks to that instrument I have met very nice people and learned a lot. To all the "dultzaina" players from Andoain and Tolosa, and the musicians from the dance group Eskola, thanks for all the good times, the past and the coming ones...

I have dedicated all this work to my family, so I want to finish this page sending greetings to them.

Thanks!

*Arantra Irigoras Balda
Andoain, April 9, 1999.*

Contents

Sarrera Orokorra	i
Bi-Egoerako Erreaktibitatea	ii
Trantsiziozko Metalei Buruzko Faktore Garrantzitsu Batzuk	v
Metodo Teoriko Erabilgarriak	vi
Prozedura Teorikoaren Diseinua	vi
General Introduction	1
Two-State Reactivity	2
Gas-Phase Metal Ion Chemistry	4
Some Important Factors to Consider about Transition Metals	5
Available Theoretical Methods	6
Conventional Quantum Chemical Methods	8
Density Functional Theory Methods	16
Designing the Theoretical Procedure	19
1 Preliminary Calculations	21
1.1 Introduction	22
1.2 Methods	23
1.2.1 Level of Theory	23
1.2.2 Basis Sets	23
1.3 Results	24
1.3.1 Ti^+	25
1.3.2 $Ti(OH_2)^+$	27
1.3.3 Dissociation Energies	28
1.4 Conclusions	30
2 The First Mechanism: The Titanium case	33
2.1 Introduction	34
2.2 Methods	35
2.3 Results and Discussion	36
2.3.1 $Ti(OH_2)^+$ Dissociation Energy	37
2.3.2 Excitation Energy	38
2.3.3 Reaction Energetics	39

2.3.4	The Doublet Stationary Points	40
2.3.5	Quartet Stationary Points	42
2.3.6	Potential Energy Surfaces	43
2.3.7	The H_2 Elimination Mechanism	47
2.4	Conclusions	49
3	The Early First-Row Transition Metal Cases	51
3.1	Introduction	52
3.2	Methods	53
3.3	Results and Discussion	54
3.3.1	Dissociation Energies	54
3.3.2	Excitation Energy	54
3.3.3	Reaction Energetics	56
3.3.4	The Stationary Points	59
3.3.5	Potential Energy Surfaces	63
3.4	Conclusions	68
4	The Middle First-Row Transition Metal Cases	71
4.1	Introduction	72
4.2	Methods	74
4.3	Results and Discussion	76
4.3.1	Dissociation Energies	76
4.3.2	Excitation Energy	76
4.3.3	Reaction Energetics	79
4.3.4	The Stationary Points	82
4.3.5	Potential Energy Surfaces	86
4.4	Conclusions	93
5	The Late First-Row Transition Metal Cases. General Conclusions	95
5.1	Introduction	96
5.2	Methods	97
5.3	Results and Discussion	98
5.3.1	Dissociation Energies	98
5.3.2	Excitation Energy	100
5.3.3	Reaction Energetics	102
5.3.4	The Stationary Points	104
5.3.5	Potential Energy Surfaces	109
5.4	Conclusions	116
	Bibliography	117
	List of Publications	127

Sarrera Orokorra

"Erreakzio kimikoa loturen aldaketa da"

Derek H.R. Barton[1]

*"Lotura kimikoa balentziazko orbital elektronikoen
elkarketarekin erlazionatuta dagoen atomoen arteko
elkarrekintza da"*

Isaac B. Bersuker[2]

Esperientzia haundiko bi ikertzaile hauek ados daude erreakzio kimiko eta konposatu kimiko berrien diseinuak duen garrantziaz; hain zuzen ere, askotan zorte onari edo eta ikertzailearen arteari egotzi baitzale erreakzio kimiko eta konposatu kimiko berrien aurkikuntza. Honi injenieritza molekularra deritzo, hau da, konposatu berrien diseinatze eta sintetizazioa.

"Hogeitabatgarren mendearen konposatu kimiko berri gehienak diseinu molekularren bitartez lortuko dira eta ikuspuntu praktiko eta psikologikotik prest egon behar dugu desafio honi aurre egin ahal izateko"

Zeharo ados nago beraien ikuspuntuekin; horregatik, geure helburua lortzeko, hau da, zientzian ebatzi gabeko paradigmen ulerpen sakonago bat lortzea, esku artean ditugun teknika guztiak elkarrekin lanean jartzeak duen garrantzia azpimarratu nahi nuke.

Gure asmoa paradigma horietako baten argitze lanetan laguntzea izan da: lehenengo lerroko trantsiziozko metalen katiolek urarekin aurkezten duten bi-egoerako erreaktibitatea. Irakurleak, emaitzak era elkartu batean eta malla berdinean aurkitzean, ulerpen sakonago bat lortuko duelakoan.

Kapitulu bakoitzaren hasieran, bertan aurkeztutako metal talde bakoitzari buruz dauden datuei buruzko laburpen bat aurki dezakezue, eta ondoren, kapitulu bakoitzean zehar erabilitako metodoen deskribapen zehatz bat ere bai. Beraz, orain, bi-egoerako erreaktibitatea eta gas-egoeran burutzen den kimikari buruzko zenbait azalpen orokor egin nahi nizkizueke. Gure sistemak ikertzeko erabil daitezkeen metodo teorikoen azalpen matematikoa ingelesezko sarrera orokorrean aurki dezakezue. Azkenean, jarraitutako lan eskemaren estrategia aipatuko dut, hau da, urarekin erreakzionatzerakoan lehenengo lerroko trantsiziozko metalen katioien bi-egoerako erreaktibitatea aztertzeko erabili dugun lan antolaketa.

Bi-Egoerako Erreaktibitatea

Lehenengo lerroko trantsiziozko metalen katioien ezaugarri garrantzizkoenetako bat energiagaz oso gertu dauden egoera eszitzatuak izatea da. Ezaugarri hau koordinatiboki ez-asetutako trantsiziozko metala duen konposatu ororentzat orokorra da[4]. Horrela, Sc^{+} -tik Fe^{+} -ra spin altuko oinarritzko egoeren eta energiagaz gertu dauden spin baxuko egoera eszitzatuen aurrean aurkitzen gara. Co^{+} -tik Cu^{+} -ra, aldiz, spin baxuko oinarritzko egoerak eta gertuko spin altuko egoera eszitzatuak ditugu. Honen ondorioz, metal hauen katioien erreaktibitatean, gutxienez, bi egoera desberdinek har dezakete parte, non oinarritzkoenak ez duen nahitanahiez erreaktiboena izan behar[5].

Erreakzio kimiko baten *energia potentzialaren gainazala*[6] (EPG), egitura molekularra zeln den energia potentzialaren aldaketa ematen duen funtzioa da. Hau da, nukleo bakoltzak besteekiko dituen mugimenduen arabera sistemaren energia potentzialak jasaten duen aldaketa adierazten du. Horrela, dimentsio anitzeko EPG molekular batean puntu bakar baten determinazioa, nukleoien orientazio erlatibo finkatu batean estruktura elektronikoaren kalkulo zabal bat suposatzen du. EPG batean N-atomoko molekula baten orientazioa deskribitzeko 3N zenbaki behar dira, hiru dimentsioko espazioan atomo bakoltzaren posizioa kontuan harturik. Baina bakarrik kontuan hartuko ditugu atomoen posizioak bata bestearekiko; horrela, molekulen errotazio eta translazio totalari dagozkien sei askatasun graduak alde batera utziz gero, molekula ez-lineal baten EPGa 3N-6 berne askatasun graduako gainazala da.

Argi dago EPGaren topologia osoa bakarrik molekula txikientzat marraztu daitekeela, baina asko ikas daiteke molekula baten jokaeraz EPGaren puntu gutxi batzuen ezagupenarekin. Horrela, EPG batean *minimo lokalak* oinarritzko puntuak dira, molekula baten isomero egonkorak errepresentatzen baitituzte. Beralek determinatzen dituzten egitura molekular eta inertzia momentuetatik errotaziozko espektroa estima daiteke. Dimentsio anitzeko EPGaren kurbadurak (pareten malda) minimo lokalean molekularen bibrazio propietateak determinatzen ditu, modu normalak eta frequentzia bibrazional harmonikoak barne.

EPGen funtsezko beste puntu bat energia gutxieneko *trantsiziozko egoera* da, zeinek bi minimo lokal edo ballara konektatzen dituen. Trantsiziozko egoera energia total baxueneko bidean minimo hauek lotzen dituen puntu altuena da. Bere propietate adierazgarrienetarikoa bat askatasun gradu bakar batekiko maximoa eta gainontzekoekiko minimoa izatean datza. Oztopo dinamiko aproxiatu bat da, minimo lokal batetik besterako eraldakuntzan bueltarik gabeko puntua baita. Horrela, erreakzio probabilitateak, edo abiadurak, trantsiziozko egoera honen altuerarekin zerikusi handia izango du.

Bi puntu hauek, bai minimo lokalak eta bai trantsizio egoerak, EPGaren *egoera geldikorak* dira; geometri koordinatu bakoltzarekiko energiaren deribatua, eta beraz atomo bakoltzaren indarra, zero da,

$$\frac{dE(q_1, q_2, \dots, q_m)}{dq_i} = 0 \quad \text{i guztientzat} \quad (1)$$

Normalean, elementu arinentzat orbital, spin eta momentu angeluar totalak ondo definituak daude erreakzio bidean zehar, eta gainera kontserbatu egiten dira[5], mekanika kuantikoaren baldintzak beteaz. Beraien erreakzioak spin bakarreko EPGen bitartez gertatzen dira[4], eta nahikoa izaten da hauen trantsiziozko egiturak, beraien entropia baldintzak, eta beralei lotutako barreira altuerak lortzea spin-bakarreko erreaktibitatea ulertzeko. Bainan irudi hau korapilatsu egiten da bi-egoerako erreaktibitatea azaltzen duen sistema bat aztertu behar dugunean, kasu hauetan bi potentzial gainazalen arteko gurutzaketak ohizkoak baitira, momentu angeluar totala baita nahi eta nahiez mantendu behar den momentu bakarra.

Lehenengo lerroko katioi metalikoak eta beren oxidoak hiru taldeetan bana daitezke, spin altuko ala baxuko egoera egonkorrak aurkezten dituzten arabera. Horrela, lehenengo taldean spin altuko egoera egonkorrak dituzten metalen katioiak eta dagozkien spin baxuko egoera egonkorrak dituzten oxidoak ditugu. Hauen EPG kualitatiboa a) grafikoan irudikatuta dago. Bigarren taldea burdinaz osatua dago bakarrik, bai bere katioiak eta baita ere bere oxido kationikoak spin altuko egoera egonkorrak baitituzte. Ikus b) grafikoa. Eta azkenik, d) grafikoan irudikatutako hirugarren taldean azken hiru katioi metalikoak eta beraien oxidoak ditugu, zeintzuk beraien katioi metalikoetan spin baxuko egoera egonkorrak aurkezten dituzten bitartean, beraien oxidoetan spin altuko egoera egonkorrak aurkezten dituzte.

Dudarik gabe, gure sistemek oso erreakzio bide bereziak aurkezten dituzte, eta baita ere jokaera bereziak lerroan zehar. Izaera "berezi" honek erreakzio faktore berrien azterketa funtsezkoa egiten du, lotura eskakizunak desberdinak baitira bi spin egoeretan; gainera, bi gainazalen arteko trantsizio probabilitateak ere kontuan eduki behar ditugu.

1. Irudia. *Trantsiziozko metalen lehenengo lerroko katioiak $M^+ + H_2O \rightarrow MO^+ + H_2$ erreakzioan aurkezten dituzten hiru gainazal desberdinen errepresentazio kualitatiboa.*

Metal Ioiien Kimika Gas-Egoeran

Bi-egoerako erreaktibilitatea aurkezten duten sistemak ikertzeko, bai esperimentalki eta bai teorikoki, dagoen ingurugirorik aproposena gas-egoera da.

Gas-egoeran burutzen den kimikari esker trantsiziozko katioi metalikoen propietateak aztertzeo aukera ematen digu, bai aske eta bai beste molekulei lotuta daudenean. Bai ere, ondo definitutako baldintzenpean erreakzio basikoak frogatzeko aukera ematen digu, disoluziotan arrunt diren faktore oztopatzailerik gabe[7], hau da, ioien parekatzea, disolbatzaile-metal elkarrekintza, eta prozezu intra- eta inter-molekularrak.

Trantsiziozko metalen bidezko oxidazioen ulerpen sakona gas-egoeran ezinbestekoa da oso arlo desberdinetan[8]. Hala nola, (a) katalisi heterogeneoetan, peroxidoak, oxigenoa, edo eta airea bezalako oxidatzaile ekonomikoak erabiliz, hidrokarburoak ballogarriagoak diren beste produktu bihurtzeko; (b) antzeko asmoekin katalisi homogeneoetan, eta bai eskala txikiko aplikazio sintetikoetan; (d) entzimen erreakzio zentruetan trantsiziozko metalek parte hartzen duten eraldakuntza biokimikoetan. Bainan gas-egoeratako ikerketak ez dira garrantzizkoak bakarrik disoluzio- eta gainazal-egoeretan burutzen diren lanen informazio iturri soil gisa, berez ere garrantzi haundikoak baitira[9]. Gas-egoeran, bai teorikoki eta bai esperimentalki, informazio termodinamiko anitz lortu da azkenengo urte hauetan: erreaktibilitatean ematen diren propietate periodikoak[10, 11], zenbait ligandoren efektuak metalen ioien kimikan (ML^+)[7, 12], ioi metaliko/ligandoen lotura energiaren determinazioa $D(M^+ - L)$ [13, 14], banan-banan zenbait ligando eranstearren eraginak (ML_n^+)[15, 16], eta azkenengo denboraldi honetan, metal taldeen ("cluster"-ak) propietateak M_n^+ [17] eta metal-karbohidrogenoen ikerketa sakona[18].

Sistema hauei buruz posible den informazio guztia lortzeko, eta ondorioz, ahal den ezagupen zehatzena lortzeko, zenbait teknikaren elkarlana beharrezkoa da. Idealki, emaitza onenak teknika posible guztiak erabiltzen direnean lortu behar irateke[9], bainan ikuspuntu praktikoa batetik, bi edo hiru metodoaren arteko akordioa nahikoa da emaitzak ontzat hartzeko. Freiser-ek esan zuen bezala, *bi metodoaren artean desadostasunak ageri direnean eta hirugarren bat frogatu behar denean, orduan gozatzen da zientziarekin*. Kasu hauetan, talde desberdinen arteko elkarlanak beharrezkoak dira, honen adibide on bat [19] erreferentzian ikus daitekeelarik. Lan horretan, hiru masa espektroskopio tekniken bitartez lortutako emaitzak bateratzen dira desberdintasun kuantitatiboak azaltzeko, ez ordea kualitatiboak. Burdina oxidoaren katioiak urarekin eta metanolarekin ematen dituen erreakzioen abiadura-konstantea eta adarkatze-proporzioa kalkulatzeko erabiltzeko hiru teknikak "Fourier transform ion cyclotron resonance (ICR)"[20], "guided ion beam (GIB)"[21], eta "selected ion flow tube (SIFT)"[22] dira, honako ondorioak atera zituztelarik: SIFT metodoaren bitartez lortutako emaitzek ziruditen egokienak, ICR metodoaren bitartez lortutakoak handi samarrak eta GIB-aren bitartez lortutakoak txikiak ziren bitartean.

Konposatu tartekariak SIFT teknikan, jasandako egonkortze termonuklear-

rak zirela eta, neurtutako adarkatze proportzioengan eragina zutela nabaritu zuten, ICR eta GIB neurketen aurrean, (azken hauek talka-bakunetako baldintzetan neurtzen baitira). Sahlaketa hauetan, ioien aktibazioa, beraien disoziazioa eta produktuen neurketa elkar-biltzen dira. Zein prozedura erabiltzen dira ioi hauek aktibatzeke? Berriz ere metodo desberdinak erabil daitezke, beraien helburu eta akatsekin, emaitzak konparatzea interesgarria suertatzen delarik. Ioiak aktibatzeke metodo erabilienak: gas inerte baten aurka azeleratuz, (collision-induced dissociation, CID)[23], azalera batean azeleratuz eta talkatuz (surface-induced dissociation, SID)[24], argiarekin irradiatuz (photodissociation (PDS)[25] eta fotoinduzitutako erreaktibitatea[26]), eta elektroiez bonbardeatuz (electron-induced dissociation(EID))[27].

Une honetan, teoria oso erabilgarria den tresna bihurtzen zaigu. Kontu handiz egindako kalkuluen bitartez, egitura-geometria eta egoera elektronikoaren buruzko datu zehatzak eman baitiezazkiguke. Ondorioz, aztertutako erreakzio bidearen buruzko informazioa ere atera dezakegularik, trantsizio egoerak barne. Azken hauetatik, gainditu beharreko erreakzioaren energia langan informazioa eskuratuz.

Beraz, ioi metalikoen kimika azaltzeko garaietan, *hiru kide* talde hau oso egokia dela dirudi, hau da, instrumentazioa, ionizatze modua eta kalkulu teorikoak.

Lan honetan aztertutako transformakuntzak ximpleak badira ere, trantsiziozko metalen bitartez suertatutako hidrokarbonoen erreakzioak ulertzeko ezinbestekoak dira[19]. Lan honetan geure kalkuluetan lortutako emaitzak erakusten ditugu eta dauden datu experimentalekin aldaratu. Guzti honekin behatutako zenbait ezaugarri azalduko ditugu. Honekin, erreakzio hauetan argi ez dauden zenbait puntu argitzea eta trantsiziozko katioi metaliko eta metal oxido kationiko hauen energia potentzial gainazalaren ulertze orokor bat eman nahi izan dugu.

Trantsiziozko Metalei Buruzko Faktore Garrantzitsu Batzuk

Trantsiziozko metalak, orokorrean, teorikoki aztertzeke talde konplikatuak dira. Hau nagusiki korrelazio zein efektu erlatibistikoak zuzenki deskribatzeko da- goen zailtasunarengatik gertatzen da.

Batez ere 70. hamarkadan[28] buruturiko hainbat kalkulu zehatzen ondorioz lorturiko esperientziak korrelazio energia sorrera fisiko desberdineko bi multzotan banatzen du: degenerazio edo la-degenerazio efektuak barne hartzen dituena, eta elektroien mugimenduen korrelazio dinamikoa kontuan hartzen duena.

Trantsiziozko metalen sistemak karakterizatzen dituzten aspektu berezietako bat beren nahasketa konfigurazional sendoa da[29]. Hau arrazoi desberdinak direla eta gertatzen da. Alde batetik sistema hauetan lotura kimiko ahulak direla eta, antiloturazko orbitalen okupazio substantziala gertatzen da.

Beste aldetik, lehen alaturiko energia maila atomikoen hurbiltasuna dela eta agertzen den la-degenerazioak transiziozko metalen atomoetan, eta azkenik, metal hauek sortuko duten lotura kimikoengan duten influentzia. Beraz, errore hau Hartree-Fock metodoaren mugapen baten ondorioz agertzen da: bi elektroi kokatzen dira orbital espazial bakoitzean[30].

Bigarren errorea partikula independenteen eredutik dator. Eredue honetan elektroiak beste elektroiek sorturiko batzbesteko potentzialean mugitzen dira, errealtatean elektroien mugimendua beste elektroi guztien posizio zehatzaren menpean dagoelarik[30].

Bi errore hauen banaketa ez da lan makala, bi efektu hauen arteko muga zehatzik ez baitago, beren deskribapena zailago eginez.

Faktore hauen eragina transiziozko metalen lerro desberdinetan desberdina da, kontuan hartu behar dugularik lehengo lerroko 3d eta 4s orbitalen arteko tamaina diferentzia beste lerroetan baino handiagoa dela, la-degenerazio efektuak emanez d loturak gertatzerakoan. Honen eraginez, nahiz eta lehengo lerroko transiziozko metalak arinenak izan, tratatzeko zailenak izatea dakar [31]. Beste aldetik, efektu erlatibistikoak lehengo lerroko transiziozko metaletan txikiagoa da. Dena dela, gustatuko litzaidake komentatzea zenbait elementu astunen konposatuetan beren estruktura eta propietate elektronikoen interpretatzea tratamendu erlatibistikorik gabe ezin dela egin adierazten duten obserbazio kimikoak badaudela[32].

Metodo Teoriko Erabilgarriak

Beraz, alde batetik, gure sistema hauek gobernatzen dituzten korrelazio efektu hauek zehazki deskribatzen dituzten prozedura teorikoak bilatu behar ditugu; bestetik, aldez, horrelako lan bolumena aurrera ateratzeko egingarria den prozedura bat zehaztu behar dugu.

Puntu honetan zenbait irakurlerentzat interesgarria izan daiteke metodo hauen garapen matematikoa, baina ekuazio jarraipen bat besterik ez denez gero eta laburtasunarengatik bitan gauza berbera ez jartze arren, ingeleseko sarrerara zuzenduko nituzke irakurle horiek.

Prozedura Teorikoaren Diseinua

$Ti^{+} + H_2O$ erreakzioak gure arreta bereganatu zuen literaturan estabaldia interesgarriak aurkitzean, hauek erakusten zutelarik teorikoki, obserbazio esperimentalekin bat etorritik, aztertzeke erreakzio interesgarria zela.

Erreakzio mekanismo osoa kalkulatzeko hasi aurretik, erabiliko zen teoria maila zehazteko beharrezkoak ziren kalkulu batzuk aurretik burutzea pentsatu genuen. Gure erreakzio mekanismoan bi energia puntu aukeratu genituen: $Ti(OH_2)^{+}$ ioi-molekularen disoziazio energia alde batetik, eta titanio katiolen 4F egoera elektronikoaren $d^{n-1}s$ and $d^{n-2}s^2$ balentziako elektroi konfigurazioen arteko interkonfigurazio energia bestetik.

Hasierako kalkuluak MCSCF metodoa erabiliz burutu ziren, lehengo lerroko transiziozko metalen kasuan erabili behar zen metodoa zirudielako. Elektroi osoko oinarritzko multzoak zein core-potentzial efektiboak erabili ziren (ikusi 1. kapituloa). Baina disoziazio energetan behestimazio nabaria lortu zen. Hau coupled cluster metodoetan ere aurkitzen zen. Beraz, DFT metodo berriek gure arreta bereganatu zuten. Dirudenez, MCSCF zein CC metodoak baino askoz ere merkeagoak dira, eta literaturan agerturiko emaitzak oso positiboak ziren. Gure taldeko inork DFT eta transizio metalen kimikan esperientziarik ez zuenez, Prof. R. Boyd-en taldean hiru hilabetez lan egiteko parada izan nuen, metodo honi buruz ikasiz. Nabaria denez, hau aukera bikaina izan zen, gure sistemen ikerketan perspektiba berriak irekitzen zituelako. Lorturiko emaitzak MCSCF edo CCSD(T) metodoak bakarrik erabiliz lorturikoak baino askoz hobekoak ziren, eta erreakzio mekanismo osoa aztertzeko bide bat ireki zen gure aurrean.

Hala ere, gure sistemetan korrelazio tratamendu desberdina egin behar zela uste genuen, behintzat puntu garrantzitsu batzuentzat, gure B3LYP emaitzen kalitatea estimatzen gai izateko. Interesgarria iruditu zitzaigun bai korrelazio dinamikoa zein ez-dinamikoa kontuan hartzen zuen metodo bat probatzea. Berriz, metodo hauen ezagupena lortzeko Dr. Leif Eriksson-en taldean egon nintzen. Garai hartan Prof. Per Siegbahn-en taldean aritzen zen, transiziozko metalen kimikan esperientzia handia zuelarik. Hurbilketa desberdinak erabili ziren, eta CASPT2 metodoa erabiltzeko interesgarria suertatu zen, gure sistemen deskribapen egokirako egoera esztatuen estimazio egokia beharrezkoa zelako. Kalkulu hauek bigarren kapituloan zehar ematen dira.

Dena dela, hobekuntza nabaririk ez zen lortu, emaitza esanguratsuak lortzeko beharrezkoa zen esfortzu izugarriaren aurrean. Argi zegoen hurbilketa on bat B3LYP/DZVP teoria malla, energia potentzial azalera osorako, erabiliz lor zitekeela, puntu klabeetan B3LYP/TZVP+G(3df,2p) teoria malla erabiliz. Hala eta guztiz ere, *ab initio* balio puru batzuk ere eman behar zirela erabaki genuen. Horrela, literaturan agerturiko emaitzekin eta gure sistemetan lorturiko esperientzia guztia kontuan hartuz, CCSD(T)/TZVP+G(3df,2p)//B3LYP/TZVP+G(3df,2p) kalkuluak ere burutzea erabaki genuen (3., 4. eta 5. kapituloak).

Hemendik aurrera lan guztia ingelesez aurkituko duzue, hori izan baita lan hau garatzeko erabili den hizkuntza, eta zientziarena orokorrean. Gainera, orri-alde horiek irakurtzeko "ausardia" duena zientzia munduan sartutako bat izango dela pentsatu dut, ingelesez irakurtzeko inongo arazorik izango ez duena alegia. Baina sarrera-laburpen orokor hau irakurle zabalago bati zuzendua egin nahi nuen, orain arte egindakoaren zergatiaren ideia bat bereganatu zezaten.

Honeraino iritsi zaretenoi... ZORIONAK!

General Introduction

"A Chemical Reaction is a Change in Bonding"

Derek H.R. Barton[1]

*"Chemical Bonding is an Interaction between Atoms
Associated with a Collectivization of the Valence
Electronic Orbitals"*

Isaac B. Bersuker[2]

Both of these experienced authors agree in the importance of being able to design what has been often attributed to the good luck or the art of the researchers: new chemical reactions and chemical compounds. This is known as molecular engineering, that is, the design and synthesis of new compounds.

"In the twenty-first century the majority of new chemical compounds will be obtained based on molecular design, and we should be prepared, from both the practical and psychological points of view, to meet this challenge."

I fully agree with their perspective and believe in the fact that it is necessary to put together all the techniques in use for reach our goal: a better understanding of the paradigms unresolved in science.

In this work we have tried to help in the clarification of one of them: the two-state reactivity of first row transition metal cations with water, with the hope that presenting the results in an unified way and on the same level, a better understanding will be reached by the readers.

In the introduction of each chapter a review of related existing data for each of the metal groups studied is given. Also a detailed description of the methods used through the chapter will be pointed out. So, now, I would like to introduce some general facts about two-state reactivity and gas-phase chemistry. A quick review of the available theoretical methods for the study of the systems of interest will come next. Finally the followed "pathway" to obtain a theoretical strategy to explain theoretically the main facts that involve the two-state reactivity of first row transition metal cations with water will be pointed out.

Two-State Reactivity

One of the characteristic aspects of first row transition metal cations is the presence of close lying excited states[3]. This is a common fact for coordinatively unsaturated transition-metal compounds in general[4]. Sc^+ to Fe^+ cations possess high-spin ground states and nearby low-spin excited states, while Co^+ to Cu^+ cations possess low-spin ground states and close lying high-spin excited states. Due to this, the reactivity of these metal cations can involve at least two states in which the ground state may not necessarily be the most reactive one[5].

The *potential energy surface*[6] of a reaction is the function that describes how the potential energy changes as the nuclei move relative to one another. Determining a single point on a many-dimensional molecular PES implies an extensive electronic structure calculation at a fixed relative orientation of the nuclei. To describe the orientation of an N-atom molecule on a PES requires $3N$ numbers, the positions in the three-dimensional space of each of the atoms. But we care only about the positions of the atoms relative to one another, so discarding six degrees of freedom for overall rotation and translation of the molecule leaves, for a nonlinear molecule, the PES is a surface of $3N-6$ *internal* degrees of freedom.

Clearly mapping out the full PES is tractable only for small molecules, but a great deal about a molecule and its behaviour can be learned from knowledge of a few selected points of the PES. *Local minima* on the PES are fundamental points since they represent stable isomers of a molecule. They determine the molecular structure and the moments of inertia by which the rotational spectra can be estimated. The curvature of the many-dimensional PES about the local minima, the steepness of the walls, determines the vibrational properties of the molecule including the normal modes and harmonic vibrational frequencies.

Another fundamental point on the PES is the lowest-energy *saddle point* connecting two local valleys or minima. The saddle point is the highest point on a lowest total energy pathway connecting these minima. It has the property that it is a maximum with respect to one degree of freedom and is a minimum with respect to all other degrees of freedom. The significance of the saddle point is that it is an approximate dynamic bottleneck, a point of no return, for a transformation from the vicinity of one local minimum or valley to another. The probability (or rate) of reaction is very strongly influenced by the height in energy of this saddle point.

Both the minima and the saddle points are *stationary points* on the PES; the derivative of the energy with respect to each of the geometry coordinates, and thus the force on each of the atoms is zero,

$$\frac{dE(q_1, q_2, \dots, q_m)}{dq_i} = 0 \text{ for all } i \quad (2)$$

Usually for light elements the orbital, spin and total angular momenta are well defined and conserved along the reaction path[5], as it is required by quantum mechanics. Their reactions proceed on a single spin potential energy surface[4], and it is sufficient to determine the transition structures, their entropic requirements, and the associated barrier heights to obtain an understanding of the single-state reactivity. But this picture becomes more complicated in the systems that exhibit two-state reactivity in which it is common to observe a crossing between the two potential energy surfaces. This is because only the total angular momenta must be rigorously conserved when heavier elements are involved.

Throughout the first row metal cations and their corresponding oxides three groups can be made based on their relative ground states. In the first group we have high-spin ground state metal cations with the corresponding low-spin ground state oxide cation; qualitative potential energy surfaces for these metals are shown in Figure 1.a. Iron forms the second group, as its metal and oxide cation has a high-spin ground state. One could think that spin should be conserved through the reaction, but the potential energy surface shows at least two spin-crossing as it is shown in Figure 1.b. Finally, the last group is formed by three late metal cations and the corresponding oxides, where low-spin ground states metal cations and high-spin ground state oxide cations are encountered, with the characteristic potential energy surface shown in Figure 1.c.

Undoubtedly we have to deal with systems that show very interesting reaction pathways and singular behaviours along the row. This "special" nature makes for the necessity of studying new reactivity factors due to the different bonding requirements in both states, and to the transition probabilities between the surfaces.

Figure 1. Qualitative representations of the three different potential energy surfaces shown by the first-row transition metals in the $M^+ + H_2O \rightarrow MO^+ + H_2$ reaction.

Gas-Phase Metal Ion Chemistry

Gas-Phase ion chemistry is the best environment to study this two-state reactivity systems both experimentally and theoretically.

Gas-Phase Chemistry gives us the opportunity to study the *intrinsic* properties of bare or ligated transition metal cations and to probe elementary reactions under well-defined conditions without the disturbing factors common in solution, that is, associations by ion pairing, solvent-shell interactions, intra- and intermolecular processes[7].

A good understanding of transition metal mediated oxidations in the gas phase is vital in very different areas[8], such as (a) heterogeneous catalysis for the conversion of hydrocarbons into more valuable products by use of economical oxidants such as peroxides, oxygen, or even air; (b) homogeneous catalysis for similar purposes as well as for small-scale synthetic applications; (c) biochemical transformations that involve one or several transition metals in the enzymes' reaction centers.

Studies in the gas-phase are not only important as a method of information supply to solution and surface phase studies. They are also of great interest in themselves[9]. Through experimental and theoretical studies in gas-phase an arsenal of thermochemical information has been obtained over these last years. Periodic properties on reactivity[10, 11], the effect of various ligands on metal ion chemistry(ML^+)[7, 12], the determination of metal ion-ligand bond strengths $D(M^+ - L)$ [13, 14], the effect of the attachment of subsequent ligands (ML_n^+)[15, 16], and lately the properties of metal clusters M_n^+ [17] and metallo-carbohedrenes[18] have been studied extensively.

To obtain as much as information and to reach a deep understanding of these systems a cocktail of techniques should be used. Ideally, the best results are obtained when all available techniques are used[9], but from a practical point of view, good agreement between a couple or more methods should be sufficient to take some data as reliable. As noted by Freiser[9] "*some of the fun occurs when there is disagreement between two methods and another method is tried to solve the discrepancy*". In these cases, collaborations between different groups are necessary and a very good example of this can be seen in ref. [19], where results from three different mass spectrometric techniques are put together to explain the quantitative differences found in the determination of rate constants and branching ratios for the iron oxide cation reaction with water and methane. These experimental techniques are Fourier transform ion cyclotron resonance (ICR)[20], guided ion beam (GIB)[21], and selected-ion flow tube (SIFT)[22] mass spectrometry. They conclude that the rate constants obtained with the SIFT method appear to be the most accurate ones, while those obtained by ICR are slightly too large, and the ones obtained by GIB are lower than the SIFT results. They also conclude that thermonuclear stabilization of the intermediates in the SIFT technique causes the difference in the branching ratios with respect to ICR and GIB measurements, which are obtained under single-collision conditions.

These experimental methods involve the activation of the ion, its dissociation and the collection of the products[9]. Which experimental procedures are used to activate the ions? Again, several methods can be used, with their particular goals and failures, and it is desirable to compare results. Ions can be activated by accelerating them against an inert gas (collision-induced dissociation, CID)[23], accelerating and colliding them into a surface (surface-induced dissociation, SID)[24], irradiating them with light (photodissociation (PDS)[25] and photoinduced reactivity[26]), and bombarding them with electrons (electron-induced dissociation(EID))[27].

At this point theory becomes relevant because through careful calculations detailed electronic and geometric structural information can be obtained as well as detailed pictures of the possible pathways of the reactions of interest. In addition a detailed description of the transition states on the surfaces is garnered and thereby a better understanding of the barriers that should be overcome in the reactions.

Thus, a *three member team* seems to be crucial for a proper description of metal ion chemistry: instrumentation, ionization sources and theoretical calculations.

Because the reaction mechanisms of transformations as simple as the ones we have described throughout our work are fundamental for the understanding of transition-metal mediated reactions with hydrocarbons in general [19], we report here the results from our calculations and the comparison with existing experimental data. This will be used to explain some of the observed patterns. We hope to shed some light onto some unclear aspects of these reactions and enhance the general understanding of transition metal cation and metal oxide potential energy surfaces.

Some Important Factors to Consider about Transition Metals

Transition metals in general represent a complicated group to be treated theoretically. This is due principally to the difficulty arising from the correct description of correlation and relativistic effects.

The experience obtained from a large amount of accurate calculations carried out mainly in the 70's[28] leads to a description of the correlation energy divided into two parts with different physical origins: one that takes into account the different degeneracy or near-degeneracy effects, and the dynamical correlation of the motion of the electrons.

One of the particular aspects that characterize the transition metal systems is their strong configurational mixing[29]. This arises from either the weak chemical bonds in these systems, and thus substantial occupation of the antibonding orbitals, and/or the related near-degeneracies in the transition metal atoms due to the closely spaced atomic energy levels, and their influence in the chemical bonds that will be formed by these metals.

The Hartree-Fock method has problems to describe this configurational mixing, since it places two electrons in the same spatial orbital[30]. The second problem with the Hartree-Fock method comes from the independent particle model where the electrons are moving in the average field of the other electrons, while, in reality the motion of the electrons depends on the instantaneous positions of all the other electrons[30]. The separation of these two errors is not a trivial work, as there is not a clear line separating these two effects, which makes their description more intricated.

The influence of these factors on the different transition metal rows is different, and we must take into account that for the first row transition metals the difference in size between the $3d$ and $4s$ orbitals is larger than for the other rows, leading to near-degeneracy effects when the d bonds are formed. This makes that although the first row transition metals are the lightest of the transition metals they have been claimed to be the most difficult to treat[31]. On the other hand, relativistic effects become smaller for the first row transition metals. It should be noted that for heavy atom compounds there exist a number of chemical observations which show that the interpretation of their electronic structure and properties cannot be achieved without relativistic treatment[32].

Available Theoretical Methods

Our goal is to obtain a procedure that describes correctly the correlation effects that govern our systems of interest, and at the same time that is feasible to perform the amount of calculations needed for the study of the trends through the series of the first row transition metals. At this point it is necessary to introduce the methods used in subsequent chapters. It is beyond the scope of this section to develop a full description of quantum mechanics and quantum chemistry, so we have omitted many mathematical demonstrations, referring the interested reader to the literature devoted to these topics (see for example ref. [33] and [34]).

The main goal of quantum chemistry is to solve the **time-independent Schrödinger equation** for molecules, i.e., a collection of nuclei and electrons, and obtain from the resultant Ψ information about the system. The hamiltonian \hat{H} for a molecule aside from relativistic terms and LS coupling has the form,

$$\begin{aligned} \hat{H} &= \hat{T}_e + \hat{T}_N + \hat{V}_{e-e} + \hat{V}_{e-N} + \hat{V}_{N-N} & (3) \\ &= -\sum_i \frac{\nabla_i^2}{2} - \sum_A \frac{1}{2M_A} \frac{\nabla_A^2}{2} - \sum_A \sum_i \frac{Z_A}{r_{iA}} + \sum_{i>j} \frac{1}{r_{ij}} + \sum_{A>B} \frac{Z_A Z_B}{R_{AB}} & (4) \end{aligned}$$

where i and j run over electrons and A and B over nuclei. \hat{T}_e and \hat{T}_N are the kinetic operators for electrons and nuclei, respectively, and the remaining three terms correspond to the interactions between particles, thus, electron-electron

repulsion (\hat{V}_{e-e}), electron-nuclei attraction (\hat{V}_{e-N}), and nucleus-nucleus repulsion (\hat{V}_{N-N}). Unfortunately, the exact resolution of such equation is only possible for systems containing just one electron. Of course, the majority of chemical species lie outside this reduced set, and the time-independent Schrödinger equation has to be solved under certain approximations.

The most basic one is that called the **Born-Oppenheimer approximation**[35], and results in the separation of the movements of the nuclei and electrons. The basic reasoning argues that since nuclei are much heavier than electrons, they move slower, and hence, one can consider the electrons in a molecule as moving in the field of fixed nuclei. Within this approximation, the term corresponding to the kinetic energy of the nuclei can be neglected and the repulsion between the nuclei can be taken as a constant. The remaining terms comprise the electronic Hamiltonian,

$$\hat{H}_e = \hat{T}_e + \hat{V}_{e-e} + \hat{V}_{e-N} \quad (5)$$

The solution to the Schrödinger equation set up by this Hamiltonian, namely,

$$\hat{H}_e \Psi_e = E_e \Psi_e \quad (6)$$

is the electronic wave function $\Psi(\{r_i\}; \{R_A\})$, which describes the motion of the electrons and depends explicitly on the electronic coordinates and parametrically on the nuclear coordinates, as does the electronic energy $E_e(\{R_A\})$.

On the other hand, to solve the problem of the motion of the nuclei, we can reasonably replace the electronic coordinates in \hat{H} by their average values, namely, $E_e(\{R_A\})$, since the electrons move much faster than the nuclei. Hence

$$\hat{H}_N = \hat{T}_N + E_e(\{R_A\}) + \hat{V}_{N-N} \quad (7)$$

The solution of the corresponding nuclear Schrödinger equation

$$\hat{H}_N \Psi_N = E \Psi_N \quad (8)$$

describes the vibration, rotation and translation of a molecule, and E is the total energy of the system. It is worth noting that the sum of $E_e(\{R_A\})$ and \hat{V}_{N-N} , namely $E_{tot}(\{R_A\})$, provides a potential for the nuclear motion. This function constitutes a **potential energy surface**.

Thus, the nuclei in the Born-Oppenheimer approximation move on a potential energy surface set up by the electronic energy, obtained by solving the electronic problem, and the internuclear repulsion. The concept of potential energy surface (PES) is fundamental in quantum chemistry, its topology determines the stability and reactivity of any chemical system and its detailed knowledge gives an understanding of the reaction mechanisms for a given chemical process. The calculation of the PES requires solution of the electronic problem.

Conventional Quantum Chemical Methods

The central approximation to resolve the electronic problem has been historically the **Hartree-Fock (HF) method**, electrons occupying orbitals, the starting point for more accurate descriptions.

The Hartree-Fock (HF) method is a variational method that approximates Ψ as an antisymmetrized product of N orthonormal spin orbitals $\chi_i(\vec{r})$ (one-electron functions, also called molecular orbitals (MO)), each a product of a spatial orbital $\phi_k(\vec{r})$ and a spin function $\sigma(s) = \alpha(s)$ or $\beta(s)$, the *Slater determinant*,

$$|\Psi_{HF}\rangle = |\chi_1, \chi_2, \dots, \chi_i, \chi_j, \dots, \chi_n\rangle \quad (9)$$

A *variational method*[36] allows one to obtain an approximation to the ground-state energy of a system without solving the Schrödinger equation. The theorem says:

"Given a system whose Hamiltonian operator \hat{H} is time independent and whose lowest-energy eigenvalue is E_1 if ϕ is any normalized, well-behaved function of the coordinates of the system's particles that satisfies the boundary conditions of the problem, then

$$\int \phi^* \hat{H} \phi d\tau \geq E_1, \phi \text{ normalized} \quad (10)$$

The variation theorem allows us to calculate an upper bound for the system's ground state energy.

The Hartree-Fock approximation[37, 38] is the method where-by the orthonormal orbitals $\chi_i(\vec{r})$ are found that minimize the expectation value for this determinantal form of Ψ .

The normalization integral $\langle \Psi_{HF} | \Psi_{HF} \rangle$ is equal to 1, and the energy expectation value is found to be given by the formula,

$$E_{HF} = \langle \Psi_{HF} | \hat{H}_e | \Psi_{HF} \rangle = \sum_{i=1}^N h_{ii} + \sum_{i,j=1}^N (J_{ij} - K_{ij}) \quad (11)$$

where

$$h_{ii} = \langle \chi_i(1) | \hat{h}_i(1) | \chi_i(1) \rangle = \int \chi_i^*(\vec{r}_1) \left[-\frac{1}{2} \nabla_1^2 - \sum_A \frac{Z_A}{r_{1A}} \right] \chi_i(\vec{r}_1) d\vec{r}_1 \quad (12)$$

$$J_{ij} = \langle \chi_i(1) | \hat{J}_j(1) | \chi_i(1) \rangle = \int \chi_i^*(\vec{r}_1) \chi_i(\vec{r}_1) \frac{1}{r_{12}} \chi_j^*(\vec{r}_2) \chi_j(\vec{r}_2) d\vec{r}_1 d\vec{r}_2 \quad (13)$$

$$K_{ij} = \langle \chi_i(1) | \hat{K}_j(1) | \chi_i(1) \rangle = \int \chi_i^*(\vec{r}_1) \chi_j(\vec{r}_1) \frac{1}{r_{12}} \chi_j^*(\vec{r}_2) \chi_i(\vec{r}_2) d\vec{r}_1 d\vec{r}_2 \quad (14)$$

J_{ij} and K_{ij} are called the *Coulomb* and the *exchange integrals*, respectively.

If we further consider that the spatial orbitals set $\{\phi_i\}$ are the same for both spin states α and β , thus, $\{\phi_i^\alpha(\vec{r})\} = \{\phi_i^\beta(\vec{r})\}$, we speak about the *restricted Hartree-Fock* method (RHF), and the expression of the energy for closed-shell systems can be written,

$$E_{RHF} = 2 \sum_{i=1}^{N/2} h_{ii} + \sum_{i,j=1}^{N/2} (2J_{ij} - K_{ij}) \quad (15)$$

where now the i and j indexes runs over the spatial orbitals $\{\phi_i\}$

Minimization of (13) subject to the orthonormalization conditions $\langle \phi_i | \phi_j \rangle = \delta_{ij}$ now gives the Hartree-Fock differential equations,

$$\hat{F}\phi_i(\vec{r}) = \sum_{j=1}^{N/2} \varepsilon_{ij} \phi_j(\vec{r}) \quad (16)$$

where \hat{F} is called the *Fock operator* and it is defined as,

$$\begin{aligned} \hat{F}(1) &= \hat{h}(1) + v^{HF}(1) \\ v^{HF}(1) &= \sum_i^{N/2} (2\hat{J}_i(1) - \hat{K}_i(1)) \end{aligned} \quad (17)$$

where $v^{HF}(1)$ can be viewed as an average potential create by the electrons.

The matrix ε consists of Lagrange multipliers associated with the orthonormality constraints. Multiplying by ϕ_i^* and integrating, one obtains the formula for *orbital energies*.

$$\varepsilon_i \equiv \varepsilon_{ii} = \langle \phi_i | \hat{F} | \phi_i \rangle = h_{ii} + \sum_{i,j=1}^{N/2} (2J_{ij} - K_{ij}) \quad (18)$$

Summing over i and comparing with (14), we find that

$$E_{RHF} = 2 \sum_{i=1}^{N/2} \varepsilon_i - V_{ee} \quad (19)$$

where V_{ee} stand for the total electron-electron repulsion energy.

An important property of the HF wave functions is that the occupied orbitals ϕ_i can be mixed among themselves without changing the expectation value E_{HF} . The operator \hat{F} is also invariant to such a transformation. This leads to a certain freedom in the choice $\{\phi_i\}$ and since the matrix ε is hermitian, one may choose a set of orbitals that diagonalize it. The corresponding orbitals are called the *canonical Hartree-Fock orbitals* and satisfy the *canonical Hartree-Fock equations*,

$$\hat{F}\phi_i(\vec{r}) = \varepsilon_i \phi_i(\vec{r}) \quad (20)$$

This equation is considerably more convenient for calculation than (14). The canonical orbitals will generally be delocalized and form a basis for an irreducible representation of the point group of the molecule, i.e., they will have certain symmetry properties characteristic of the symmetry of the molecule. Once the canonical orbitals have been obtained it would be possible to obtain an infinite number of equivalent sets by a unitary transformation of the canonical set. In particular, there are various criteria for choosing a unitary transformation so that the transformed set of orbitals is in some sense localized, more in line with our intuitive feeling for chemical hybrid bonds.

Solution of (18) must proceed iteratively, since the set of orbitals $\{\phi_i\}$ that solve the problem appear in the operator \hat{F} . Consequently, the Hartree-Fock method is a *self consistent field* (SCF) method. In actual implementations of the Hartree-Fock theory, one usually employs some set of fixed one-electron basis functions (*basis set*), in terms of which the $\{\phi_i\}$ are expanded

$$\phi_i = \sum_{\nu} C_{\nu i} \varphi_{\nu} \quad (21)$$

Quite often, the φ_{μ} are hydrogenic-like functions centered in one atom (*atomic orbitals*), and then, we say that the molecular orbitals $\{\phi_i\}$ (MO) are expanded as a linear combination of atomic orbitals (LCAO), i.e., the MO-LCAO approximation. In this context solving the variational problem means to find the set of the MO-LCAO expansion coefficients $\{C_{\nu i}\}$ for which (18) is satisfied. This problem can be transformed into a matrix eigenvalue problem, in which the matrix elements are calculated from arrays of integrals evaluated for the basis functions. This can be done by expanding $\{\phi_i\}$ in equation (18), multiplying by φ_{μ}^* and integrating,

$$\sum_{\nu} C_{\nu i} \int d\vec{r}_1 \phi_{\mu}^*(1) \hat{F}(1) \phi_{\nu}(1) = \varepsilon_i \sum_{\nu} C_{\nu i} \int d\vec{r}_1 \phi_{\mu}^*(1) \phi_{\nu}(1) \quad (22)$$

Defining now the RHS integral as an element $S_{\mu\nu}$ of the *overlap matrix* \mathbf{S} and the integral on the LHS as $F_{\mu\nu}$, an element of the *Fock matrix* \mathbf{F} , we obtain the following matrix equation (*the Roothan matrix equation*),

$$\mathbf{F}\mathbf{C} = \mathbf{S}\mathbf{C}\varepsilon \quad (23)$$

The elements $F_{\mu\nu}$ and $S_{\mu\nu}$ are sometimes all computed from first principles, hence one says that one has an *ab initio method*. Sometimes these are determined by some recourse to experimental data, in which case one has a *semiempirical method*.

If spatial parts of spin orbitals with α spin are allowed to be different from spatial parts of spin orbitals with β spin,

$$\{\phi_i^{\alpha}(\vec{r})\} \neq \{\phi_i^{\beta}(\vec{r})\} \quad (24)$$

we speak about the *unrestricted Hartree-Fock* (UHF) approximation. This is the method of choice if we are dealing with open-shell systems, and can yield

the proper homolytic dissociation products in contrast with the RHF method. In UHF we will have a two sets of equations, matrices and integrals, one for the α - and one for the β -spin cases, and they have to be solved in a SCF way. The basis sets are the same for α - and β - spin orbitals, what differs is that since they are treated separately, we will find different expansion coefficients for the two set of orbitals.

However, the exact wave function for a system of many interacting electrons is *never a single determinant*. We can define:

The correlation energy for a specific state of a system is defined as the difference $E_{corr} = E - E_{HF}$ between the exact eigenvalue E and the Hartree-Fock energy E_{HF} of the same Hamiltonian for the state under consideration[39].

In other words, we can say also that the total energy of an atomic or molecular system is divided in the SCF energy which is obtainable from a wave function consisting of a single configuration and the other part is the correlation energy[28].

Which methods evaluate the correlation energy? The methods for evaluation of the correlation energy are based in two approximations: the variational and perturbational theories.

Suppose now that we have a system with time-independent Hamiltonian \hat{H} which Schrödinger equation we are not able to solve, $\hat{H}\Psi_n = E_n\Psi_n$, for the eigenfunctions and eigenvalues of the bound stationary states. Suppose also that we are able to solve another system which Hamiltonian \hat{H}^0 is only slightly different from the Hamiltonian \hat{H} . The difference of this two Hamiltonians is defined as the *perturbation* \hat{H}' [40],

$$\hat{H}' \equiv \hat{H} - \hat{H}^0 \quad (25)$$

Physicist and chemists have developed various perturbation-theory methods [41, 42] to deal with systems of many interacting particles, and these methods constitute *many-body perturbation theory* (MBPT). In 1934, Moller and Plesset proposed a perturbation treatment of atoms and molecules in which the unperturbed wave function is the HF function, and this form of MBPT is called **Moller-Plesset** (MP) *perturbation theory*.

The basic variational method for obtaining the correlation energy is based on the idea of representing the exact wave functions as a linear combination of N-electron trial functions and use linear variational method: the **configuration interaction**[43] (CI). We define the full CI wavefunction as a mixture of all the possible different configurations,

$$|\Psi_{CI}\rangle = C_0|\Psi_0\rangle + \sum_S C_S|S\rangle + C_D|D\rangle + C_T|T\rangle + \dots \quad (26)$$

where $|S\rangle$, $|D\rangle$, $|T\rangle$, and so on, stands for all the single ($|\Psi_{ab}^r\rangle$), double ($|\Psi_{abcd}^{rst}\rangle$), triple ($|\Psi_{abc}^{rst}\rangle$), and so on, excitations, respectively, which are

adapted to a given spin state. The full CI matrix that has to be calculated is,

	$ \Psi_0\rangle$	$ S\rangle$	$ D\rangle$	$ T\rangle$	$ Q\rangle$...
$\langle\Psi_0 $	$\langle\Psi_0 \hat{H} \Psi_0\rangle$	0	$\langle\Psi_0 \hat{H} D\rangle$	0	0	...
$\langle S $	0	$\langle S \hat{H} S\rangle$	$\langle S \hat{H} D\rangle$	$\langle S \hat{H} T\rangle$	0	...
$\langle D $	$\langle D \hat{H} \Psi_0\rangle$	$\langle D \hat{H} S\rangle$	$\langle D \hat{H} D\rangle$	$\langle D \hat{H} T\rangle$
$\langle T $	0	$\langle T \hat{H} S\rangle$	$\langle T \hat{H} D\rangle$
$\langle Q $	0	0

Notice that the terms $\langle\Psi_0|\hat{H}|S\rangle$ are zero (see Brillouin's theorem in reference [44]), and any element relating Slater determinants which differ by more than 2 spin orbitals also vanishes (see Slater rules in reference [44]). Due to the fact that the single excitations do not mix directly with $|\Psi_0\rangle$, they can be expected to have a very small effect on the ground state energy. Their effect is not zero because they do mix indirectly; that is, they interact with the doubles which in turn interact with $|\Psi_0\rangle$. Besides, because it is the double excitations that mix directly with $|\Psi_0\rangle$, it is expected that these excitations play an important role in determining the correlation energy. Despite the negligible effect of the single excitations on the correlation energy, their inclusion turns out to be essential for a satisfactory description of the charge density and, hence, for properties which are sensitive to this quantity.

To solve the problem, we can apply the linear variation method, thus, write,

$$\hat{H}|\Psi_{CI}\rangle = \mathcal{E}_0|\Psi_{CI}\rangle \quad (27)$$

or equivalently, subtracting E_0 from the above equation,

$$(\hat{H} - E_0)|\Psi_{CI}\rangle = (\mathcal{E}_0 - E_0)|\Psi_{CI}\rangle = E_{corr}|\Psi_{CI}\rangle \quad (28)$$

Then, successively multiply this equation by $\langle\Psi_0|$, $\langle\Psi_a^r|$, $\langle\Psi_{ab}^{r*}|$, etc. For instance, multiplying by $\langle\Psi_0|$ and considering an intermediate normalization $\langle\Psi_0|\Psi_{CI}\rangle = 1$ we obtain,

$$E_{corr} = \sum_{a<b;r<*} c_{ab}^{r*} \langle\Psi_0|\hat{H}|\Psi_{ab}^{r*}\rangle \quad (29)$$

and we can see how the correlation energy is determined solely by the coefficients of the double excitations in the intermediate normalized CI function. This does not mean that only double excitations need to be included for an exact CI description of the ground state; as mentioned, these coefficients are affected by the presence of the other excitations. Multiplying equation (27) by the rest of configurations we would end up with a hierarchy of equations that must be solved simultaneously to obtain the correlation energy. This set of coupled equations is extremely large if all possible excitations are included, and one has to truncate the serie (25) in somewhere.

One of the most common truncations is to cut the series at double excitations, this is quite reasonable since as we have seen they seem to be the main

contributors to the correlation energy. The so truncated wave function is called the SDCI wave function,

$$|\Psi_{SDCI}\rangle = C_0|\Phi_0\rangle + \sum_S C_S|S\rangle + C_D|D\rangle \quad (30)$$

and one solves the linear variation problem for this reduced number of configurations. The obtained result will be an upper bound to the true energy.

One of the problems of the truncation of a full-CI wave function is that the property called *size-consistency*[45] is lost. A size-consistent quantum-mechanical method is one for which the energy and hence the energy error in the calculation increases proportionally to the size of the molecule. Size consistency is important whenever calculations on molecules of substantially different sizes are to be compared. Full CI wave functions are size consistent, however truncated CI wave functions are not, and it has been shown that the correlation energy recovered by truncated CI expansions per particle goes to zero as the number of particles goes to infinity. Nevertheless, it has been observed that for small molecules[45] (up to 50 electrons) CI-SDTQ comes reasonably close to the full CI and hence will be approximately size consistent. However, these calculations are fairly expensive.

An alternative is to use an approximate formula due to Davidson[46] to estimate the energy contribution of the quadruple excitations, namely,

$$\Delta E_Q \approx (1 - a_0^2)(E_{SDCI} - E_{SCF}) \quad (31)$$

where a_0 is the coefficient of the HF wave function in the normalized CI expansion. When this correction is added to E_{SDCI} the result is reasonable close to the SDTQCI result and thus, considerably reduces the size-consistency error.

One of the more advanced multi-determinant correlation methods is the **Coupled Cluster Approximation**[47]. This coupled-pair theory is related to the perturbational methods in the respect that it is non-variational; i.e. there is no lower bound to the correlation energy. The formalism is, however, very similar to that of the CI methods, and in particular to DCI. The main difference from the DCI result is that CC-calculations are size-consistent, whereas DCI are not. Due to products of coefficients of the doubly excited configurations (as will be shown below) it is, furthermore, non-linear, and the correlation energy can thus not be obtained by a simple matrix diagonalization, as is the case in CI.

The fundamental equation in the CC theory is:

$$\Psi_{CC} = e^T \Phi_0 \quad (32)$$

where Ψ is the exact non-relativistic ground-state molecular electronic wave function, Φ_0 is the normalized ground-state Hartree-Fock wave function, the

operator $e^{\hat{T}}$ is defined by the Taylor-series expansion

$$\begin{aligned} e^{\hat{T}} &\equiv 1 + \hat{T} + \frac{\hat{T}^2}{2!} + \frac{\hat{T}^3}{3!} + \dots \\ &= \sum_{k=0}^{\infty} \frac{\hat{T}^k}{k!} \end{aligned} \quad (33)$$

and the cluster operator \hat{T} is

$$\hat{T} \equiv \hat{T}_1 + \hat{T}_2 + \dots + \hat{T}_n \quad (34)$$

where n is the number of electrons in the molecule.

Inclusion of only \hat{T}_2 gives the approximate CC approach called the coupled-cluster doubles (CCD) method. The next step in improving the CCD method is the inclusion of the \hat{T}_1 operator, so taking $\hat{T} = \hat{T}_1 + \hat{T}_2$ in $e^{\hat{T}}$, resulting in the singles and doubles (CCSD) method. And finally, including also \hat{T}_3 we obtain the accurate CC singles, doubles, and triples (CCSD(T)) method[48].

Actually, MOs for the CI calculation can be chosen freely. Any set of MOs, and in particular the SCF MOs, built with the basis set functions will produce the same final wave function provided a full-CI calculation is carried out. Moreover, properly chosen MOs will converge faster to the true wave function than SCF MOs, thereby allowing for fewer configurations to be included in a truncated wave function. One method that uses this idea is the **multiconfiguration self-consistent-field (MCSCF) method** that we will comment on next.

The MCSCF wave function[49] is a truncated CI expansion,

$$|\Psi_{MCSCF}\rangle = \sum_I C_I |\Psi_I\rangle \quad (35)$$

in which the expansion coefficients of both the configurations $|\Psi_I\rangle$ (thus, C_I) and of the orthonormal orbitals used to set up the configurations, are optimized. Thus, the MCSCF orbitals for each configuration will differ from the corresponding SCF and/or CI orbitals. In addition, the energy will be lower, since the orbitals are optimal for the MCSCF wave function, rather than being optimal for the HF wave function. The general equations, which must be solved to obtain the MCSCF wave-functions are considerably more complicated than those corresponding to HF method, and its derivation is beyond the scope of this section.

A commonly used kind of MCSCF method is the *complete active space* SCF (CASSCF) method. In this method, one defines three set of orbitals: *inactive*, *active* and *external* orbitals (unoccupied orbitals). The inactive orbitals are kept doubly occupied in all configurations, and one writes the MCSCF wave function as a linear combination of all configurations that can be formed by

distributing the remaining electrons (*active electrons*) among the active orbitals in all possible ways and that have the same spin and symmetry eigenvalues as the state to be treated. One then does an MCSCF calculation to find the optimum orbitals and coefficients of the expansion.

The choice of the active space is critical in CASSCF studies, and leads to the possibility of a lack of objectivity in CASSCF computations. From the outset, it must be recognized that in CASSCF theory, one is not attempting to compute the true dynamic electron correlation energy; rather, one is seeking a wavefunction that will yield a balanced representation of the potential energy surface in the region of products, reactants and transition states. For those potential energy surfaces where degeneracies or near-degeneracies occur between different electronic configurations, HF theory breaks down, but CASSCF wavefunctions, with properly chosen active spaces, can yield a balanced description of all the stationary points. To be able to describe all the degeneracies, one obvious option would be to include all the valence orbitals into the active space. In calculations on larger systems this will, of course, not be possible. It is also not necessary. Studies of an energy surface, i.e., for a chemical reaction, will normally be concentrated in regions where only one or two of the chemical bonds are broken or formed. The calculation can then be performed by choosing as active orbitals only those taking part in the bond-breaking or bond-formation process.

There exists a strong interplay between near-degeneracy effects and dynamical correlation. Strong near-degeneracy effects lead to effective separation of the electron pair, and thus, to a reduction in the dynamical correlation effects. A method which only takes into account near-degeneracy effects will in general not give a balanced description of the total correlation effects over an energy surface, for example along a dissociation channel. This is the reason why full valence MCSCF calculations, in general, give binding energies which are too low. It is sometimes possible to counter-balance this effect by adding a few more active orbitals. The principle behind this is that the active space should contain one correlating orbital for each strongly occupied orbital. When this is not possible (large systems), one can do CASSCF calculations but assuming that only semi-quantitative results can be expected from them, and to improve the results additional dynamical correlation effects have to be included via configuration interaction or perturbational calculations.

So, in the conventional CI method one starts with a SCF wavefunction Φ_1 (the reference function), and moves electrons out of occupied orbitals of Φ_1 into virtual SCF orbitals to produce CSFs Φ_2, Φ_3, \dots , and one writes the wave function as $\Psi = \sum_i a_i \Phi_i$; one then varies the a_i 's to minimize the variational integral.

The conventional CI method and the MCSCF methods can be combined obtaining a **multireference CI (MRCI) method**[50]. Here, one first does an MCSCF calculation to produce a wave function that consists of several CSF's $\Phi_1, \Phi_2, \dots, \Phi_m$ with optimized orbitals and that has the proper behavior for all

nuclear configurations. One then takes this MCSCF function and moves electrons out of occupied orbitals of the CSF's $\Phi_1, \Phi_2, \dots, \Phi_m$ (called the reference CSF's) into virtual orbitals to produce further CSF's $\Phi_{m+1}, \dots, \Phi_n$. One writes $\Psi = \sum_{i=1}^n a_i \Phi_i$ and does a CI calculation to find the optimum a_i 's. Typically, the reference CSF's will contain singly and doubly excited CSF's, and as in the final wave function, one will consider single and double excitations from the reference CSF's, the final MRCI wave function will include some triple and quadruple excitations.

So, in this scheme, near-degeneracy correlation effects are treated effectively using the multiconfigurational SCF method; and dynamical correlation is included through subsequent multireference MRCI calculations. But, this approach has severe limitations as regards of the size of the system that can be treated, both with respect to the number of electrons and the basis set dimension. Lately, another approach has been developed to obtain a correct description of the dynamical correlation based on a multiconfigurational wave function, with the goal of being able to apply it to all the systems that can be treated by the MCSCF method, this can be done extending low-order perturbation schemes to the case with a multiconfigurational reference function: a quasidegenerate perturbation theory, a **second-order perturbation theory with a complete active space self-consistent field reference function (CASPT2)**[51, 52].

Density Functional Theory Methods

In this section, we will introduce a different approach to the electronic problem. We will consider the electron density $\rho(\vec{r})$, a function of only 3 variables, as the descriptor of an electronic state and calculate the energy and all the properties of our system in terms of this $\rho(\vec{r})$. This formalism is called *density functional theory (DFT)*[53, 54].

In 1964, Hohenberg and Kohn proved that the ground-state molecular energy, wave function, and all other molecular electronic properties are uniquely determined by $\rho(\vec{r})$. Hence, the ground-state energy E_0 is a functional of $\rho(\vec{r})$, and therefore, if we know the ground-state electron density it is possible to calculate all the ground-state properties from ρ . In a second theorem, Hohenberg and Kohn established an energy variational principle for this functional, that is, for a trial density $\tilde{\rho}(\vec{r})$ such that $\tilde{\rho}(\vec{r}) \geq 0$ and $\int \tilde{\rho}(\vec{r}) d\vec{r} = N$, it is satisfied that,

$$E_0 \leq E[\tilde{\rho}(\vec{r})] \quad (36)$$

This is analogous to the variational principle (23) for wave functions. Once we know the exact form of the $E[\rho]$ functional, the variational principle gives us a way to search for the ground state density (as it is the case for the wave function). However, the Hohenberg and Kohn theorems do not tell us how to

calculate E_0 from ρ since the exact form of the functional is not known.

Kohn and Sham invented an indirect approach to this functional, the *Kohn-Sham method*, and thereby turned DFT into a practical tool for rigorous calculations. They showed that the exact ground-state purely electronic energy E_0 of an N-electron molecule with ground-state electron probability density ρ is given by,

$$E_0 = -\frac{1}{2} \sum_{i=1}^N \langle \psi_i | \nabla_1^2 | \psi_i(1) \rangle + \int v(r) \rho(1) dr_1^3 \quad (37)$$

$$+ \frac{1}{2} \iint \frac{\rho(1)\rho(2)}{r_{12}} dr_1^3 dr_2^3 + E_{xc}[\rho]$$

where $v(r) = -\sum_{\alpha} \frac{Z_{\alpha}}{r_{1\alpha}}$ is the external potential due to the nuclei, ψ_i are the *Kohn-Sham orbitals*, and the $E_{xc}[\rho]$ is the *exchange-correlation energy*.

In the Kohn and Sham procedure, the exact ground state ρ can be found from the Kohn-Sham orbitals according to,

$$\rho = \sum_{i=1}^N |\psi_i|^2 \quad (38)$$

The Kohn-Sham orbitals are found by solving the one-electron equations

$$\hat{F}_{KS}(1)\psi_i(1) = \varepsilon_i\psi_i(1) \quad (39)$$

where the Kohn-Sham operator \hat{F}_{KS} is

$$\hat{F}_{KS} = -\frac{1}{2}\nabla_1^2 + v(1) + \sum_{j=1}^n \hat{J}_j(1) + V_{xc}(1) \quad (40)$$

where \hat{J} is the Coulomb operator, and V_{xc} is called the *exchange-correlation potential*. \hat{F}_{KS} is like the Fock operator in HF equations, except that the exchange operators are replaced by V_{xc} , which handles the effects of both the exchange and electron correlation. The physical significance of the Kohn-Sham orbitals is still under debate. Some authors claim that they do not have any significance other than in allowing the exact ρ to be calculated from (37). Likewise, the Kohn-Sham orbital energies should not be confused with molecular orbital energies. However, based on the fact that the Kohn-Sham orbital energy for the HOMO is just the negative of ionization potential, and due to the fact that the set of Kohn-Sham equations remind us, as in the HF case of, the independent particle model, others associate to the Kohn-Sham orbitals a similar physical significance and legitimacy as to the HF canonical orbitals.

As in HF, these equations have to be solved iteratively. Thus one proposes a guess density, which is used to build the \hat{F}_{KS} , then one solve the set of equations (38) and obtain a new density, which in turn is used to build a second \hat{F}_{KS} , and so on, until self-consistency.

There is only one problem in using the the Kohn-Sham equations to find ρ and E . No one knows what the exact functional $E_{xc}[\rho]$ is for molecules, however, approximate functionals have been proposed.

If ρ varies very slowly with position, one can show that $E_{xc}(\rho)$ is given by

$$E_{xc}^{LDA}(\rho) = \int \rho(\vec{r}) \varepsilon_{xc}(\rho) d\vec{r} \quad (41)$$

where $\varepsilon_{xc}(\rho)$ is the exchange plus correlation energy per electron in a homogeneous electron gas with electron density ρ . An accurate expression for $\varepsilon_{xc}(\rho)$ has been found by Vosko, Wilk and Nusair[55]. Application of this expression to study ρ in a molecule leads to the *local density approximation* (LDA), or *local spin density approximation* (LSDA)[56], if one uses different orbitals and densities ρ^α and ρ^β for electrons with different spins. Of course, in the case of molecules these are only approximations to the true functionals, since ρ is far from being homogeneous. To yield accurate chemical descriptions, one usually has to add corrections by means of terms involving the gradient of ρ . These corrections are called *non-local gradient corrections*, and they are added to both exchange and correlation terms. For the exchange term in this thesis we have used the corrections proposed by Becke[57] (B), and for the correlation part those introduced for Lee, Yang and Parr[58] (LYP), and so, we will speak about the BLYP method. Also, it has been observed one can get better results using hybrid functionals of the type,

$$(1 - a_0)E_x^{LSDA} + a_0E_x^{HF} + a_xE_x^{B88} + a_cE_c^{LYP} + (1 - a_c)E_c^{VWN} \quad (42)$$

being the values of the parameters $a_0=0.20$, $a_x=0.72$ and $a_c=0.81$. This functional is known as the Becke's 3 parameter functional, B3LYP[59].

Because density-functional calculations do not use the exact E_{xc} they are not, strictly speaking, ab-initio calculations. However, they do not use parameters fitted to experimental data, and so are closer in spirit to ab-initio calculations than to semiempirical ones. One of the main advantages of these methods is that with a similar computational cost to HF methods, they include some kind of electron correlation, being the major drawback that the correlation effects cannot be sorted out exactly. They are already mixed from the beginning with the uncorrelated solution. Besides, there is not a systematic way to improve the calculations by applying more and more sophistication, so the results must be accepted as they stand. In spite of these facts, DFT have been found to yield good results for ground state properties of various chemical

systems, with a quality comparable to MP2 results[60], or even better in some cases. Due to their relative low computational cost, DFT is the method of choice for large systems, for which the inclusion of electron correlation by MP or CI methods is prohibitive.

Designing the Theoretical Procedure

The $Ti^+ + H_2O$ reaction gained our attention first as interesting discussions were found in the literature showing that it was a good case for studying theoretically and in accordance with experimental observations. Before starting to calculate the full reaction mechanism we first thought it would be convenient to carry out various calculations to determine what levels of theory were necessary. We choose two point energies in our reaction mechanism: the $Ti(OH_2)^+$ ion-molecule dissociation energy and the interconfigurational energy ordering of the two valence electronic configurations $d^{n-1}s$ and $d^{n-2}s^2$ of the titanium cation's 4F electronic state.

The very first calculations were carried out using the MCSCF method as it seemed that it was the method to use with first row transition metals. Both full electron basis sets and effective core potentials were used (see chapter 1). But a clear underestimation was obtained in the dissociation energies. This was also the case for the coupled cluster methods. Thus, the new DFT methods gained our attention. They are much cheaper to use than MCSCF or CC methods, and the results in the literature were very encouraging. As nobody from our group had experience in DFT and transition metal chemistry, I had the opportunity to work in Prof. R. Boyd's group for three months and learn about this new method. This proved to be a good choice as a new perspective for the studying of our systems was gained. The results obtained were better than the only MCSCF or CCSD(T) methods, and a way for studying the full reaction mechanism was opened in front of us.

We still had the feeling that a different treatment of correlation should be used in our systems, at least for some important points, in order to be able to estimate the reliability of our B3LYP results. We found it interesting to try some methods that include both dynamical and non-dynamical correlation. I had the opportunity to get insight into these methods under the direction of Dr. Leif Eriksson. He was at that time in Prof. Per Slegbahn's group, which has great experience with transition metal chemistry. Different approaches were used and CASPT2 seemed to be an interesting method to apply, as a good estimation of excitation energies was desirable for the correct description of our system. These calculations are shown through chapter 2.

In the end, not much improvement was obtained compared to the considerable effort needed to obtain reliable results. It was clear that a good approximation could be obtained just using B3LYP/DZVP level of theory for the full potential energy surfaces, and some B3LYP/TZVP+G(3df,2p) level calculations for the key data. However, we decided that some pure *ab initio* value should also

be given. Thus, collecting all the experience gained in our work and the results in the literature, we decided that also CCSD(T)/TZVP+G(3df,2p)//B3LYP/TZVP+G(3df,2p) calculations should be carried out (chapters 3, 4 and 5).

Chapter 1

Preliminary Calculations

The dissociation energy of the $Ti(OH_2)^+$ ion-molecule complex has been calculated by the Multiconfigurational Self-Consistent-Field Theory, Coupled Cluster Theory and two Density Functional Theory based methods, using both all electron basis sets and Effective Core Potentials. The calculations show that approximate Density Functional Theory gives results in better agreement with experiment than both the Multiconfigurational Self-Consistent-Field Theory and the Coupled Cluster Theory, with both all electron basis sets and Effective Core Potentials. Nevertheless, optimized geometries and harmonic vibration frequencies are very similar, irrespective of the level of theory used. The interconfigurational energy ordering of the two valence electronic configurations $d^{n-1}s$ and $d^{n-2}s^2$ of the titanium cation's 4F electronic state, have been also calculated and discussed.

1.1 Introduction

Solvation of the first transition-row metal ions by water has been the subject of much recent research work. Both experimental and theoretical methods have been used to gain insight into the bonding energies of water molecules to transition metal positive ions. In particular, the $Ti(OH_2)^+$ cluster has been studied earlier, by both experimentalists and theoreticians. The bond dissociation energy of the $Ti(OH_2)^+$ complex was first reported by Magnera *et al.*, obtained by the use of collision-induced dissociation in a triple-quadrupole mass spectrometer[61]. They gave a value of 38.0 ± 3 kcal/mol. Later, Dalleska *et al.*[62], reported the bond dissociation energies for the $M-O$ bond of the ion-molecule complex as determined by collision-induced dissociation in a guided ion beam mass spectrometer. The threshold energy for the collision-induced reactions is equivalent to the 0K bond dissociation energy[63]. Therefore, their value for the dissociation energy of the $Ti(OH_2)^+$ ion molecule complex at 0K is 36.9 ± 1.4 kcal/mol(see Table 3 in ref. [62]. Simultaneously, *ab initio* molecular orbital theory was also used to estimate the dissociation of $Ti(OH_2)^+$. Rossi and Bauschlicher[64] reported on calculations with the modified coupled pair functional (MCPF) method and a fairly large basis set. They obtained a value of 37.5 kcal/mol, using for the ZPVE correction, the corresponding energy correction of the $Cu(OH_2)^+$ system. Then, Magnusson and Moriarty[65] used both Møller Plesset (MP) perturbation theory and truncated Configuration Interaction (CI) methods, with a variety of basis sets. Their results show, as indeed Rossi and Bauschlichers' do, that in every case the dissociation energy of the $Ti(OH_2)^+$ is overestimated, with respect to the experimental value of Dalleska *et al.*

During the last years, however, there has been an increasing interest in the use of gradient corrected approximate density functionals[57, 66]. In particular, there is a growing evidence that approximate functionals yield accurate bonding energies for both, the first[67, 68] and second-row[69] transition metal complexes. Thus, in this work we consider the bonding energy of the $Ti(OH_2)^+$. Our goal is to determine the reliability of the approximate density functionals BLYP and B3LYP used in conjunction with effective core potentials and valence basis sets of double and triple zeta quality. Comparison of experimental available data, with respect to both BLYP and B3LYP and multiconfigurational-self-consistent-field (MCSCF) and Coupled Cluster (CCSD(T)) calculations with all-electron double zeta and triple zeta basis sets and effective core potentials, will be made. Inclusion of corrections due to the zero-point-vibrational energy and to the basis set superposition energy, estimated with the counterpoise method[70] will also be explicitly considered.

1.2 Methods

All calculations reported in this chapter have been carried out with the GAUSSIAN94/DFT[71] and the GAMESS[72] suites of programs.

1.2.1 Level of Theory

Both *ab initio* molecular orbital MCSCF and CCSD(T) methods and BLYP and B3LYP approximate Density Functional Theory (DFT) methods have been used in the present study. For the MCSCF calculations, initially a full optimization at the Hartree-Fock level of theory was carried out to select the active space window properly. In particular, we have chosen six orbitals, corresponding to the five $3d$ and the one $4s$ valence orbitals of titanium, to allocate three electrons. This active space will be denoted, as usual, (3/6). Both Ti^+ and $Ti(OH_2)^+$ have been fully optimized at this level of theory, while for H_2O only the Hartree-Fock level was used. These structures were confirmed to be true minima by inspection of the force constants matrix, evaluated at the corresponding level of theory.

The singles and doubles, with a noniterative estimate for the triples, Coupled Cluster, CCSD(T), calculations were carried out at the CCD optimized structures. Also, at this level of theory the zero-point vibrational energy corrections, ($\Delta ZPVE$), were taken from a frequency calculation at the CCD level of theory.

The approximate DFT methods that have been used are associated with the well known Becke[57] and Lee, Yang and Parr[66] (BLYP) approximate functionals, and the three parameter hybrid approximate functional of Becke[59] and the gradient-corrected correlation functional of Lee, Yang and Parr[66] (B3LYP). The choice of these two approximate DFT methods is largely motivated by their satisfactory performance reported recently[68, 73] for transition metal containing systems.

1.2.2 Basis Sets

All Electron Basis Sets

As indicated by Hay *et al.*[74], good uncontracted basis sets are normally too large for application to molecules, so they should be appropriately contracted. In the present chapter three different contracted basis sets[75], two of double zeta plus polarization quality, namely the DZVP and DZVP2 given by Salahub *et al.*[76, 77], and one of triple zeta plus polarization quality have been used for the calculations. The triple zeta quality basis set, TZVP, used in the present chapter is, for the titanium, that given by Schäfer, Hubert and Ahlrichs[78], supplemented by the two $4p$ polarization function optimized by Wachters[79] for the excited states and augmented with a diffuse s function (with an exponent 0.30 times that of the most diffuse s function on the original set) and one diffuse

d function (optimized by Hay)[80]. For both the oxygen and hydrogen we have taken the standard 6-311++G(d,p) basis set of Pople *et al.*[81].

Effective Core Potentials (ECP)

The use of atomic effective core potentials (ECP) and model potentials (MP) to eliminate chemically inactive atomic core electrons from quantum mechanical calculations has become routine during the past decade[82]. Because of their economic advantages associated with reduced sizes of the basis sets that can be achieved with the ECP method and corresponding nodeless pseudo-orbitals, the SKBJ's Relativistic Compact Effective Potentials[82] have been used. These consider the first ten electrons of the titanium and the first two electrons of the oxygen to be part of the core, and the rest are described by the SKBJC valence basis set. Three different sets have been built from the standard SKBJC's set. The smallest one has one extra heavy atom polarization function on the oxygen (SKBJC(d)); the intermediate one has one extra d polarization function on the oxygen and p type polarization function on the hydrogens (SKBJC(d,p)); finally the largest one has a d polarization function on the oxygen plus two p polarization functions on the hydrogens (SKBJC(d,2p)). The contractions for these three sets are:

- SKBJC(d)→[4sp3d/2sp1d/2s]
- SKBJC(d,p)→[4sp3d/2sp1d/2s1p]
- SKBJC(d,2p)→[4sp3d/2sp1d/2s2p]

Since the importance of the relativistic effects decreases steadily from the third row transition metal series to the first one, it is customarily[64, 65] assumed that they are small enough for titanium, hence they have been not considered explicitly in the all electron basis sets. Therefore, the dissociation energies, reported in this chapter for all electron basis sets, were calculated as the difference between the energy of the isolated monomers and the complex, without considering relativistic effects, but including both BSSE and ZPVE corrections. All the structures shown in this chapter have been confirmed to be true minima by a frequency calculation at the corresponding computational level. Further, these calculations have provide us with the zero point vibrational energy (ZPVE) corrections.

1.3 Results

Discussion here is directed at finding out which of the methods used can be selected as a computational strategy that is economic and, at the same time, reliable. Multiconfigurational methods are adequate to describe properly the different configurations that arise from the non-equivalence of d orbitals in

$d^{n-2}s^2$, $d^{n-1}s$ and d^n states [83]. On the other hand DFT, a monoconfigurational method that includes correlation and that seems to work properly for this kind of systems[67, 68, 69, 73], is computationally a less demanding method than the correlated *ab initio* MCSCF and CCSD(T) methods.

1.3.1 Ti^+

It has been pointed out earlier[84] that the correct prediction of the interconfigurational energy ordering of the two valence electronic configurations, $d^{n-1}s$ and $d^{n-2}s^2$, of transition metal atoms is crucial for the accurate description of the dissociation energies of the clusters. In particular, the ground state of the Ti^+ cation is the 4F state, which corresponds to the $3d^24s^1$ electronic configuration, and the first excited state, the $^4F(3d^3)$, lies 0.10 eV above[85]. However, it has been demonstrated[86] that subtraction of the relativistic corrections from the energies of both states switches the stability order, rendering a $^4F(3d^3)$ ground state with the $^4F(3d^24s^1)$ being the first excited state, 0.07eV above.

Table 1.1. *Total(E), in a.u., and relative energy (Δ_{sd}), in eV, and expectation value of the S^2 operator for the sd^2 and d^3 electronic configurations of $Ti^+(^4F)$ calculated with the B3LYP and various basis sets and ECPs.*

	Electronic Configuration	E	$\langle S^2 \rangle$	Δ_{sd}
SKBJC(d)	sd^2	-57.68400	3.75	-0.06
	d^3	-57.68193	3.75	
DZVP	sd^2	-848.98009	3.75	0.54
	d^3	-848.99986	3.75	
DZVP2	sd^2	-848.98681	3.75	0.38
	d^3	-849.00070	3.75	
TZVP	sd^2	-849.11515	3.75	0.19
	d^3	-849.12219	3.75	

Inspection of table 1.1 reveals that the B3LYP method describes correctly the above mentioned energy ordering. Thus, for the all-electron basis function sets used in the present research, of which neither accounts for the relativistic effects, the $^4F(3d^3)$ state should be found to be the ground state, as it is the case, and the $^4F(3d^24s^1)$ the first excited state. But, for the SKBJ(d) effective core potential, which does account for the relativistic effects, the $^4F(3d^24s^1)$ is predicted to be ground state. Nevertheless, it is particularly worth noting that for the all-electron basis functions, the relative energy difference is overestimated with respect to the experimental energy corrected for the relativistic effects. The best relative energy is obtained at the B3LYP/TZVP level of theory, $\Delta_{sd} = 0.19$ eV, which is to be compared with the relativistic corrected

experimental energy of 0.07eV. However, for the ECP's the relative energy difference is only slightly underestimated. Indeed we predict a difference of 0.06 eV, while the experimental value is 0.1 eV. This raises again the question of the legitimacy of employing effective core potentials derived from atomic HF calculations in approximate DFT methods. A question which has been addressed recently, and given an empirical justification[69, 87].

Table 1.2. *Total(E), in a.u., and relative energy (Δ_{sd}), in eV, for the sd^2 and d^3 electronic configurations of $Ti^+(^4F)$ calculated at MCSCF(3/6) level with various basis sets and ECPs.*

	Electronic Configuration	E	Δ_{sd}
SKBJC(d)	sd^2	-57.25419	-0.24
	d^3	-57.24549	
DZVP	sd^2	-848.02548	-0.23
	d^3	-848.01714	
DZVP2	sd^2	-848.02904	-0.30
	d^3	-848.01807	
TZVP	sd^2	-848.18782	-0.46
	d^3	-848.17087	

Table 1.3. *Total(E) in a.u., and relative energy (Δ_{sd}), in eV, for the sd^2 and d^3 electronic configurations of $Ti^+(^4F)$ calculated at CCSD(T) level with various basis sets and ECPs.*

	Electronic Configuration	E	Δ_{sd}
SKBJC(d)	sd^2	-57.44871	-0.72
	d^3	-57.42224	
DZVP	sd^2	-848.02363	-0.19
	d^3	-848.01670	
DZVP2	sd^2	-848.02780	-0.26
	d^3	-848.01831	
TZVP	sd^2	-848.19397	-0.21
	d^3	-848.18645	

Results obtained with the MCSCF and CCSD(T) methods, collected in Tables 1.2 and 1.3 respectively, deserve also a short comment. It is observed that both, irrespective of whether effective core potentials or all-electron basis sets are used, predict a $^4F(3d^24s^1)$ ground state, with the $^4F(3d^3)$ state lying more than 0.2 eV above. While this energy ordering is qualitatively correct for the ECP's, it should be regarded as incorrect for the all-electron basis, for

which the ${}^4F(3d^3)$ should be the lowest energy state, as stated above. Notice, also, that the qualitatively correct energy level ordering prediction obtained with the ECP's, is unsatisfactory from a quantitative point of view, since the experimental energy difference is 0.1 eV while the MCSCF theory predicts 0.24 eV and the CCSD(T) theory 0.72 eV.

Table 1.4. MCSCF(3/6) optimized relevant geometric data for the 4B_2 state of the $Ti(OH_2)^+$ ion-molecule complex with various basis sets. Distances are in Angstroms and angles in degrees.

Basis set	R(Ti-O)	r(O-H)	<TiOH
SKBJC(d)	2.200	0.968	127.0
SKBJC(d,p)	2.194	0.963	126.8
SKBJC(d,2p)	2.196	0.962	126.4
DZVP	2.178	0.951	126.4
DZVP2	2.185	0.950	126.6
TZVP	2.196	0.951	126.6

Table 1.5. B3LYP and BLYP approximate density functional theory optimized geometries for the corresponding 4B_1 and 4B_2 states of the $Ti(OH_2)^+$ ion-molecule complex with various basis sets. Distances in Å and angles in degrees.

Basis set	BLYP			B3LYP		
	R(Ti-O)	r(O-H)	<TiOH	R(Ti-O)	r(O-H)	<TiOH
SKBJ(d)	2.107	0.999	127.0	2.109	0.989	127.0
SKBJ(d,p)	2.104	0.995	126.9	2.107	0.985	126.9
SKBJ(d,2p)	2.097	0.996	126.8	2.108	0.985	127.0
DZVP	2.107	0.984	126.4	2.103	0.973	126.6
DZVP2	2.105	0.985	126.4	2.099	0.974	126.6
TZVP	2.115	0.971	126.4	2.106	0.982	126.2

1.3.2 $Ti(OH_2)^+$

Tables 1.4, 1.5 and 1.6 show the optimized geometry of the $Ti(OH_2)^+$ ion-molecule complex at various levels of theory. Data is given only for the 4B_2 state, however it is worth of noting that a 4B_1 state, nearly degenerate in energy, and with a nearly coincident optimum geometry, has also been found in every case. Inspection of the data of Tables 1.4, 1.5 and 1.6 reveals that both, the approximate density functionals BLYP and the hybrid procedure B3LYP yield a shorter $Ti-O$ bond length than the MCSCF(3/6) method, for the basis set investigated. This is a tendency reported recently for hydrogen bonded

complexes[88] and for charge-transfer complexes[89]. However, for our ion-molecule complex the discrepancies between the approximate density functional and molecular orbital theories are not as severe as those found for the above mentioned systems. On the other hand, the Coupler Cluster (CCD) theory $Ti-O$ and $O-H$ optimized distances lie in between MCSCF and DFT values, as shown in Table 1.6. The largest discrepancy with the ECPs is found for the SKBJC(d), for which the B3LYP method renders a $Ti-O$ bond length 0.091 Å shorter, with respect to the MCSCF(3/6) method. Nevertheless, it should be pointed out that the $O-H$ bond is predicted to be ~ 0.035 Å larger by both of the DFT based methods used in the present chapter. The agreement found for the $TiOH$ bond angle for all the methods, is also remarkable, see column 4 of Tables 1.4 and 1.6 and columns 4 and 7 of Table 1.5.

Table 1.6. CCD optimized relevant geometric data for the 4B_1 state of the $Ti(OH_2)^+$ ion-molecule complex with various basis sets. Distances are in Angstroms and angles in degrees.

Basis set	R(Ti-O)	r(O-H)	<TiOH
SKBJC(d)	2.149	0.993	127.3
SKBJC(d,p)	2.148	0.984	127.2
SKBJC(d,2p)	2.150	0.982	127.4
DZVP	2.173	0.970	127.0
DZVP2	2.177	0.970	127.2
TZVP	2.166	0.968	125.6

In summary the MCSCF(3/6) method predicts a bond length close to 2.2 Å for the $Ti(OH_2)^+$ ion-molecule complex, the CCD theory prediction lies in the range between 2.18 Å and 2.15 Å, depending on the basis set used, and both of the DFT based methods used, predict it to be around 2.1 Å, irrespective of whether an all-electron basis function set or an effective core potential is used.

1.3.3 Dissociation Energies

Table 1.7 shows the electronic energies, zero point vibrational energy corrections, basis set superposition error energy corrections and the dissociation energies of the $Ti(OH_2)^+$, calculated at various levels of theory. In every case, the dissociation energy has been calculated as the energy difference between the 4B_2 state of the $Ti(OH_2)^+$ and the most stable electronic configuration of the 4F state of the Ti^+ plus the energy of one water molecule. In addition, both the zero point vibrational energy correction and the basis set superposition error energy correction have been taken into account.

Inspection of Table 1.7 reveals that both approximate density functional based methods, BLYP and B3LYP, overestimate slightly the dissociation energy of the 4B_2 state of $Ti(OH_2)^+$, with respect to the best experimental value

of 36.9 kcal/mol. The best value obtained using DFT with ECP's has been achieved at the B3LYP/SKBJC(d,2p) level of theory, i.e.: 37.9 kcal/mol, only 1 kcal/mol higher than experiment. However, it should be mentioned that provision of the basis set superposition energy error must be taken into account, in order to arrive at such good estimate, for it can as large as 2.3 kcal/mol. When all-electron basis sets are used with our approximate DFT methods, the BSSE error appears to be smaller than for ECP's, and the dissociation energies get even closer to the experimental value. Remarkably, at the B3LYP/TZVP level of theory we obtain $D_0 = 36.7$ kcal/mol, only 0.2 kcal/mol below the experimental result. Notice that for the all electron basis set, both the BLYP and B3LYP lead to estimates of D_0 within the error bars of the experimental value, namely 36.9 ± 1.4 kcal/mol. In addition, the B3LYP method fits also the estimate for D_0 , with the SKBJC(d,2p) within the error bars. These data contribute to the mounting evidence that B3LYP performs reliably also for open-shell transition metal containing compounds[68, 69, 73].

Table 1.7. Total energies E , in hartree/particle, zero-point vibrational energy corrections $\Delta ZPVE$, in kcal/mol, basis set superposition error corrections BSSE, in kcal/mol, dissociation energies D_0 , in kcal/mol, for the $Ti(OH_2)^+$ ion-molecule complex.

Method		E	$\Delta ZPVE$	BSSE	D_0
BLYP	SKBJC(d)	-74.82757	1.5	2.2	39.6
	SKBJC(d,p)	-74.83640	1.6	2.5	39.5
	SKBJC(d,2p)	-74.83839	1.5	2.9	38.7
	DZVP	-925.50760	1.6	1.2	38.1
	DZVP2	-925.51685	1.6	0.4	37.1
	TZVP	-925.60812	1.7	0.7	36.5
B3LYP	SKBJC(d)	-74.91565	1.6	1.7	38.9
	SKBJC(d,p)	-74.92534	1.6	2.0	38.9
	SKBJC(d,2p)	-74.92722	1.7	2.3	37.9
	DZVP	-925.51190	1.8	0.9	37.3
	DZVP2	-925.52189	1.8	0.4	37.3
	TZVP	-925.62064	1.8	0.8	36.7
MCSCF(3/6)	SKBJC(d)	-74.15448	1.5	3.7	30.4
	SKBJC(d,p)	-74.16708	1.6	3.7	30.6
	SKBJC(d,2p)	-74.16872	2.2	3.6	29.2
	DZVP	-924.11855	1.8	2.7	30.0
	DZVP2	-924.12735	1.8	2.3	28.2
	TZVP	-924.27208	1.8	1.8	29.7
CCSD(T)	SKBJC(d)	-74.53349	1.6	3.7	31.6
	SKBJC(d,p)	-74.55629	1.3	3.6	31.5
	SKBJC(d,2p)	-74.56032	1.4	3.5	30.2
	DZVP	-924.32465	1.6	1.9	33.4
	DZVP2	-924.32823	1.5	2.1	31.2
	TZVP	-924.49505	1.5	1.0	32.9

On the other hand, both molecular orbital theory methods, MCSCF(3/6) and CCSD(T), with ECP's severely underestimate the dissociation energy of the title compound by 7.7 and 6.7 kcal/mol, at the MCSCF(3/6)/SKBJC(d,2p) and CCSD(T)/SKBJC(d,2p) levels of theory respectively. Using all-electron basis sets, instead of ECP's, does not remedy the apparent weakness of the method, although it improves the estimation. Notice that at the MCSCF(3/6)/TZVP the dissociation energy is still underestimated by 7.2 kcal/mol, and by 4.0 kcal/mol at the CCSD(T)/TZVP level of theory. This is suggestive of the slower convergence of the CCSD(T) method with the basis set, with respect to B3LYP. Hence, in the small basis sets used in this work, it yields poorer agreement with experiment. However this might not be so in the complete basis set. It is worth of pointed out that both the MCSCF and CCSD(T) calculations are affected by a noticeable large BSSE error of 3.6 kcal/mol, when ECP's are used[64].

Finally our calculations highlight one more interesting point. Namely, the approximate $\Delta ZPVE$ value of 1.7 kcal/mol, used by Bauschlicher *et al.*[64] for the first transition-row metal positive water clusters is well justified, even for approximate density functional based methods.

1.4 Conclusions

Our calculations show that the approximate DFT functionals BLYP and B3LYP, with both double zeta quality all electron basis sets, and effective core potentials, correctly predict the energy ordering of the two electronic configurations associated with the ground 4F state of Ti^+ . However, the calculated relative energies are overestimated with respect to their corresponding experimental values, for every all-electron basis set used in the present study. On the other hand for the Stevens *et al.* SKBJC(d) effective core potentials a good estimate, only 0.04 eV smaller, of true experimental interconfigurational energy is obtained. Noticeably, both the MCSCF and CCSD(T) method perform more poorly than the B3LYP procedure, yielding only a qualitative correct estimate for Δ_{ad} with the SKBJC(d) effective core potential. All-electron basis sets do not succeed even to predict the expected energy level ordering.

Optimum molecular geometries of the 4B_2 state of the $Ti(OH_2)^+$ ion-molecule complex do not depend appreciably of the basis sets used, but they do depend on the method. Thus, the MCSCF method leads the largest $Ti-O$ optimum bond distances, namely 2.2Å, DFT yields the shortest, around 2.1Å and CCSD(T) predicts it in between, close to 2.15Å.

Finally, the dissociation energy of the $Ti(OH_2)^+$ (4B_2), is best reproduced at the B3LYP/TZVP level of theory, and good reasonable estimates are obtained with at both the BLYP/SKBJC(d,2p) and B3LYP/SKBJC(d,2p) levels of theory. On the other hand both molecular orbital theory methods, MCSCF and CCSD(T), severely underestimate the dissociation energy.

Therefore, it is concluded that the B3LYP method used in conjunction

with either the SKBJC effective core potentials or triple-zeta quality basis sets represents a feasible computational strategy to deal with the molecular and electronic structures of the first-row transition metal ligand complexes. In particular it should be an efficient and accurate method to help understanding recent experiments[90] on primary reactions of Ti^+ with small molecules in the gas phase.

Chapter 2

The First Mechanism: The Titanium case

The reaction of $Ti^+(^4F, ^2F) + OH_2$ has been studied in detail for both doublet and quartet spin states. The only exothermic products are $TiO^+(^2\Delta)$ and H_2 ; formation of several endothermic products is also examined. An in-depth analysis of the reaction paths leading to each of the observed products is given, including various singlet, triplet and quartet minima, several important transition states, and a discussion of the two H_2 elimination mechanisms proposed in the literature. The experimentally observed spin-forbidden crossing is given a possible explanation. Throughout this work comparison to experimental results in energetics, reaction products, and suggested mechanisms has been central.

2.1 Introduction

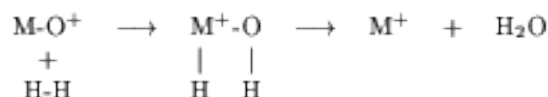
Transition metal cation chemistry has been the subject of many experimental studies in recent years. At the same time, theoretical studies have seen a rapid increase in applicability thanks to improved computational methods and new computational technologies [31]. These developments in both the experimental and theoretical fields provide new opportunities to study quantitatively the reactions, mechanisms, bonding, and structure of complexes incorporating transition metals [91, 92].

Of particular interest among recent works *e.g.* [61, 62, 93, 94, 95, 96] are the results presented by Castleman and co-workers [90] indicating that Ti^+ is very active toward breaking $C-H$, $O-H$, $N-H$ and $C-O$ bonds in small alkene molecules, ammonia, water, and methanol. All the reactions are exothermic bimolecular reactions at thermal energies. For these reactions, the dehydrogenation rate constant is found to be proportional to the bond strength of the $X-H$ bonds. The result can be explained on the basis of dehydrogenation mechanisms. For example:



Here, a H migration from O to Ti occurs in the mechanism, following the initial insertion of Ti^+ into the $O-H$ bond.

More recently Armentrout and co-workers [97] have found, after an exhaustive experimental study, that the early transition metal ions (Sc^+ , Ti^+ and V^+) are more reactive than their oxides, while the contrary occurs with the late metals (Cr^+ , Mn^+ and Fe^+). The energetics measured for these reactions correspond to production of M^+ primarily in an excited low-spin electronic state; formation of ground-state M^+ is also observed, even though this reaction channel does not conserve spin. Their proposed mechanism that appears to be consistent with all their experimental and molecular orbital considerations is:



where the intermediate HM^+OH moiety conserves spin with the $MO^+ + H_2$ reactants and the low-spin $M^+ + H_2O$ products, but not the ground-state $M^+ + H_2O$ products.

Their data for the titanium and vanadium systems are dominated by production of excited low-spin $Ti^+(^2F)$ and $V^+(^3F)$ states. Their estimated potential energy surface, based on their results and theoretical predictions of Tilson and Harrison [98], shows for Sc^+ a crossing of the triplet and singlet surfaces, probably occurring in the region between HSc^+OH and $Sc(OH_2)^+$. Similar crossing should also exist in the titanium and vanadium systems, and thus the inefficiency of forming the ground-state metal ions in these systems

can be explained by the need to undergo a spin-forbidden surface crossing. The $MO^+ + D_2 \rightarrow M^+ + D_2O$ reaction channel is the first bimolecular, transition metal reaction to their knowledge that shows convincing evidence that excited-state products can be formed preferentially over ground-state products. The overriding constraint in these systems is conservation of spin rather than overall reaction energetics [97].

Finally Armentrout and co-workers [99] studied the reverse of the above mentioned reactions. They found that the a^2F state of Ti^+ reacts much more efficiently than the a^4F ground state in forming the MD^+ , MO^+ and MOD^+ product ions. All evidence is consistent with the hypothesis that the reactions occur primarily through a low-spin state of a DM^+OD intermediate. Furthermore, they suggest that this species is likely to eliminate H_2 through a four-centered transition state. This is in contrast with the mechanism proposed by Castleman and co-workers [90], in which the initial step of Ti^+ insertion into the $O-H$ bond to form HTi^+OH is followed by hydrogen migration to form H_2TiO^+ , which then loses H_2 to form TiO^+ .

The data provided and questions raised by these experimental works provide an excellent point of departure for theoretical investigation. In Chapter 1 we have discussed the preliminary work done in our group determining the dissociation energies of the $Ti(OH_2)^+$ ion-molecule complex comparing MCSCF, CCSD(T) and DFT methods[100]. This present work is the first theoretical investigation of the possible mechanisms of bond activation and dissociation involved in the $Ti(OH_2)^+$ system. We report full reaction mechanism geometries and energetics for both the doublet and quartet spin states for numerous possible reactions of Ti^+ with H_2O .

2.2 Methods

The computational method used for optimization and frequency calculations was Density Functional Theory (B3LYP functional) [57, 58] with the DZVP basis sets given by Salahub *et al.*[76, 77] because of the good results obtained in Chapter 1[100]. The choice of the B3LYP DFT method is largely motivated by its satisfactory performance reported recently [31, 68, 73] for transition metal containing systems. Some of the more relevant structures have been reoptimized at the B3LYP/LanL2DZ level to see how the triple zeta treatment of the $3d$ electrons influences geometries and energies. Reactants and products of the possible reactions have been reoptimized both at the B3LYP/6-311+G(2d,2p) and B3LYP/TZVP+G(3df,2p) for the system. All the calculations have been corrected with the ZPVE calculated at the corresponding theoretical level. The triple zeta quality basis set, TZVP+G(3df,2p), used for titanium was that given by Schäfer, Hubert and Ahlrichs [78], supplemented with a diffuse s function (with an exponent 0.33 times that of the most diffuse s function on the original set), two sets of p functions optimized by Wachters [79] for the excited states, one set of diffuse pure angular momentum d function (optimized by

Hay) [80], and three sets of uncontracted pure angular momentum f functions, including both tight and diffuse exponents, as recommended by Ragavachari and Trucks[101]. For the oxygen and hydrogen atoms the 6-311++G(2df,2p) basis set of Pople *et al.*[81] was used.

In order to give very accurate energies for the energy differences between the different spin states of each species, CASPT2 calculations have been carried out[51, 52]. In the CASPT2 calculations the Wachters primitive basis for titanium[79] was extended by adding two sets of p -functions in the $4p$ region, one $5d$ set of diffuse d -functions, and three $7f$ sets of f -functions, yielding a (14s, 11p, 6d, 3f) primitive basis. This was contracted to a [6s, 5p, 3d, 1f] basis as explained in ref. [102]. For oxygen the primitive (9s, 5p) basis of Huzinaga [103] was used, contracted to [3s, 2p] plus one set of pure angular momentum d functions. For hydrogen the primitive (5s) augmented with one set of p functions and contracted to [3s, 1p] was used. The active spaces used for the CASPT2 calculations are given in Table 1.1. The criteria used to choose this active spaces is the "chemically reasonable" one [104]. That is, all MOs taking part in forming and breaking bonds were included in the active space.

Table 2.1. Active Spaces Used for Multireference Calculations.

System	Orbitals included	Size [†]
Ti^+	$b_1(d_{xz})b_2(d_{yz})a_2(d_{xy})a_1(d_{xz-yy})a_1(d_{2xz-zx-yy})a_1(s)$	(3/6)
H_2O	$\sigma(O-H, bond)\sigma^*(O-H, antibond)$	(4/4)
$TiOH_2^+$	$\sigma(O-H, bond)\sigma^*(O-H, antibond)$	(4/4) + Ti^+ (3/6)
$TiO^+(^4B_1)$	(Ti-O, bond)(Ti-O, antibond)8a ₁ 9a ₁ 4b ₁ 3b ₂ 4b ₂ 1a ₂	(7/10)
$TiO^+(^2A_2)$	2(Ti-O, bond)2(Ti-O, antibond)8a ₁ 9a ₁ 4b ₁ 1a ₂	(5/8)
H_2	$\sigma_g\sigma_u^*$	(2/2)
$TiOH^+$	(Ti-O, bond)(O-H, bond)	(6/9)
	(Ti-O, antibond)(O-H, antibond)4a [*] 5a [*] 10a [*] 11a [*]	(6/9)
$HTiO^+$	2(Ti-O, bond)(Ti-H, bond)	(6/9)
	2(Ti-O, antibond)(Ti-H, antibond)4a [*] 5a [*] 10a [*]	(6/9)

[†] The notation (m/n) denotes an active space of m electrons in n orbitals.

All DFT calculations reported in this chapter have been carried out with the GAUSSIAN94/DFT [71] suites of programs, and the CASPT2 calculations were carried out with the MOLCAS program[105]. Also NBO [106, 107] calculations have been done to clarify some structures and MOLDEN [108] was used to draw MO pictures.

2.3 Results and Discussion

Our discussion will focus first on the $Ti(OH_2)^+$ dissociation energy, then the quartet→doublet splitting for several relevant species. Following these are total

energies for the experimentally observed reactions, and this report finishes with a detailed analysis of the PES.

2.3.1 $\text{Ti}(\text{OH}_2)^+$ Dissociation Energy

Dissociation energies of the $\text{Ti}(\text{OH}_2)^+$ ion-molecule have been calculated with new levels of theory and compared with the ones calculated in Chapter 1 [100] in order to test the quality of these methods in describing these reactions. Dissociation energies were calculated as the difference between the energy of the isolated monomers and the complex, including both BSSE and ZPVE corrections.

$\text{Ti}(\text{OH}_2)^+$ dissociation energies predicted by various levels of theory [64] and those experimentally observed [61, 62] are given in Table 2.2. The $\Delta ZPVE$ for the multireference methods were taken as the average of all other results reported for this system [100]. It can be seen that a slightly higher D_0 is predicted by the B3LYP/LanL2DZ than for the B3LYP/DZVP theory level, although the results obtained with Los Alamos effective core potentials are similar to the ones obtained previously with the SKBJC effective core potentials [100].

The predictions of the CASPT2 method demonstrate the importance of properly including dynamic/non-dynamic correlation in order to obtain a good description of the system. When the $1s$ through $3p$ orbitals of the titanium and the $1s$ orbital of oxygen are not correlated (10 frozen core orbitals), the dissociation energy obtained is clearly underestimated. This shortcoming is quickly resolved through reducing the frozen core to include only the $1s2s2p$ orbitals of Ti and the $1s$ orbital of O. Further reduction of the frozen core does not change the predicted dissociation energy.

Table 2.2. Total energies (E), in hartree, zero-point vibrational energy corrections ($\Delta ZPVE$), basis set superposition error corrections (BSSE), and dissociation energies (D_0) in eV, for the $\text{Ti}(\text{OH}_2)^+$ ion-molecule complex.

Method		E	$\Delta ZPVE$	BSSE	D_0
B3LYP	DZVP	-925.51190	0.078	0.039	1.619
	LanL2DZ	-134.22460	0.078	0.148	1.684
	TZVP+G(3df,2p)	-925.64949	0.074	0.022	1.573
CASPT2(7/10)[11]*	Wachters	-924.51653	0.069	0.178	1.536
CASPT2(7/10)[6]*	*	-924.73265	0.069	0.221	1.654
CASPT2(7/10)[0]*	*	-924.74928	0.069	0.230	1.654
Experimental [61]					1.65±0.13
Experimental [62]					1.60±0.06
Theoretical [64]					1.626

For the CASPT2 results the numbers in parenthesis (m/n) indicates the size of the active space (m electrons in n orbitals), and in square brackets are the number of frozen core orbitals.

2.3.2 Excitation Energy

In the reactions of interest there are three quartet-doublet relative energies that are exceptionally important, thus we describe them more exhaustively. These three are the Ti^+ , $Ti(OH_2)^+$, and TiO^+ moieties. Excitation energies for these systems are shown in Table 2.3.

Table 2.3. Relative energies in eV for the $^4F(sd^2)$ and $^2F(sd^2)$ states of Ti^+ (Δ_1), the 4B_1 and 2B_2 states of $Ti(OH_2)^+$ (Δ_2), and the $^4\Delta$ and $^2\Delta$ states of TiO^+ (Δ_3).

Method	Δ_1	Δ_2	Δ_3
B3LYP/DZVP	0.599	0.593	-3.045
B3LYP/LanL2DZ	0.647	0.510	-2.991
B3LYP/TZVP+G(3df,2p)	0.545	0.488	-3.111
CASPT2[9,10]/Wachters	0.507	0.850	-3.450
CASPT2[5,6]/Wachters	0.596	1.023	-3.517
CASPT2[0,0]/Wachters	0.597	1.117	-3.524
Experimental [99, 85]	0.574	0.565 ^a	-3.5 ^a

^a estimated

In square brackets the total number of frozen orbitals are shown, the first number corresponds to the Ti^+ and the second one to $Ti(OH_2)^+$ and TiO^+ moieties. The CAS active space used for each calculation can be found in Table 2.1.

It is known that DFT calculations can describe properly ground states even for transition metal systems, and also that this method gives good results for some excited state calculations [31, 68, 73]. For the Ti^+ system, for example, the doublet state is a three electron doublet state, which can be formed through various orbital occupations. Thus it is difficult to describe properly with single-determinant methods. However, the results obtained with the B3LYP method are reasonably close to other theoretical predictions as well as experimental observations.

The CASPT2 calculation results are even closer in agreement with the experimental value for the $Ti^+ \ ^4F \rightarrow \ ^2F$ excitation energy. Note that again, when the $1s - 3p$ orbitals of Ti are frozen an underestimation of the energy is observed but the results obtained from the freezing of the $1s$ through $2p$ orbitals are equivalent with the non-frozen core results.

Quartet \rightarrow Doublet excitation energies for the $Ti(OH_2)^+$ ion-molecule also have been calculated at numerous levels of theory. Armentrout and co-workers [99] assumed this energy difference to be the same as for the Ti^+ cation. At the B3LYP level, with both basis sets used, the energy difference found is lower than the predicted $Ti^+ \ ^4F \rightarrow \ ^2F$ energy gap. However, this energy difference predicted by the various CASPT2 levels is approximately twice that predicted by the B3LYP method.

The last system studied at these levels was the TiO^+ molecule. Here the doublet is the ground state. Armentrout and co-workers [99] estimated that the high-spin states of TiO^+ lie above the low-spin ground state by about 3.5eV. The CASPT2 predictions are in good agreement with their estimations and the B3LYP numbers are only slightly lower.

2.3.3 Reaction Energetics

Five reactions leading to the experimentally observed product ions have been studied for this system:

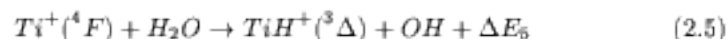
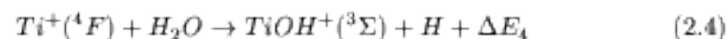
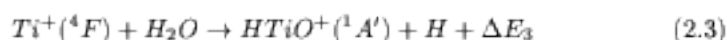
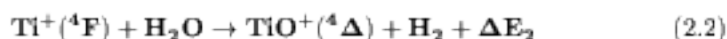
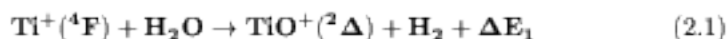


Table 2.4. Overall energies for reactions (2.1)-(2.5) at several levels of theory. Energies given are in eV and for the various B3LYP levels of theory include ZPVE corrections calculated at the corresponding level of theory.

Method	ΔE_1	ΔE_2	ΔE_3	ΔE_4	ΔE_5
B3LYP/DZVP	1.365	-1.680	-1.661	-0.470	-2.739
B3LYP/LanL2DZ	1.642	-1.349	-1.470	-0.200	-
B3LYP/6-311+G(2d,2p)	1.536	-1.573	-1.306	-0.341	-
B3LYP/TZVP+G(3df,2p)	1.543	-1.568	-1.293	-0.321	-2.632
CASPT2[9,10]	1.308	-2.142	-1.572	-0.676	-
CASPT2[5,6]	1.314	-2.203	-1.434	-0.669	-
CASPT2[0]	1.315	-2.209	-1.420	-0.664	-
Exp. [99]	1.77±0.06	-1.73 ^a	-	-0.39±0.12	-2.74±0.09

^a estimated

Equations (2.1)-(2.5) represent the main ionic products observed in the reaction of Ti^+ (4F) and H_2O . The energetics of these reactions have been calculated with the B3LYP and CASPT2 methods, and here larger basis sets also have been used with the B3LYP method. The various predicted values and the energies given by Armentrout and co-workers [99] are listed in Table 2.4.

In some of these energetics we see very large discrepancies between the B3LYP predictions resulting from the use of different basis sets. In each case the difference between the B3LYP/DZVP result and the B3LYP/LanL2DZ result is startling. However, some consistency is seen with the larger 6-311+G(2d,2p) and TZVP+G(3df,2p) basis sets. This consistency and the reasonable agreement with experimental [99] results implies that the B3LYP/TZVP+G(3df,2p) level of theory provides results worthy of a high level of confidence.

In agreement with experiment, we find only one exothermic reaction, the formation of low-spin $TiO^+ + H_2$ (Reaction 2.1). Our best value of 1.543eV is 0.23eV below the experimentally observed energy. Considering that a spin-crossing is involved in this reaction, our energy predictions are good, but not entirely satisfactory. The result, -0.321eV, obtained for the low-lying endothermic reaction leading to $TiOH^+ + H$, Reaction 2.4, is within the error bars of the experimental result, $-0.39 \pm 0.12eV$. The experimental value for Reaction 2.2 (-1.73eV) is based on an estimated doublet→quartet splitting of 3.5eV [99] and is not radically different from our calculated -1.568eV.

2.3.4 The Doublet Stationary Points

The various B3LYP/DZVP doublet stationary points are depicted in Figure 2.1. The C_{2v} symmetry $Ti(OH_2)^+$ ion-molecule complex has a $Ti-O$ distance of 2.104Å and a $Ti-O$ stretching frequency of $401cm^{-1}$. As seen in the dissociation energies section, this interaction is rather strong. However, the OH_2 moiety itself is only slightly changed from its unassociated parameters. In comparison to free H_2O described by the same level of theory, the $O-H$ bond length in this complex is 0.008Å longer and the symmetric stretching and $H-O-H$ bending frequencies change by -93 and 21 cm^{-1} respectively.

TS1 characterizes the first hydrogen transfer from oxygen to titanium. This transition state has C_s symmetry and the one imaginary frequency clearly corresponds to hydrogen transfer.

The HTi^+OH minimum also has C_s symmetry. This intermediate is a well-characterized minimum with a covalent $Ti-H$ bond. The $Ti-H$ stretching frequency is $897cm^{-1}$ and the $H-Ti-O$ bend has a frequency of $482cm^{-1}$. The lowest vibrational frequency of $281cm^{-1}$ corresponds to $Ti-O-H$ bend.

The second oxygen to titanium hydrogen transfer occurs through TS2. In this transition state the $H-H$ distance is still quite long (0.983Å) and the $Ti-O$ distance (1.691Å) is closer to the $HTiOH$ value than that in the following $(H_2)TiO$ species. The one imaginary frequency corresponds to $H-H$ bond formation.

The final doublet stationary point located was the $(H_2)TiO^+$ species. This $(H_2)TiO^+$ structure of C_s symmetry is a curious intermediate. Earlier arguments against H_2 elimination from an H_2TiO^+ structure have considered two covalent $Ti-H$ bonds [90]. The $(H_2)TiO^+$ minimum which exists on the PES has no $Ti-H$ σ bonds *per se*, but should be considered a ion-molecule complex. Note that the $Ti-H$ bond distance has increased from 1.656Å in the

HTi^+OH minimum to 2.115\AA here. Examination of the MOs shows an interaction between the singly occupied d orbital of Ti and the $H-H$ σ^* orbital (see Figure 2.2). NBO analysis gives this interaction a value of 7.87kcal/mol . It is through this interaction that the $H-H$ bond is activated. In comparison with separated $TiO^+(^2\Delta) + H_2$ the $Ti-O$ bond length of this complex is only 0.004\AA longer, while the aforementioned $H-H$ bond activation lengthens the H_2 bond length by 0.02\AA .

Figure 2.1. Geometrical parameters of the various stationary points on the doublet $B3LYP/DZVP$ potential energy surface. Bond lengths are reported in \AA , bond angles in degrees.

Figure 2.2. The singly occupied orbital of the doublet $(H_2)TiO^+$ intermediate as seen looking down the $Ti-O$ axis.

2.3.5 Quartet Stationary Points

Figure 2.3 depicts the various B3LYP/DZVP quartet stationary points. The stationary points found on the quartet surface are in many aspects related to those of the doublet surface. The $Ti(OH_2)^+$ ion-molecule is very similar indeed. The geometrical parameters of both are essentially equal and the vibrational frequencies which vary the greatest are the water wagging frequency which decreases here by $52cm^{-1}$ and the $Ti-O$ stretching frequency which increases by $57cm^{-1}$.

The HTi^+OH species, on the other hand, is quite different on the quartet surface. The $Ti-O$ bond is 0.048\AA longer for the quartet minimum and the $Ti-H$ bond an astounding 0.666\AA longer. This difference is also seen in the $Ti-O$ and $Ti-H$ stretching frequencies which are 101 and $1287cm^{-1}$ lower for the quartet than the doublet species.

The $(H_2)TiO^+$ ion-molecule complex on the quartet surface has a slightly stronger interaction between the H_2 molecule and the TiO^+ unit than that found on the doublet surface. However, as was the case on the doublet surface, this structure should not be considered to have two covalent $Ti-H$ bonds, but rather a $d \rightarrow \sigma^*$ donation. For the quartet species, this interaction is given a value of $9.85kcal/mol$ by NBO analysis.

Figure 2.3. Geometrical parameters of the various stationary points on the quartet B3LYP/DZVP potential energy surface. Bond lengths are reported in \AA , bond angles in degrees.

2.3.6 Potential Energy Surfaces

Figure 2.4 shows the potential energy surface starting from the $Ti^+ + OH_2$ separated reactants and leading to $TiO^+ + H_2$ for the doublet and quartet spin states at the B3LYP/DZVP level of theory.

On the doublet surface, the first step is the formation of the ion-molecule complex. Then, through *TS1*, one hydrogen atom is passed from oxygen to titanium, leading to the HTi^+OH molecule, the intermediate whose existence was surmised by experimentalists.

A second hydrogen transfer from oxygen to titanium passing through *TS2* leads to the most stable complex encountered on the surface, $(H_2)TiO^+$. From this intermediate the loss of H_2 proceeds without transition state to the observed major products, doublet TiO^+ and H_2 .

The first step on the quartet surface can also be formation of the ion-molecule complex. However, following the reaction from that point is significantly more complicated than was the case for the doublet surface. Despite numerous varied strategies for finding a transition state between this complex and the HTi^+OH molecule, none was found. Here we note that while the quartet $Ti(OH_2)^+$ ion-molecule complex lies below that of the doublet, their relative positions are reversed in the HTi^+OH moieties. Thus, the two surfaces have crossed somewhere between these two points. This explains the experimentally observed "forbidden crossing" and seriously complicates the location of the quartet transition state.

Once this quartet HTi^+OH intermediate is formed possibly from $Ti(OH_2)^+$ rearrangement, possibly from direct Ti^+ insertion into an $O-H$ bond of H_2O , another intermediate, $(H_2)TiO^+$, can be realized by passing through another probably high-lying H transfer transition state. From that isomer, the loss of an H_2 molecule gives one of the scarcely observed reaction products quartet TiO^+ . The high relative energy of this product agrees well with the fact that TiO^+ in this spin state is a rarely observed reaction product.

Figure 2.5 depicts the doublet and quartet B3LYP/DZVP potential energy surfaces for the reactions leading to the other experimentally observed products, $TiOH^+$ and TiH^+ , sequential H atom loss leading to TiO^+ , and the possible reactions leading to $HTiO^+$ and $TiH^+ + OH$. Energies given (in eV) are relative to $Ti(^4F) + H_2O$ (as was the case in Figure 2.4).

The doublet process begins with the formation of the $Ti(OH_2)^+$ ion-molecule, and passes through the H atom transfer transition state, resulting in the HTi^+OH intermediate. This doublet HTi^+OH may lose one of its hydrogen atoms, leading to either the singlet $HTiO^+$ or $TiOH^+$. These two species are relatively close in energy, but as would be expected, the $TiOH^+$ isomer is lower in energy. Note that the energy difference between these two singlet isomers is much smaller than the energy difference between the corresponding triplet isomers.

The quartet surface is, again, more complicated than that of the doublet. Considering the $Ti(OH_2)^+$ ion-molecule complex, it is possible (passing through *TS3*) that one H atom is directly lost from the oxygen, leading to the

Figure 2.4. *B3LYP/DZVP potential energy surface following the $Ti^+ + OH_2 \rightarrow TiO^+ + H_2$ reaction path. Energies given are in eV and relative to the separated ground state reactants, $Ti^+(^4F) + OH_2$. Bond lengths are reported in Å, bond angles in degrees.*

Figure 2.5. *B3LYP/DZVP potential energy surface following the reaction paths leading to the other experimentally observed products. Energies given are in eV and relative to the separated ground state reactants, $Ti^+(^4F) + OH_2$. Bond lengths are reported in \AA , bond angles in degrees.*

triplet $TiOH^+$ species. This molecule also could lose its remaining hydrogen atom through TS4. This pathway leads to eventual formation of doublet TiO^+ , but is very much kinetically disfavored as compared to the pathway in Figure 2.2 because it passes through a very high-lying transition state (TS4).

Considering the quartet HTi^+OH species, it is possible that either of the two H atoms could be lost individually, resulting in the triplet $TiOH^+$, or high-lying $HTiO^+$ triplet. Again, there is the possibility of forming the doublet TiO^+ product from either of these minima through loss of the second hydrogen atom. However, these sequential H loss mechanisms lie very high in energy when compared to the mechanism seen in Figure 2.2.

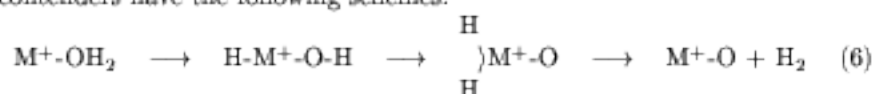
The observed reaction leading to $HTi^+(^3\Delta) + OH$ is also possible from the HTi^+OH quartet intermediate. A simple breaking of the $Ti - O$ bond leads to these energetically high-lying products. A similar process on the doublet surface, leading to singlet $TiH^+ + OH$ is even more energetically disfavoured with a final energy 0.891eV higher than that of triplet $TiH^+ + OH$. Thus it lies outside of the energy range depicted in Figure 2.3.

Equilibrium geometry parameters for the various reaction products are given in Figure 2.6.

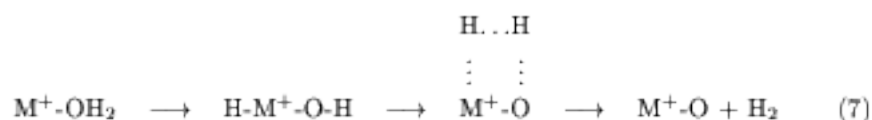
Figure 2.6. Equilibrium geometry parameters for the various reaction products at the $B3LYP/DZVP$ level of theory. In parenthesis are the parameters predicted at the $B3LYP/TZ+G(3df,2p)$ level of theory. Bond lengths are reported in \AA , bond angles in degrees.

2.3.7 The H₂ Elimination Mechanism

There has been much discussion in the literature as to what is the process of H₂ elimination induced by transition metal ions [90, 97, 99]. The two leading contenders have the following schemes:



and



Our theoretical results imply that neither of these is entirely correct, nor are they entirely in error.

Our predictions agree with Mechanism 6 in so much as the hydrogen atoms are last associated with Ti⁺ before elimination. However, a quick examination of the bonding shows that there are not two Ti-H covalent bonds, rather this species should be considered an ion-molecule complex. There is *d* → *σ*^{*} donation which activates the H-H bond, but the H-H bond is intact and no covalent Ti-H bond exists.

Mechanism 7 is incorrect, according to our predictions, *only* in that the four centered transition state is shown leading directly to MO⁺ + H₂. We predict the existence of another intermediate, (H₂)TiO⁺, through which the reaction passes.

In examining the two intermediates, HTi⁺OH and (H₂)TiO⁺, it is seen that the connection between the two *must* be a four-centered transition state. From the HTi⁺OH intermediate a second hydrogen transfer to Ti⁺ does not occur, rather a hydrogen transfer to hydrogen is seen. This process is multifaceted. It involves the breaking of the O-H bond, the forming of the H-H bond, the breaking of one covalent Ti-H bond, and the formation of a Ti-O π bond.

Armentrout and co-workers [97] suggest that for the four-centered transition state TiO_(3π) → H-H(*σ*^{*}) donation is important. This implies a planar four-center transition state. Indeed we find that there is significant interaction between the TiO π system and the H-H bond being formed. Figures 2.7 depicts the *σ*_{H-H} + *π*_{TiO} orbital with large positive overlap for all the atoms. Figure 2.8 illustrates that the *σ*_{H-H} - *π*_{TiO} orbital is stabilized by positive overlap with one lobe of the in-plane *d* orbital on Ti. Figure 2.9 shows the singly occupied orbital of this doublet. The interaction here is *π*_{TiO}^{*} + *σ*_{H-H}^{*}.

Planar transition states for H₂ rotation also were found for both the doublet and quartet (H₂)TiO⁺ species, lying only 0.004 and 0.026eV above their respective minima. We suggest that these low-lying transition states could be

Figure 2.7. *The $\sigma_{H-H} + \pi_{TiO}$ molecular orbital of the doublet four-centered transition state.*

Figure 2.8. *The $\sigma_{H-H} - \pi_{TiO}$ molecular orbital of the doublet four-centered transition state.*

Figure 2.9. *The singly occupied $\pi_{TiO}^* + \sigma_{H-H}^*$ molecular orbital of the doublet four-centered transition state.*

related to the four-centered transition state.

Thus our results support the hypothesis of a four-centered transition state that leads eventually to H_2 elimination. The difference between our predictions and that original hypothesis is that we have found another intermediate $(H_2)TiO^+$ through which the reaction passes.

Another possible reaction path, originally discussed by Irkura and Beauchamp in studying $OsO_x^+(x = 1 - 4) + H_2$ [109] involves direct separation of H_2 from the O atom of the $Ti(OH_2)^+$ structure without any hydrogen transfer to titanium (or in the reverse reaction H_2 attaching directly to the oxygen atom of $Ti - O^+$). Transition states corresponding to the direct loss of a hydrogen molecule from the initial $Ti(OH_2)^+$ ion-molecule on both surfaces were sought. However, the imaginary frequencies of the $Ti - O^+ \cdots H_2$ stationary points located were indicative of sequential H loss, rather than loss of H_2 . Thus, this proposed reaction mechanism is ruled out in this case.

2.4 Conclusions

The reaction of Ti^+ with water has been investigated in detail. Both the doublet and quartet potential energy surfaces have been characterized at the B3LYP/DZVP level of theory. Energy differences between key doublet and quartet species and total reaction energies for the experimentally observed products have been predicted at even higher levels of theory including B3LYP/TZVP+G(3df,2p) and CASPT2/Wachters. From these data, the following conclusions are drawn:

1. The only exothermic products of the $Ti^+(^4F, ^2F) + H_2O$ reaction are $TiO^+(^2\Delta) + H_2$.
2. The HTi^+OH intermediate hypothesized by the experimentalists is a well-defined minimum on each potential energy surface.
3. The doublet and quartet potential energy surfaces cross between this aforementioned intermediate and the $Ti(OH_2)^+$ ion-molecule complex.
4. The much-discussed H_2 elimination process occurs neither from a H_2TiO^+ species with two covalent $Ti - H$ bonds nor directly from a four-centered transition state, but rather passes from the HTi^+OH intermediate through a four-centered transition state to another ion-molecule intermediate $(H_2)TiO^+$, from which intermediate H_2 is eliminated.

Chapter 3

The Early First-Row Transition Metal Cases

The study of the reaction of water with the early first row transition metal ions has been completed in this work, in both high- and low-spin states. In agreement with experimental observations, the only exothermic products are the low lying states $MO^+ + H_2$; formation of other endothermic products is also examined. An in-depth analysis of the reaction paths leading to each of the observed products is given, including various minima, and several important transition states. All results have been compared with existing experimental data, and our earlier work covering the $Ti^+ + H_2O$ reaction in order to observe existent trends for the early first row transition metal ions.

3.1 Introduction

The recent excitement in the study of transition metals is in part due to improved methods of studying, both experimentally and theoretically, the plethora of low-lying electronic states and their effects on reaction properties. The different gas-phase reactivity that transition metals show depending on the spin, electron configuration, and even spin-orbit level has been discussed extensively by Armentrout and co-workers[3, 5, 110]. As they have pointed out in those works, studies of excited electronic states of transition metal ions can help validate the molecular orbital ideas that are used routinely to understand the activation of covalent bonds by transition metals. Thus, such studies are a perfect field for interaction between experiment and theory.

The reactions of transition metal cations and water have received much attention recently in large part due to two curious effects. The first is that the early transition metal cations (Sc^+ , Ti^+ and V^+) are more reactive than their oxides, while the contrary occurs with the late metals (Cr^+ , Mn^+ and Fe^+)[97]. Even more interesting, however, is that the primary product observed in the reverse reaction ($MO^+ + H_2 \rightarrow M^+ + H_2O$) is a low-spin excited state of the cation[97], meaning that spin, rather than reaction energetics, is the overriding constraint of the reaction.

With regards to the importance of spin in these reactions evidence comes from both the forward reaction ($M^+ + H_2O \rightarrow MO^+ + H_2$) and its reverse. In the forward transition metal cation plus water reaction, two factors point to the importance of the spin-state. The first is that if ground-state high-spin cations are used for the reaction, the observed MO^+ product is, nevertheless in its low-spin ground state. Of course, if an excited-state low-spin cation is used the MO^+ product will also be in its ground state. However, the grand difference between using high-spin or low-spin cations as reactants is not the final product but rather the efficiency of the reaction. While the high-spin cations do react to give low-spin MO^+ products, the efficiency is actually quite low. On the other hand, the reaction starting with a low-spin cation proceeds rapidly and efficiently[93, 99].

There is also a point of difference between Sc^+ , Ti^+ , and V^+ that is rather interesting. The ground-state high-spin cations of Sc^+ and Ti^+ do produce (though inefficiently) low-spin MO^+ . However, the ground state $V^+(^5D(d^4))$ cation *does not* make the spin crossing to produce triplet VO^+ . The first quintet excited state of $V^+(^5F(sd^3))$, on the other hand, follows the trend established by the high-spin Sc^+ and Ti^+ cations, *i.e.* production of low-spin MO^+ , though be it inefficiently. Of question is whether this is due to the occupation scheme (both high-spin ground state Sc^+ and Ti^+ have a singly occupied s orbital) or due simply to the extra kick of energy available in the 5F state. We address this question in the discussion of the potential energy surfaces.

From the experimental data we gather that the reaction pathway is a low-spin pathway and that somewhere along the line the high-spin complex must

undergo a spin-forbidden crossing. The reaction pathway demonstrated in our earlier work is: $Ti^+ + H_2O \rightarrow Ti^+ - OH_2 \rightarrow HTi^+OH \rightarrow (H_2) - TiO^+ \rightarrow TiO^+ + H_2$. In the $Ti^+ - OH_2$ ion-molecule complex the high-spin state still lies below the low-spin state, but in the HTi^+OH intermediate that situation is reversed implying that the high- and low-spin surfaces cross between these two moieties.

Another topic of interest concerning these reactions is the process of H_2 elimination (or addition in the reverse reaction). Two possibilities were proposed: elimination from an H_2MO^+ intermediate[90], or elimination from a four-centered transition state[93, 99]. Our earlier work[112] on the high- and low-spin $Ti^+ + H_2O$ reaction does predict a final intermediate before H_2 elimination in which the H atoms are most closely associated with the Ti atom. However, *no* $H - Ti$ covalent σ bonds existed. Instead the intermediate immediately preceding H_2 elimination could be viewed as an ion-molecule complex with some donation of electron density from the $H - H$ σ bond to the Ti atom and some back donation from a Ti d orbital to the $H - H$ σ^* orbital.

Multiconfiguration self-consistent-field (MCSCF) and configuration interaction (MCSCF+1+2) calculations [98] have been already done for some of the products of the reaction $Sc^+(^3D) + H_2O$. Also, a MP4(SDTQ)**//MP2/6-31G** study of the dehydrogenation reaction of water by Sc^+ has recently appeared in the literature[111]. No previous theoretical works have appeared on the vanadium system. We present the full reaction mechanism geometries and energetics for both the high and low-spin states, considering the possible transition states.

3.2 Methods

The experience of this group [100, 112] shows that the Density Functional Theory (B3LYP functional) [57, 58] with the DZVP basis sets given by Salahub *et al.*[76, 77] is a reasonable choice for optimization and frequency calculations of these systems. Recent calibration calculations on transition metal compounds affirms this choice[113]. The choice of the B3LYP DFT method is largely motivated by its satisfactory performance reported recently [31, 68, 113, 114, 73, 115, 116] for transition metal containing systems. Reactants and products of the possible reactions have been reoptimized at the B3LYP/TZVP+G(3df,2p) level of theory. All the calculations have been corrected with the ZPVE calculated at the corresponding theoretical level.

In order to confirm the B3LYP results, some single point CCSD(T)/TZVP+G(3df,2p) calculations have been carried out at the B3LYP/TZVP+G(3df,2p) equilibrium geometries. The $1s$ electrons of O and $1s$ to $2p$ electrons of the metals were frozen in the CCSD(T) calculations. This CCSD(T)/TZVP+G(3df,2p)//B3LYP/TZVP+G(3df,2p) method will be named as CCSD(T)//B3LYP.

The triple zeta quality basis set, TZVP+G(3df,2p), used for titanium was that given by Schäfer, Hubert and Ahlrichs [78], supplemented with a diffuse s

function (with an exponent 0.33 times that of the most diffuse s function on the original set), two sets of p functions optimized by Wachters [79] for the excited states, one set of diffuse pure angular momentum d function (optimized by Hay) [80], and three sets of uncontracted pure angular momentum f functions, including both tight and diffuse exponents, as recommended by Ragavachari and Trucks[101]. For the oxygen and hydrogen atoms the 6-311++G(2df,2p) basis set of Pople *et al.*[81] was used.

All DFT and CCSD(T) calculations reported in this chapter have been carried out with the GAUSSIAN94/DFT [71] suites of programs. Also NBO [106, 107] calculations have been done to give additional insight into the bonding properties of some structures.

3.3 Results and Discussion

3.3.1 Dissociation Energies

Dissociation energies of the $Sc(OH_2)^+$ and $V(OH_2)^+$ ion-molecules calculated at the B3LYP/DZVP, B3LYP/TZVP+G(3df,2p) and CCSD(T)//B3LYP levels of theory are shown in Table 3.1. Results for the $Ti(OH_2)^+$ ion-molecule at the same levels of theory [100, 112] are shown also. Dissociation energies were calculated as the difference between the energy of the isolated monomers and the complex, including both BSSE and ZPVE corrections. $M(OH_2)^+$ dissociation energies predicted by various levels of theory [64, 98, 111] and those experimentally observed [61, 62, 117] are given also in Table 3.1. Note that the temperature of references [61] and [117] works is not specified.

Good values are obtained with both the B3LYP and CCSD(T) methods when used in conjunction with the TZVP+G(3df,2p) basis set, as was expected from our experience with the Ti calculations. The difference found between the B3LYP/DZVP and B3LYP/TZVP+G(3df,2p) results is around 0.050 eV and both are in reasonable agreement with the experimental and theoretical values that can be found in Table 3.1, especially the more recent and precise data from Armentrout's group. The CCSD(T)//B3LYP values are systematically lower as is usual for dissociation energies. Test works with the DZVP basis set have shown that the use of a larger basis set is essential with the CCSD(T) method as CCSD(T)/DZVP dissociation energies were drastically smaller. The MP4(SDTQ)**//MP2/6-31G** values[111] are clearly too large implying that this is not a good method for treating this system, as has been proven by other authors[68].

3.3.2 Excitation Energy

In the reactions of interest there are three high-low spin relative energies that are exceptionally important, thus we describe them more exhaustively. These three are the M^+ , $M(OH_2)^+$, and MO^+ moieties. Excitation energies for these systems are shown in Table 3.2 ($M = Sc$) and Table 3.3 ($M = V$).

Table 3.1. Total energies (E), in hartree, zero-point vibrational energy corrections ($\Delta ZPVE$), basis set superposition error corrections ($BSSE$), and dissociation energies (D_0) in eV, for the $M(OH_2)^+$ ion-molecule complexes ($M = Sc, Ti, V$).

M	Method	E	$\Delta ZPVE$	BSSE	D_0
Sc	B3LYP/DZVP	-836.79492	0.061	0.056	1.641
	B3LYP/TZVP+G(3df,2p)	-836.91655	0.065	0.018	1.580
	CCSD(T)//B3LYP	-836.18785	0.065	0.068	1.410
	Exp. [61]*				1.36±0.13
	Theo. [64]				1.497
	Theo. [111]				2.500
	Theo. [98]				1.571
Ti	B3LYP/DZVP	-925.51190	0.078	0.039	1.619
	B3LYP/TZVP+G(3df,2p)	-925.64949	0.074	0.022	1.573
	CCSD(T)//B3LYP	-924.87741	0.074	0.073	1.471
	Exp. [61]*				1.65±0.13
	Exp. [62]**				1.60±0.06
	Theo. [64]				1.628
V	B3LYP/DZVP	-1020.03778	0.056	0.039	1.628
	B3LYP/TZVP+G(3df,2p)	-1020.19640	0.065	0.017	1.588
	CCSD(T)//B3LYP	-1019.38614	0.065	0.065	1.406
	Exp. [61]*				1.57±0.13
	Exp. [62]**				1.52±0.05
	Exp. [117]*				1.523±0.174
	Theo. [64]				1.506

* Temperature not specified.

** Values at 0K .

Table 3.2. Relative energies in eV for the $^3D(sd)$ and closed-shell singlet $^1S(s^2)$ states of Sc^+ (Δ_1), the $^3D(sd)$ and open-shell singlet $^1D(sd)$ states of Sc^+ (Δ_2), the 3A_2 and closed-shell singlet 1A_1 states of $Sc(OH_2)^+$ (Δ_3), the 3A_2 and open-shell singlet 1A_1 states of $Sc(OH_2)^+$ (Δ_4), and the $^3\Delta$ and $^1\Sigma$ states of ScO^+ (Δ_5).

Method	Δ_1	Δ_2	Δ_3	Δ_4	Δ_5
B3LYP/DZVP	0.891	0.169	0.713	0.180	-3.081
B3LYP/TZVP+G(3df,2p)	0.916	0.173	0.697	0.211	-3.192
CCSD(T)//B3LYP	0.550	0.154	0.375	0.225	-3.496
Experimental [85, 99]	-	0.32	-	-	-
Theoretical [98]	-	-	-	-	-3.45
Theoretical [111]		0.304	0.543		-5.234 ^a

^a this energy difference corresponds to the $^3\Sigma$ and $^1\Sigma$ states.

Table 3.3. Relative energies in eV for the ${}^5D(d^4)$ and ${}^3F(sd^3)$ states of V^+ (Δ_1), the 5A_1 and 3A_1 states of $V(OH_2)^+$ (Δ_2), and the ${}^5\Sigma$ and ${}^3\Sigma$ states of VO^+ (Δ_3).

Method	Δ_1	Δ_2	Δ_3
B3LYP/DZVP	0.965	0.889	-2.654
B3LYP/TZVP+G(3df,2p)	0.923	0.783	-2.677
CCSD(T)//B3LYP	0.860	0.660	-2.920
Experimental [85, 99]	1.07	0.6 ^a	–
Experimental [118]	–	–	3.3 – 4.2

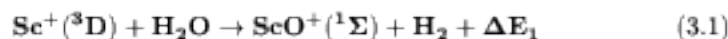
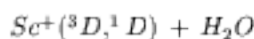
^a estimated

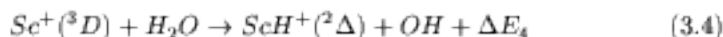
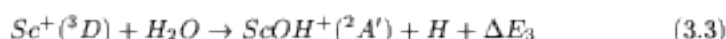
There are two values for singlet-triplet splittings of both Sc^+ and $Sc(OH_2)^+$ given in Table 3.1. Considering first the cationic atom, the larger of the two splittings is the separation between the triplet and the closed-shell singlet and the result in relative agreement with the experimental value (though slightly underestimated) is the separation between the triplet and the open-shell singlet. The V^+ singlet-triplet splittings are also lower than the experimental values given by Moore[85]. However, the ordering of the states is correct and the relative gaps are reasonably well described and these are the important points for a correct understanding of the PESs.

High \rightarrow Low-spin excitation energies for the $M(OH_2)^+$ ion-molecules also have been calculated. The experimental values for these excitation energies are estimations. Thus we compare the theoretical values. In the case of the 3A_2 to (closed-shell) 1A_1 excitation of $Sc(OH_2)^+$, the B3LYP and CCSD(T) predictions using the large basis set lie to either side of the values predicted by Ye [111]. The predictions for the triplet \rightarrow open-shell singlet excitation energy show less variance and are slightly greater than those of the Sc^+ cation. For the vanadium system, the disagreement between the B3LYP and CCSD(T) is less than was seen for the open to closed-shell excitation of the $Sc(OH_2)^+$ complex and the agreement with the experimental estimation is reasonable.

The last system studied at these levels was the MO^+ molecule. Here the low-spin moieties are the ground states as was expected and open-shell low-spin cases need not be considered. Our values agree much better with the estimated experimental values than do Ye's values for ScO^+ . Also we note that the CCSD(T) numbers are closer to the experimental values than are the B3LYP numbers.

3.3.3 Reaction Energetics





Equations (3.1)-(3.4) represent the main ionic products observed in the reaction of $\text{Sc}^+(^3D, ^1D)$ with H_2O . The various predicted values and the energies given by Armentrout and co-workers [99] experimentally, and Tilson and co-workers[98] and Ye[111] theoretically are listed in Table 3.4.

Table 3.4. Overall energies for Reactions (3.1)-(3.4) at several levels of theory. Energies given are in eV and for the various B3LYP levels of theory include ZPVE corrections calculated at the corresponding level of theory.

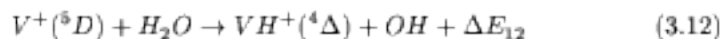
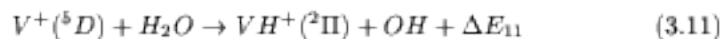
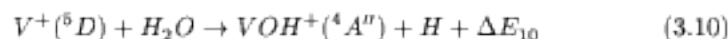
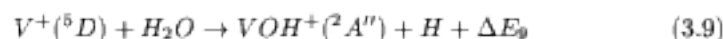
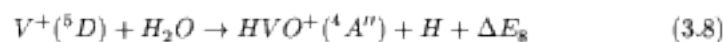
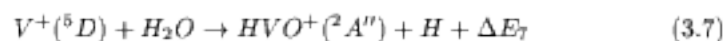
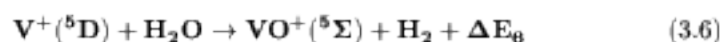
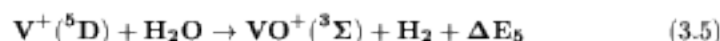
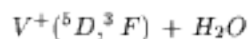
Method	ΔE_1	ΔE_2	ΔE_3	ΔE_4
B3LYP/DZVP	1.689	-1.392	0.084	-2.429
B3LYP/TZVP+G(3df,2p)	1.939	-1.253	0.180	-2.401
CCSD(T)//B3LYP	1.956	-1.518	0.010	-2.665
Exp.[99]	2.03±0.06	-	-0.04±0.009	-2.74±0.09
Exp.[119, 120, 121, 122]	1.866±0.304	-	-	-
Theo.[98]	1.415	-2.035	-0.395	-
Theo.[111]	4.687	-0.547*		

* this energy difference corresponds to the $^3\Sigma$ and $^1\Sigma$ states.

In agreement with experiment, we find only one definitely exothermic reaction, the formation of low-spin $\text{ScO}^+ + \text{H}_2$ (Reaction 3.1). Our best value of 1.956eV is in good agreement with the experimental values listed in Table 3.4, and our even worst value obtained with the B3LYP/DZVP level of theory, 1.689eV, is better than the value given by Tilson. Again it is seen that the Møller-Plesset methods give poor values, 4.687eV in this case. The energies shown for Reaction 2 reflect the already discussed $^3\Delta \rightarrow ^1\Sigma$ ScO^+ excitation energy.

Our results also indicate that the reaction leading to $\text{ScOH}^+(^2A') + \text{H}$ (Reaction 3.3) would be exothermic, but only very slightly so. The experimental result[99] is that this reaction would be very slightly endothermic. While our numbers are on the opposite side of zero from the experimental numbers, the error is still quite small.

The agreement between our results and the experimental value for Reaction 3.4 is also quite good. Thus we see that for each of these reactions our results hold well with the experiments. It should be noted that the CCSD(T)//B3LYP results are especially satisfying.



Equations (3.5)-(3.12) represent the main ionic products observed in the reaction of $V^+(\text{}^5D, \text{}^3F)$ and H_2O . The various predicted values and the energies given by Armentrout and co-workers [93] are listed in Table 3.5. No other theoretical values have been published for this system, as far as we know.

Table 3.5. Overall energies for Reactions (3.5)-(3.12) at several levels of theory. Energies given are in eV and for the various B3LYP levels of theory include ZPVE corrections calculated at the corresponding level of theory.

Method	B3LYP /DZVP	B3LYP /TZVP+G(3df,2p)	CCSD(T) /TZVP+G(3df,2p)	Exp.[93]
ΔE_5	0.569	0.687	0.726	0.88±0.10
ΔE_6	-2.085	-1.990	-2.169	-
ΔE_7	-2.560	-2.229	-2.234	-
ΔE_8	-3.769	-3.559	-3.434	-
ΔE_9	-1.687	-1.540	-1.608	-
ΔE_{10}	-0.878	-0.780	-0.855	-0.71±0.15
ΔE_{11}	-4.548	-4.499	-4.736	-
ΔE_{12}	-2.854	-2.767	-2.945	-3.12±0.06

Our theoretical estimations for the only exothermic reaction, which leads to $VO^+(\text{}^3\Sigma) + H_2$, are below again the value given by Armentrout and co-workers, as was also observed for the Sc and Ti cases.

The other experimental results available are those for Reaction 3.10 and 3.12. For the low-lying endothermic reaction leading to $VOH^+ + H$ (10), both the B3LYP and CCSD(T) methods give values within the experimental errors bars when the triplet zeta basis set is used. The predicted values for Reaction 3.12 are slightly lower than the experimental value, but not far off the mark.

3.3.4 The Stationary Points

The following figures show the most relevant stationary points found for the $M(OH_2)^+$, $TS1^+$, HM^+OH , $TS2^+$ and $(H_2)MO^+$ moieties respectively at the B3LYP/DZVP level of theory, where $M = Sc, V$.

Figure 3.1. Geometrical parameters of the various $M(OH_2)^+$ stationary points on the B3LYP/DZVP potential energy surfaces. Bond lengths are reported in Å, bond angles in degrees.

Figure 3.1 illustrates the $M(OH_2)^+$ ion-molecule complexes. The C_{2v} symmetry $Sc(OH_2)^+$ ion-molecule complex has a $Sc - O$ distance of 2.143Å in the closed-shell singlet, 2.177Å in the open-shell singlet and 2.190Å in the triplet isomer. The open-shell singlet is closer in geometry (and energy) to the triplet, having similar orbital occupancies. The ground state open-shell singlet is a 1A_1 state, but a 1A_2 state lies very nearby in energy. Similarly, there exists a 3A_1 state lying very near to the 3A_2 ground state.

The $V(OH_2)^+$ ion-molecule complex has a $V - O$ distance of 2.085Å in the low-spin (triplet) case and a bond length of 2.109Å in the high-spin (quintet) state. The $Ti - O$ bond length in the related doublet and quartet isomers is 2.10Å, as it was pointed out in Chapter 2 [112]. Thus as we progress from Sc to V this $M - O$ distance shrinks. In all cases the H_2O moiety itself is only

slightly changed from its unassociated parameters, and there is not appreciable difference between the various $O - H$ or $M - O - H$ values.

Figure 3.2. Geometrical parameters of the various $TS1^+$ transition states on the *B3LYP/DZVP* potential energy surfaces. Bond lengths are reported in \AA , bond angles in degrees.

$TS1$ shown in Figure 3.2 characterizes the first hydrogen transfer from oxygen to the metal. This transition state has near- C_s symmetry and the one imaginary frequency clearly corresponds to hydrogen transfer. Although the exact position of the hydrogen being transferred varies significantly (the surfaces are very flat in this area) again a $M - O$ bond distance decrease is observed from *Sc* to *V*.

Figure 3.3. Geometrical parameters of the various HM^+OH stationary points on the *B3LYP/DZVP* potential energy surfaces. Bond lengths are reported in \AA , bond angles in degrees.

The HM^+OH minimum has C_s symmetry. This intermediate is a well-characterized minimum in all reactions. However, there is a large difference between the low- and high-spin $M-H$ bond distances as can be seen in Figure 3.3. The low-spin cases follow the expected trend, the $M-H$ bond distance decreases as does the $M-O$ distance from Sc to V .

The high-spin cases, however, have very long $M-H$ bonds (*e.g.* 2.606 Å in the HSc^+OH $^3A'$ isomer). These bonds can not be considered covalent bonds, and clearly the surfaces are very flat with regards to the movement of this hydrogen, resulting in the large differences seen among the high-spin isomers. We should point out that the $M-H$ distance in HSc^+OH is remarkably longer than for the other two cations, as could be expected since no electron is free to contribute to $Sc-H$ bonding. This minimum corresponds essentially to $H + ScOH^+$. The $Sc-O-H$ angle also differs for Sc . In this case we found an angle of almost 180.0 degrees, while for Ti a 160.3 degree angle was found and a 153.5 degree angle for V .

Figure 3.4. Geometrical parameters of the various $TS2^+$ transition states on the $B3LYP/DZVP$ potential energy surfaces. Bond lengths are reported in Å, bond angles in degrees.

The second oxygen to scandium hydrogen transfer occurs through $TS2$ depicted in Figure 3.4. In the case of the low-spin isomers, these transition states show $H-H$ distances which are still quite long (1.070 Å for Sc , 1.143 Å for $Ti[112]$, and 1.166 Å for V) and the $M-O$ distance (1.722 Å for Sc , 1.666 Å for $Ti[112]$, and 1.635 Å for V) is closer to the HM^+OH value than that in

the following $(H_2)MO^+$ species. The one imaginary frequency corresponds to $H-H$ bond formation, and $O-H$ bond-breaking. The high-spin four-centered transition states show an almost-fully formed $H-H$ bond and very long $M-H$ and $O-H$ bond distances. Also, the imaginary frequency is reminiscent of direct H_2 elimination.

Figure 3.5. Geometrical parameters of the various $(H_2)MO^+$ stationary points on the B3LYP/DZVP potential energy surfaces. Bond lengths are reported in Å, bond angles in degrees.

The final stationary points located were the $(H_2)MO^+$ species illustrated in Figure 3.5. These $(H_2)MO^+$ structures of C_s symmetry are curious intermediates. As it was pointed out for the Ti system[112] this minimum should be considered a ion-molecule complex. Note that the $V-H$ bond distance has incremented from 1.603Å in the HV^+OH minimum to 2.083Å in the corresponding $(H_2)VO^+$ minimum. Also for the V system the examination of the MOs shows an interaction between the singly occupied d orbital of M and the σ_{H-H}^* orbital (see Figure 2.2). NBO analysis gives this interaction a value of 5.45kcal/mol for V , smaller than for the Ti case (7.87kcal/mol). It is through this interaction that the $H-H$ bond is activated. In comparison with separated low-spin $MO^+ + H_2$ the $M-O$ bond length of this complex is only 0.003Å longer, while the aforementioned $H-H$ bond activation lengthens the H_2 bond length by 0.021Å. The donation from the σ_{H-H} orbital to the metal s orbital should also be remarked upon as the NBO analysis gives that donation

a value of 7.09kcal/mol in the case of Ti and 4.87kcal/mol in the case of V .

In the Sc system a similar $(H_2)ScO^+$ isomer with the hydrogens above and below the plane of symmetry corresponds to a transition state, where the negative eigenvalue corresponds to the rotation of H_2 . The local minimum which is found in this region of the singlet PES is a planar $(H_2)ScO^+$ structure with a $Sc-O$ bond length only 0.006\AA larger than in the separated $ScO^+ + H_2$ products and an $H-H$ distance shorter than the in the other $(H_2)MO^+$ structures. Of course, in the singlet $(H_2)ScO^+$ system there is no singly occupied d orbital and thus the $d \rightarrow \sigma_{H-H}^*$ interaction is impossible. Instead, this structure is a dipole-induced ion complex, which, clearly would not be possible were the hydrogens located above and below the plane of symmetry. In the NBO analysis of this stationary point, a donation from the σ_{H-H} orbital to the Sc atom was given a value of 9.11kcal/mol and a donation from the highest σ_{Sc-O} orbital to the σ_{H-H}^* orbital a value of 4.57kcal/mol . The triplet $(H_2)ScO^+$ species does have a singly occupied d orbital and follows nicely in the trend set by the other metals.

3.3.5 Potential Energy Surfaces

Figures 3.6 and 3.7 show the potential energy surface starting from the $M^+ + OH_2$ separated reactants and leading to $MO^+ + H_2$ for the low- and high-spin states at the B3LYP/DZVP level of theory for Sc and V respectively. That the different spin structures are located in the same column should not be taken to mean that they are connected by simple vertical excitation. The geometrical parameters are significantly different as can be seen in Figures 3.2-3.5.

On both low-spin surfaces, the first step is the formation of the ion-molecule complex. Then, through $TS1$, one hydrogen atom is passed from oxygen to the metal, leading to the HM^+OH molecule, the intermediate whose existence was surmised by experimentalists. Here we observe one of the important differences between V and Sc and Ti . That is, on the V triplet state surface the $TS1$ transition state lies above the energy of the $V^+(^5D) + H_2O$ reactants by 0.568eV while the singlet $TS1$ on the Sc surface lies energetically below the $Sc^+(^3D) + H_2O$ reactants by 0.364eV . The corresponding value for the Ti doublet surface is $+0.056\text{eV}$, that is, almost isoenergetic with the separated reactants.

Here we have a possible explanation for the observed experimental behavior of the ground state metal cations when reacting with water. Both $Sc^+(^3D)$ and $Ti^+(^4F)$ are seen to exhibit at least some spin-forbidden crossing, leading to low-spin products[99]. $V^+(^5D)$, however, does not make that crossing[93]. The low- and high-spin surfaces must cross between the $M(OH_2)^+$ and HM^+OH moieties since the relative positions are switched. In the case of Sc and Ti , that crossing of surfaces occurs at an energy below that of the high-spin reactants, whereas in the case of V , the crossing occurs at an energy above that of the reactants according to our calculations. Also, it is clear that the reactivity through this pathway should decrease from Sc to V as the initial activation

Figure 3.6. *B3LYP/DZVP potential energy surface following the $Sc^+ + OH_2 \rightarrow ScO^+ + H_2$ reaction path. Energies given are in eV and are relative to the separated ground state reactants, $Sc^+(^3D) + OH_2$.*

Figure 3.7. *B3LYP/DZVP potential energy surface following the $V^+ + OH_2 \rightarrow VO^+ + H_2$ reaction path. Energies given are in eV and are relative to the separated ground state reactants, $V^+(^6D) + OH_2$.*

energy needed to go through *TS1* increases. Of course, some caution must be taken with these numbers because dynamical factors, too, would play a role in the evolution of the reaction.

As noted earlier, the 5F state of V^+ does demonstrate some surface crossing. The main differences between the 5D and 5F states of V^+ are the occupation scheme (d^4 for 5D vs. sd^3 for 5F) and the relative energy. Which, then, is the cause of the difference in reactivity?

If the reaction path we propose here (and that suggested by others[93, 99]) is the true path of the reaction, the occupation scheme should not cause a difference by arguments of symmetry. Both the 5D and 5F initial states transform smoothly to the same ${}^5A_1 V(OH_2)^+$ ion-molecule complex. Considering this we investigated the energy of the triplet *TS1* at the B3LYP/TZVP+G(3df,2p) level of theory and found it to lie 0.473eV above the separated $V^+({}^5D) + H_2O$ reactants. The 5F state of V^+ at that same level of theory lies 0.557eV above the 5D state and thus our mystery is solved, or at least the energetic argument is strengthened. The reactants starting with V^+ in the 5F state do have enough energy to reach the point where the surfaces cross and therefore $VO^+({}^3\Sigma)$ is produced (though inefficiently), whereas the reactants in their ground state do not have enough energy to reach the point where the crossing is made.

It should also be pointed out that the open-shell singlet $Sc(OH_2)^+$ species is converted to the closed-shell singlet HSc^+OH isomer in the process of *H* transfer. The passing of the *H* atom occurs through this near- C_s structure which mixes the two singly occupied orbitals and falls to the lower-energy (at this point) electronic structure of the closed-shell singlet.

The HSc^+OH singlet state is much more stable than the $Sc(OH_2)^+$ singlet species (1.492eV), while the HTi^+OH doublet state is more stable than the $Ti(OH_2)^+$ doublet species by 0.626eV. In contrast, on the triplet surface of *V* we found that the triplet $HVOH^+$ isomer is actually 0.22eV *less* stable than the corresponding $V(OH_2)^+$ triplet species.

The second hydrogen transfer from oxygen to the metal takes place through *TS2*. Again this transition state lies lower in energy than the reactants for *Sc* and *Ti* low-spin structures, but not for the *V* triplet transition state. This transition state leads to the final intermediate found on the reaction path: the $(H_2)MO^+$ ion-molecule complex. In the case of $M = Sc$, this complex is bound by 0.270eV, while it is bound by 0.375 in the case of *Ti* and 0.353eV for *V*. It should be remembered that the bonding of this complex is very different for *Sc* due to the lack of singly occupied *d* orbitals (see stationary points section). From this intermediate the loss of H_2 proceeds without transition state to the observed major products, low-spin MO^+ and H_2 .

The first step on the high-spin surface can also be formation of the ion-molecule complex. However, following the reaction from that point is significantly more complicated than was the case for the low-spin surfaces. Despite numerous varied strategies for finding a transition state between this complex and the HSc^+OH molecule, none was found, as happened in the *Ti* quartet surface. But this was not the case for the quintet surface for *V*, a quintet *TS1*

Figure 3.8. *Equilibrium geometry parameters for the various $Sc^+ + OH_2$ reaction products at the B3LYP/DZVP level of theory. In parenthesis are the parameters predicted at the B3LYP/TZVP+G(3df,2p) level of theory. Bond lengths are reported in \AA , bond angles in degrees.*

Figure 3.9. *Equilibrium geometry parameters for the various $V^+ + OH_2$ reaction products at the B3LYP/DZVP level of theory. In parenthesis are the parameters predicted at the B3LYP/TZVP+G(3df,2p) level of theory. Bond lengths are reported in \AA , bond angles in degrees.*

has been found in this surface corresponding to the migration of one hydrogen from oxygen to vanadium, and this high-spin transition state is less stable than the corresponding triplet $TS1$ by 0.143eV .

Once the high-spin HM^+OH intermediate is formed, another intermediate, $(H_2)MO^+$, can be realized by passing through another high-lying H transfer transition state, $TS2$. This $TS2$ is much less stable than the corresponding low-spin $TS2$. From that isomer, the loss of an H_2 molecule gives one of the scarcely observed reaction products, high-spin MO^+ . The high relative energy of this product agrees well with the fact that MO^+ in this spin state is a rarely observed reaction product.

Equilibrium geometry parameters for the various reaction products are given in Figures 3.8 and 3.9.

3.4 Conclusions

The reactions of Sc^+ and V^+ with water have been investigated in detail completing this study of the reactivity of the early first row transition metals. Both the low- and high-spin potential energy surfaces have been characterized at the B3LYP/DZVP level of theory. Energy differences between key low- and high-spin species and total reaction energies for the experimentally observed products have been predicted at even higher levels of theory including B3LYP/TZVP+G(3df,2p) and CCSD(T)/TZVP+G(3df,2p)//B3LYP/TZVP+G(3df,2p). From these data, the following conclusions are drawn:

1. The only exothermic products of the $M^+ + H_2O$ reaction are the ones corresponding to formation of $MO^+ + H_2$ at their low-spin ground state. The exothermicity of these reactions decreases from Sc to V .
2. The HM^+OH intermediate hypothesized by the experimentalists is a well-defined minimum on each potential energy surface. HSc^+OH and HTi^+OH lie lower than the corresponding $M(OH_2)^+$ ion-molecule complex while the contrary is true for V .
3. The low- and high-spin potential energy surfaces cross between this aforementioned intermediate and the $M(OH_2)^+$ ion-molecule complex. In the case of Sc and Ti , the crossing of surfaces occurs at an energy below that of the high-spin reactants, whereas in the case of V , the crossing occurs at an energy *above* that of the ground-state reactants. It has been shown that such a crossing is possible from the $V^+(\text{}^5F)$ excited state due to its elevated energy according to the level of theory applied.
4. The H_2 elimination process passes from the HM^+OH intermediate through a four-centered transition state to an ion-molecule intermediate $(H_2)MO^+$, from which intermediate H_2 is eliminated without transition state. In the case of $(H_2)ScO^+$, this ion-molecule complex is planar whereas the $(H_2)TiO^+$ and $(H_2)VO^+$ complexes are minima when the (H_2) unit is

coordinated perpendicular to the MO^+ unit. This is due to the fact that there are no occupied d orbitals in ScO^+ which could exemplify $d \rightarrow \sigma_{H-H}^*$ donation.

Chapter 4

The Middle First-Row Transition Metal Cases

The study of the reaction of water with the first row transition metal ions is continued in this work. Here we report the study of the reaction of water with the middle (Cr^+ , Mn^+ and Fe^+) first row transition metal cations in both high- and low-spin states. In agreement with experimental observations, the oxides are predicted to be more reactive than the metal ions and no exothermic products are observed. Formation of endothermic products is examined. An in-depth analysis of the reaction paths leading to the observed products is given, including various minima, and several important transition states. All results have been compared with existing experimental and theoretical data, and our earlier works covering the (Sc^+ , Ti^+ , V^+) + H_2O reactions in order to observe existent trends for the early first row transition metal ions. The $MO^+ + H_2$ energy relative to $M^+ + H_2O$ increases through the series from left to right. Additionally, the Fe^+ case is seen to be significantly different from the entire $Sc^+ - Mn^+$ series because both its low- and high-spin cases involve paired electrons, and Mn^+ shows some differences because of the complete half-filling of its valence shell in the high-spin case.

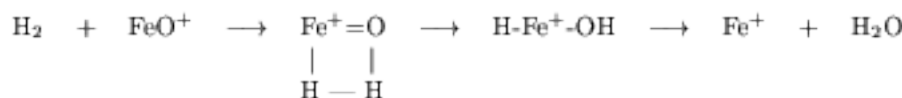
4.1 Introduction

The $H-H$ bond activation by MO^+ is a simple system that can be studied in detail both experimentally and theoretically [8]. Thus, it can be used as a model for other reactions of MO^+ with organic substrates. It was pointed out by Armentrout and co-workers that the early transition metal cations (Sc^+ , Ti^+ and V^+) are more reactive than their oxides, while the contrary occurs with the middle metals (Cr^+ , Mn^+ and Fe^+) [97]. Our earlier works [112, 123] agreed well with experimental work regarding the reactions of the early transition metals and here we expand upon those works investigating the middle transition metals to unveil some of the details underlying the observed reversed reactivity.

Indeed, the reactivity of the middle transition metals has been the subject of several earlier investigations. As early as 1986, Kang and Beauchamp [121, 124] studied the reactivity of the CrO^+ ion by ion-beam reactive scattering techniques. They pointed out that in comparison with other first-row transition-metal oxides which are either too stable (Sc^+ , Ti^+ and V^+) or too reactive (Mn^+ , Fe^+ , Co^+ , and Ni^+), CrO^+ exhibits a balance in being reactive but selective toward olefins. Thus, the chromium oxide ion undergoes facile reactions with alkanes larger than methane, but not with H_2 or CH_4 even though those reactions are exothermic.

More recently the reactivity of the manganese oxide cation with dihydrogen and alkanes has been studied both experimentally and theoretically by Ryan *et al.* [125]. They compare results from the Fourier transform ion cyclotron resonance mass spectrometry with those calculated at the CASPT2D level of theory. They found that thermalized MnO^+ reacts very efficiently with H_2 to eliminate either a H radical or H_2O from the collision complex, both reactions commencing with H-atom abstraction.

Extensive theoretical and experimental works have been carried out concerning the reactivity of iron with many small molecules. The reactivity of FeO^+ with molecular hydrogen was first studied experimentally by Schröder *et al.* [126]. They found that approximately only 1 in 100 collisions of FeO^+ with H_2 results in product formation. This does not follow simple spin selection rule arguments since the sextet ground state of FeO^+ correlates with the electronic ground state of the product ion $Fe^+(^6D)$, and also the electronic ground state of the $H-Fe^+-OH$ and $Fe(OH_2)^+$ intermediates correspond to a sextet. Additionally, the symmetry breaking through the approaching H_2 molecule does not violate any spatial symmetry selection rule. The reactive coordination of the hydrogen molecule to FeO^+ was suggested to be at the origin of the barrier of the higher exothermic oxidation of H_2 . The most likely pathway in their opinion proceeds via a multicentered coordination to generate the $H-Fe^+-OH$ intermediate:



Almost at the same time, Armentrout's group[127] reported on the state-specific reactions of $Fe^+(a^6D, a^4F)$ with D_2O and the reactions of FeO^+ with D_2 as a function of translational energy in a guided ion beam tandem mass spectrometer. The only products observed from single-collision events in the $Fe^+(a^6D, a^4F) + D_2O$ reaction were the endothermic FeD^+ and $FeOD^+$. At low energies, they also observe the $FeOD_2^+$ adduct as a result of secondary stabilizing collisions with D_2O . In the reaction of FeO^+ with D_2 , three ionic products (Fe^+ , FeD^+ and $FeOD^+$) are observed. An inefficient exothermic process that forms $Fe^+ + D_2O$ is observed; however, formation of these products also occurs via another more efficient pathway that involves a reaction barrier of 0.6eV. It is important to point out that they are able to show that FeO^+ and $Fe^+(a^4F)$ have comparable reactivities that greatly exceed that for $Fe^+(a^6D)$.

Recently a comparison of Fourier transform ion cyclotron resonance (ICR), guided ion beam (GIB), and selected-ion flow tube (SIFT) mass spectrometry methods in the study of gas-phase ion-molecule reactions has been carried out. The purpose was to interpret the experimental findings that agree well in the qualitative description of the low efficiencies of the reaction of $FeO^+ + H_2$, but disagree in the quantitative description of rate constants and branching ratios [19].

In collaborative work of groups in Berlin and Jerusalem[128], DFT augmented with CASPT2D computations was used to explore the reaction surface of $FeO^+ + H_2$ and to unravel the origin of the extremely low reactivity observed for this system. According to these calculations, the reaction violates spin-conservation rules and involves a curve crossing from the sextet ground state to the excited quartet surface, giving rise to a multicentered, energetically low-lying transition structure, from which the hydrido iron hydroxide cation $H - Fe - OH^+$ is formed as the initial oxidation product.

Shalk and co-workers [129] continued their studies of the oxidative activation of $H - H$ by FeO^+ using spin-orbit coupling (SOC) calculations. They found that the process involves two spin inversion (SI) junctions between the sextet and quartet states: near the FeO^+/H_2 complex at the entrance channel, and near the Fe^+/H_2O complex at the exit channel. This reduces the probability of the oxidation process even though the quartet surface provides a low-energy path. These groups continued studying this oxidation mechanism[130] with three different DFT functionals: B3LYP, BP86 and FT97. Three mechanisms were considered, addition-elimination, rebound, and oxene-insertion.

In the past few years great effort has been made to understand the reaction of MO^+ with hydrogen to yield M^+ and water as products. We have reported here a summary of the works that have focused on the middle transition metal oxide cations reactivity in general, and especially the FeO^+ paradigm. We feel that the debate is still open, and that more data and new perspectives are required. That is, the problem should be examined from another angle and high level calculations should be used to describe as accurately as possible the systems of interest that might serve as models for other more complicated

organic substrates[8]. Hence, we present here a study of the three middle first row transition metals in high and low-spin states in hopes that through the examination of their similarities and differences (and those with the early first row transition metals) a more complete understanding of their reactivities may be attained.

We present the full reaction mechanism geometries and energetics for both the high and low-spin states, considering the various possible transition states, intermediates, and products.

4.2 Methods

Chapters 1 to 3 show that Density Functional Theory (B3LYP functional) [57, 58] with the DZVP basis sets given by Salahub *et al.*[76, 77] is a reasonable choice for optimization and frequency calculations of these systems. Recent calibration calculations on transition metal compounds affirms this choice[113]. The choice of the B3LYP functional is largely motivated by its satisfactory performance reported recently [31, 68, 73, 113, 114, 115, 116, 130] for transition metal containing systems. Reactants and products of the possible reactions have also been reoptimized at the B3LYP/TZVP+G(3df,2p) level of theory. All the calculations have been corrected with the ZPVE calculated at the corresponding theoretical level.

In order to confirm the B3LYP results, some single point CCSD(T)/TZVP+G(3df,2p) calculations have been carried out at the B3LYP/TZVP+G(3df,2p) equilibrium geometries. The $1s$ electrons of O and $1s$ to $2p$ electrons of the metals were frozen in the CCSD(T) calculations. For the sake of brevity, we will abbreviate CCSD(T)/TZVP+G(3df,2p)//B3LYP/TZVP+G(3df,2p) as CCSD(T)//B3LYP.

The triple zeta quality basis set, TZVP+G(3df,2p), used for the metals was that given by Schäfer, Hubert and Ahlrichs [78], supplemented with a diffuse s function (with an exponent 0.33 times that of the most diffuse s function on the original set), two sets of p functions optimized by Wachters [79] for the excited states, one set of diffuse pure angular momentum d function (optimized by Hay) [80], and three sets of uncontracted pure angular momentum f functions, including both tight and diffuse exponents, as recommended by Ragavachari and Trucks[101]. For the oxygen and hydrogen atoms the 6-311++G(2df,2p) basis set of Pople *et al.*[81] was used.

All DFT and CCSD(T) calculations reported in this chapter have been carried out with the GAUSSIAN94/DFT [71] suites of programs. Also NBO [106, 107] calculations have been done to give additional insight into the bonding properties of some of the structures.

Table 4.1. Total energies (E), in hartree, zero-point vibrational energy corrections ($\Delta ZPVE$), basis set superposition error corrections (BSSE), and dissociation energies (D_0) in eV, for the $M(OH_2)^+$ ion-molecule complexes ($M = Cr, Mn, Fe$).

M	Method	E	$\Delta ZPVE$	BSSE	D_0
Cr	B3LYP/DZVP	-1044.02468	0.065	0.045	1.481
	B3LYP/TZVP+G(3df,2p)	-1044.19124	0.065	0.025	1.408
	CCSD(T)//B3LYP	-1043.48777	0.065	0.069	1.230
	Exp. [62]**				1.34±0.09
	Exp. [61]*				1.259±0.13
	Exp. [117]*				0.950±0.174
	Theo. [64]MCPF/[8s6p4d1f]				1.306
	Theo. [65]QCISD(T)/[8s6p4d1f]				1.390
	Theo. [132]CCSD(T)(FULL)				
	/6-311++G(d,p)***				1.328
Mn	B3LYP/DZVP	-1150.51830	0.056	0.059	1.258
	B3LYP/TZVP+G(3df,2p)	-1150.73035	0.056	0.023	1.196
	CCSD(T)//B3LYP	-1150.01097	0.056	0.064	1.134
	Exp. [62]**				1.23±0.06
	Exp. [61]*				1.411±0.13
	Exp. [117]*				1.150±0.174
	Theo. [64]MCPF/[8s6p4d1f]				1.237
	Theo. [65]QCISD(T)/[8s6p4d1f]				1.425
	Theo. [132]CCSD(T)(FULL)				
	/6-311++G(d,p)***				1.202
Fe	B3LYP/DZVP	-1263.16028	0.056	0.027	1.469
	B3LYP/TZVP+G(3df,2p)	-1263.40430	0.061	0.013	1.410
	CCSD(T)//B3LYP	-1262.62861	0.061	0.071	1.328
	Exp. [62]**				1.33±0.05
	Exp. [61]*				1.250±0.13
	Exp. [117]*				1.424±0.174
	Theo. [130]B3LYP/[8s6p4d]				1.515
	Theo. [130]FT97/[8s6p4d]				1.332
	Theo. [130]BP86/[8s6p4d]				2.174
	Theo. [64]MCPF/[8s6p4d1f]				1.463
	Theo. [131]B3LYP/[8s6p4d1f]				1.441
	Theo. [65]QCISD(T)/[8s6p4d1f]				1.393
	Theo. [132]CCSD(T)(FULL)				
	/6-311++G(d,p)***				1.406

* Temperature not specified.

** Values at 0K.

*** Values at 298K.

4.3 Results and Discussion

4.3.1 Dissociation Energies

Dissociation energies of the $Cr(OH_2)^+$, $Mn(OH_2)^+$ and $Fe(OH_2)^+$ ion-molecules calculated at the B3LYP/DZVP, B3LYP/TZVP+G(3df,2p) and CCSD(T)//B3LYP levels of theory are shown in Table 4.1. Dissociation energies were calculated as the difference between the energy of the isolated monomers and the complex, including both BSSE and ZPVE corrections.

$M(OH_2)^+$ dissociation energies predicted by various levels of theory (MCPF/[8s6p4d1f] and B3LYP/[8s6p4d1f] results from Rosi and Bauschlicher [64, 131, 67], QCISD(T) results from Magnusson and Moriarty [65] and the recent CCSD(T)(FULL)/6-311++G**//MP2(FULL)/6-311++G** results from Trachtman *et al.* [132]) and those experimentally observed [62, 61, 117] are given also in Table 4.1. For the $Fe(OH_2)^+$ ion-molecule the more recent DFT results from Filatov and Shaik [130] are also listed in Table 4.1. Note that the temperature is not specified in references [61] and [117].

Good values are obtained with both the B3LYP and CCSD(T) methods when used in conjunction with the TZVP+G(3df,2p) basis set, as expected from our experience with the early transition metal calculations [112, 123, 100]. The difference found between the B3LYP/DZVP and B3LYP/TZVP+G(3df,2p) results is around 0.065eV and both are in reasonable agreement with the experimental and theoretical values that can be found in Table 4.1, especially with the more recent and precise data from Armentrout's group [62]. The CCSD(T) values are systematically lower as is usual for dissociation energies. They are in good agreement with the 1.397eV CCSD(T)/[8s6p4d1f] D_e value given by Ricca and Bauschlicher [131]. It has been pointed out in our previous work [112, 123] that the use of the TZVP+G(3df,2p) basis set with the CCSD(T) method is essential in order to yield reliable results, for CCSD(T)/DZVP dissociation energies (not shown) are consistently found to be unrealistically low.

4.3.2 Excitation Energy

For the reactions of interest there are three high-/low-spin relative energies that deserve particular attention. These three are the relative energies between the high- and low-spin states of M^+ , $M(OH_2)^+$, and MO^+ species. Excitation energies for these systems are shown in Table 4.2 ($M = Cr$), Table 4.3 ($M = Mn$) and Table 4.4 ($M = Fe$).

The high-/low-spin splittings for these three metal ions follow the trends observed for the early transition metal ions. That is, our values are always lower than the experimental ones and the best overall fitting is obtained at the CCSD(T)//B3LYP level of theory. Cr^+ and Mn^+ excitation energies are predicted satisfactorily by the B3LYP and CCSD(T) methods, indeed it is the B3LYP method which holds a slight advantage in average error for the two

Table 4.2. Relative energies in eV for the ${}^4D(sd^4)$ state of Cr^+ with respect to the ${}^6S(d^6)$ ground state (Δ_1), the 4A_1 state of $Cr(OH_2)^+$ with respect to the 6A_1 ground state (Δ_2), and the ${}^6\Pi$ state of CrO^+ with respect to the ${}^4\Pi$ ground state (Δ_3).

Method	Δ_1	Δ_2	Δ_3
B3LYP/DZVP	2.303	1.531	1.321
B3LYP/TZVP+G(3df,2p)	2.263	1.437	0.136
CCSD(T)//B3LYP	2.257	1.350	0.080
Exp. [85]	2.46		

Table 4.3. Relative energies in eV for the ${}^5S(sd^5)$ state of Mn^+ with respect to the ${}^7S(sd^5)$ ground state (Δ_1), the 5A_1 state of $Mn(OH_2)^+$ with respect to the 7A_1 ground state (Δ_2), and the ${}^7\Pi$ state of MnO^+ with respect to the ${}^5\Pi$ ground state (Δ_3).

Method	Δ_1	Δ_2	Δ_3
B3LYP/DZVP	0.656	0.185	0.464
B3LYP/TZVP+G(3df,2p)	0.856	0.399	0.484
CCSD(T)//B3LYP	0.815	0.677	0.398
Exp. [85]	1.17		
Theo. [8]			0.5
Theo. [125]CAPT2D/[8s7p6d4f2g]	1.302		0.885
Theo. [64]MCPF/[8s6p4d1f]		1.866	

Table 4.4. Relative energies in eV for the ${}^4F(d^7)$ state of Fe^+ with respect to the ${}^6D(sd^6)$ ground state (Δ_1), the 4B_2 state of $Fe(OH_2)^+$ with respect to the 6A_1 ground state (Δ_2), and the ${}^4\Phi$ state of FeO^+ with respect to the ${}^6\Sigma$ ground state (Δ_3).

Method	Δ_1	Δ_2	Δ_3
B3LYP/DZVP	-0.454	-0.701	0.260
B3LYP/TZVP+G(3df,2p)	-0.183	-0.377	0.319
CCSD(T)//B3LYP	0.234	0.119	0.540
Exp. [85]	0.25		
Theo. [128]DFT(NLSD)			1.1
Theo. [128]CASPT2			0.8
Theo. [130]B3LYP/[8s6p4d]	-0.104	-0.234	0.347
Theo. [130]BP86/[8s6p4d]	-0.187	-0.356	0.551
Theo. [130]FT97/[8s6p4d]	-0.282	-0.486	0.673
Theo. [64]MCPF/[8s6p4d1f]	0.408	0.191*	
Theo. [131]B3LYP/[8s6p4d1f]	-0.165	-0.382*	
Theo. [131]MCPF/[8s6p4d1f]	0.451		
Theo. [131]CCSD(T)/[8s6p4d1f]	0.360		

*Relative energies for their 6A_1 and quartet ground state 4A_1 .

species. However, in the case of the ${}^6D(sd^6) \rightarrow {}^4F(d^7)$ splitting of Fe^+ , the B3LYP method is far from the mark, even incorrectly predicting the ordering of the states. This is a known problem that has been extensively discussed in the literature [67, 130, 131, 133], and that has been attributed to a bias toward $3d^n$ configurations over $3d^{n-1}4s^1$, which is inherent in density functionals, regardless of whether they are pure or hybrid. We have taken the 6D state of the iron ion as the energy of reference for all the calculations throughout this work, even at the B3LYP levels of theory. Notice that with the CCSD(T) method the ordering of the states is correct and the relative gaps are well described. The value obtained is in very good agreement with the experimental result of Moore[85], and it is in better agreement than is the value calculated by Bauschlicher and co-workers at the MCPF level.

High \rightarrow Low-spin excitation energies for the $M(OH_2)^+$ ion-molecules also have been calculated. Here the $Cr(OH_2)^+$ ion-molecule maintains the trend observed for the early transition metals, that is, CCSD(T) values give smaller splittings than B3LYP, but this is not the case for the $Mn(OH_2)^+$ ion-molecule, where we obtain a higher gap at the CCSD(T) level of theory, but much smaller than the one calculated by Rosi and Bauschlicher[64]. For the $Fe(OH_2)^+$ ion-molecule, again, we cannot properly describe the ordering of the states with the B3LYP method, as the relative stability of the $Fe(OH_2)^+$ system is dependent upon the ${}^6D(sd^6) \rightarrow {}^4F(d^7)$ splitting in Fe^+ . At the B3LYP level of theory the 4A_2 state is the most stable. In Table 4.5 we have listed several states calculated at the B3LYP/DZVP, B3LYP/TZVP+G(3df,2p) and CCSD(T)//B3LYP levels of theory. Ab initio MCPF results from Rosi and Bauschlicher [64] predict a quartet state 4A_1 0.191eV above the 6A_1 sextet ground state. That value is in good accordance with our CCSD(T)//B3LYP value. From Table 4.5 it can be seen that the relative energies among the various sextets are quite consistent across the table. It is in describing the low-spin \rightarrow high-spin splitting that the B3LYP method gives results which contrast so sharply with those of the CCSD(T) method.

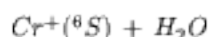
Table 4.5. Relative energies in eV for the different states of $Fe(OH_2)^+$.

State	B3LYP/DZVP	B3LYP/TZVP+G(3df,2p)	CCSD(T)//B3LYP
6A_1	0.000	0.000	0.000
6A_2	-0.005	-0.005	0.002
6B_2	0.104	0.095	0.100
4B_2	-0.701	-0.377	0.119
4A_2	-0.716	-0.379	0.176
4A_1	-0.710	-0.375	0.177
6B_1	0.202	0.196	0.187
4B_1	-0.606	-0.294	0.196

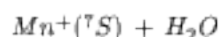
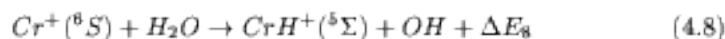
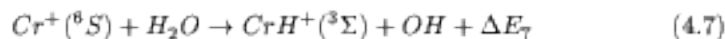
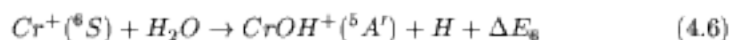
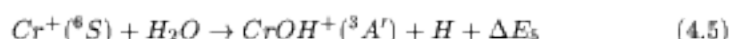
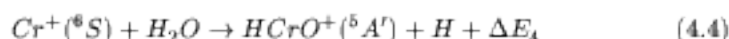
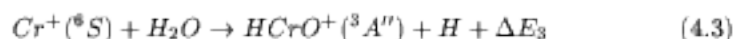
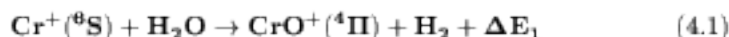
The last species studied at these levels was the metal oxide cation MO^+ molecule. For Cr^+ and Mn^+ the low-spin moieties are still the ground states

but for Fe^+ the high-spin moiety is the ground state. This is because the CrO^+ and MnO^+ molecules have no paired electrons in a $M - O$ σ bond, while the sextet $Fe - O^+$ molecule with one electron more than MnO^+ , places that electron in the $M - O$ σ bond. Now the tendencies are correctly described at all theoretical levels used. Smaller gaps are obtained at the CCSD(T)//B3LYP level of theory, and in general they agree with the other theoretical values found in the literature, the range of predicted values is, however, quite large.

4.3.3 Reaction Energetics

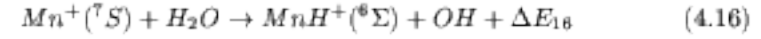
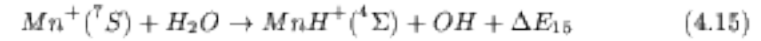
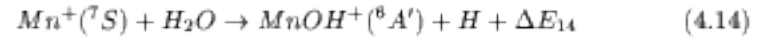
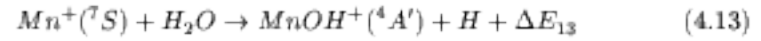
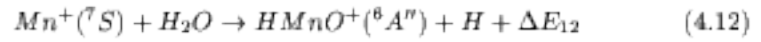
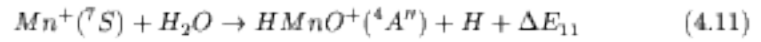
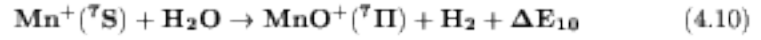


Equations (4.1)-(4.8) represent the main ionic products observed in the reaction of $Cr^+(^6S)$ with H_2O . The predicted ΔE energies are listed in Table 4.6 together with the estimation of Kang and Beauchamp [124] for reaction (4.1), and the values for several other reactions extracted from the available thermodynamical data[137].



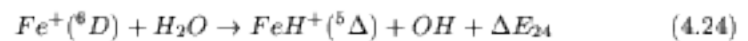
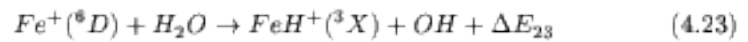
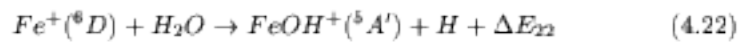
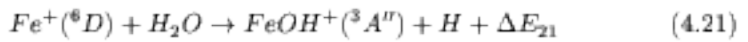
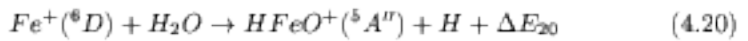
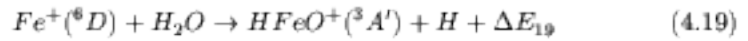
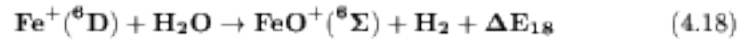
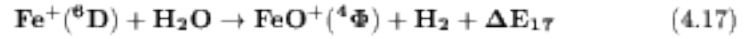
Equations (4.9)-(4.16) represent the main ionic products of the reaction of $Mn^+(^7S)$ and H_2O . Table 4.7 lists the calculated ΔE values along with the three experimental measurements of Ryan and co-workers [125], and the values for several other reactions extracted from the available thermodynamical data[137].





$Fe^+(\text{}^6D) + H_2O$

The corresponding equations for the main ionic products resulting in the reaction of $Fe^+(\text{}^6D)$ with H_2O are shown below. The various predicted ΔE values and the values extracted from the available thermodynamical data[137], along with the theoretical estimates of Fiedler and co-workers[128] and Filatov[130], are listed in Table 4.8.



4.3.4 The Stationary Points

Tables 4.9-4.13 show the most relevant stationary points found for the $M(OH_2)^+$, $TS1^+$, HM^+OH , $TS2^+$ and $(H_2)MO^+$ species respectively, calculated at the B3LYP/DZVP and B3LYP/TZVP+G(3df,2p) (in parentheses) levels of theory, where $M = Cr, Mn$ and Fe .

Table 4.9. Geometrical parameters of the various $M(OH_2)^+$ stationary points on the B3LYP/DZVP and B3LYP/TZVP+G(3df,2p) potential energy surfaces. Bond lengths are reported in Å, bond angles in degrees.

Metal	State	B3LYP/DZVP			B3LYP/TZVP+G(3df,2p)		
		M-O	O-H	\widehat{MOH}	M-O	O-H	\widehat{MOH}
Cr	4A_1	2.048	0.972	126.1	2.021	0.966	125.7
Cr	6A_1	2.093	0.971	126.5	2.087	0.965	126.2
Mn	5A_1	2.042	0.973	126.1	2.045	0.967	125.8
Mn	7A_1	2.193	0.974	126.7	2.191	0.968	126.5
Fe	4B_2	2.006	0.971	126.3	2.006	0.965	126.2
Fe	6A_1	2.119	0.975	126.2	2.101	0.969	126.1

In Table 4.9 are listed the geometrical parameters for the $M(OH_2)^+$ ion-molecule complexes. The C_{2v} symmetry $Cr(OH_2)^+$ ion-molecule complex has a $Cr - O$ distance of 2.048Å in the quadruplet state and 2.093Å in the sextet isomer. The ground states at the quadruplet and sextet states are 4A_1 and 6A_1 respectively. Excited states have been calculated and all of them lie far from these ground states.

The $Mn(OH_2)^+$ ion-molecule complex has a $Mn - O$ distance of 2.042Å in the low-spin (5A_1) case and a bond length of 2.193Å in the high-spin (7A_1) state. Note that there is a large difference between the $Mn - O$ distance of the low-spin and high-spin cases. While this difference is of 0.151Å for Mn , it was of 0.047Å, 0.001Å, 0.024Å and 0.045Å for Sc , Ti , V and Cr respectively. The septet Mn^+ ion with its complete half-filling of shells (s^1d^6) is not predisposed to accepting donations from the H_2O molecule for it will reduce its large stabilizing exchange-energy. Indeed pairing the spin of two of its electrons causes a substantial decrease of the $Mn - O$ bond length, at the B3LYP/TZVP+G(3df,2p) level of theory 0.156Å for the resulting 5A_1 state and 0.165Å for the resulting 5B_2 state, and a concomitant energy destabilization, 0.399eV for the 5A_1 state and 0.880eV for the 5B_2 state.

Things are a bit more involved for the $Fe(OH_2)^+$ ion-molecule complex. As it can be seen in Table 4.5 several states lie very close in energy, and the B3LYP and CCSD(T) results are not in accordance. While the high-spin ground state (6A_1) is the lowest lying of all the states listed in Table 4.5 at the CCSDT//B3LYP level, it is the 4A_2 low-spin state that corresponds to the ground state at either B3LYP/DZVP or B3LYP/TZVP+G(3df,2p) levels.

We took the CCSD(T)//B3LYP predictions as the correct ones, and so we show the values for the corresponding 4B_2 and 6A_1 states. For the 4B_2 state the $Fe - O$ bond length is of 2.006eV and 2.119eV at the 6A_1 state.

As we pointed out in our previous work [123] as we progress from Sc to V this $M - O$ distance among these complexes shrinks, the $V - O$ distance being 2.085Å and 2.109Å for the 3A_1 and 5A_1 states respectively. The trend holds on the low-spin state but it breaks at Mn on the high-spin state, but as we have pointed out earlier, this is due to the fact that $Mn(OH_2)^+ ({}^7A_1)$ has the maximum attainable exchange energy.

$TS1^+$ characterizes the initial hydrogen transfer from oxygen to the metal. Geometrical data corresponding to this transition state can be found in Table 4.10. This transition state has near- C_s symmetry and the one imaginary frequency clearly corresponds to the hydrogen migration over the metal atom.

The HM^+OH minimum has C_s symmetry in all cases. This intermediate is a well-characterized minimum for all the reactions. However, as it can be seen in Table 4.11 there is an appreciable difference between the low- and high-spin $M - H$ bond distances for the Cr and Mn moieties in accordance with the previous values reported for the early transition metal ions. The Mn species in the high-spin state is the only one that exhibits a *trans* conformation. No *cis* conformer was found in spite of extensive search. The low-spin cases follow the expected trend, with the $M - H$ bond distance decreasing from Cr to Fe .

A drastic reduction of the $M - H$ bond is also observed for the high-spin cases. The reduction seen in moving from Cr to Mn is not out of the ordinary, but the change from Mn to Fe is remarkable (2.10Å to 1.59Å). This is because in the case of ${}^7A'$ HMn^+OH there are no paired electrons in the $Mn - H$ interaction. The ${}^6A'$ HFe^+OH intermediate, however, has a pair of electrons in the $Fe - H$ σ bond, according to our NBO analysis.

Our geometrical prediction agrees well with earlier results from other groups [128, 130], but we disagree concerning the bonding nature of ${}^6A'$ HFe^+OH . They explain that the lengthening in $Fe - H$ distance from the quartet to the sextet electromers (1.51Å versus 1.59Å in Fiedlers' results[128], and 1.523Å versus 1.587Å in Shalks' results[130]) is due to the different character in the $Fe - H$ bonding. As was the case for all the other metals studied, they assign a weak coordination of H to a high-spin $FeOH^+$. However our NBO results clearly assign a covalent bond in both the low- and high-spin cases, and the comparison to HMn^+OH is also supportive of the argument for a covalent bond. The assignment of two electrons to a covalent $Fe - H$ bond, however, leaves us with a lack of paired electrons for $Fe - O$ bonding. The same NBO analysis which gives a pair of electrons to the $Fe - H$ bond reports two singly-occupied $Fe - O$ bonds, and a strong donation from an O lone-pair into the σ_{Fe-H}^* bond.

The second oxygen to metal hydrogen transfer occurs through $TS2^+$ depicted in Table 4.12. For the low-spin isomers, these transition states show $H - H$ distances which are still quite long for a bond (1.011Å for Cr , 0.904Å for Mn , and 0.933Å for Fe), even though they are slightly shorter than the

values found for $Sc - V$ series[112, 123]. The one imaginary frequency corresponds to $H - H$ bond formation and $O - H$ bond-breaking.

The high-spin four-centered transition states show an almost-fully formed $H - H$ bond and very long $M - H$ and $O - H$ bond distances for Cr . Also, the imaginary frequency is reminiscent of direct H_2 elimination. However the corresponding $TS2^+$ in the Fe system this $H - H$ bond is even larger than the corresponding bond at the low-spin transition state, again demonstrating the similarities between the low- and high-spin structures on the $Fe^+ + H_2O$ surface, and again due to the presence of a pair of electrons in the valence shell of Fe^+ even in the high-spin cases - something *all* the earlier high-spin M^+ ions lacked.

The final stationary points located were the $(H_2)MO^+$ hydrogen molecule metal oxide adduct illustrated in Table 4.13. As it was pointed out for the Ti system[112] this minimum should be considered a ion-molecule complex. For all of them the $M - H$ bond distance has increased from the HM^+OH minimum to the corresponding $(H_2)MO^+$ minimum, as it was expected but this increase is much less in the $M = Fe$ case, where there has been an increase of only 0.252\AA while for the $M = Cr$ case the increase is 0.437\AA . Also for these three systems the examination of the MOs shows an interaction between the singly occupied d orbital of M and the σ_{H-H}^* orbital (see Figure 2.2). The NBO analysis gives this interaction a value of 3.45kcal/mol for Cr , 1.96kcal/mol for Mn , and 5.09kcal/mol for Fe , smaller than for the Ti (7.87kcal/mol) and V (5.45kcal/mol) cases reported previously. It is through this interaction that the $H-H$ bond is activated by the oxide in the reverse reaction. The back donation from the σ_{H-H} orbital to the metal's s orbital should also be remarked upon. The NBO analysis gives that donation a value of 5.56kcal/mol in the case of Cr and 11.77kcal/mol in the case of Fe . No donation was found for the Mn case as the s orbital is the one used in the bonding with oxygen, however a $\sigma_{H-H} \rightarrow \sigma_{Mn-O}^*$ donation of 6.97kcal/mol is encountered.

It should be pointed out that we found another ${}^5A'$ structure for the $(H_2)MnO^+$ species, where the interaction between the singly occupied d orbital of Mn and the σ_{H-H}^* orbital is of 2.36kcal/mol . This slightly high-lying excited state (0.293eV at the B3LYP/DZVP level) has an smaller $Mn - O$ distance (1.595\AA) than the ground state (1.724\AA), and has a 5.85kcal/mol donation from the σ_{H-H} orbital to the metal s orbital, where one of the d orbitals is used in the bonding with oxygen.

4.3.5 Potential Energy Surfaces

For the $Sc^+ - Mn^+$ reactions the principal product of the $M^+ + H_2O$ reaction was the low-spin metal-oxide ion, but this is not the case for the Fe^+ reaction, where the ${}^6\Sigma$ high-spin state is the ground state FeO^+ . This is the reason for discussing the PESs in two subsections. Also, the iron system is particularly difficult to describe at the B3LYP level of theory since the correct ordering for the spin states of the Fe^+ cation is not obtained as pointed out earlier[67,

130, 131, 133]. Thus, results obtained with higher levels of theory will also be discussed.

That the different spin structures are located in the same column should not be taken to mean that they are connected by simple vertical excitation. The geometrical parameters are significantly different as can be seen in Table 4.9-4.13.

The Chromium and Manganese cases

Figures 4.1 and 4.2 show the potential energy surface starting from the $M^+ + OH_2$ separated reactants and leading to the products $MO^+ + H_2$ for the low- and high-spin states at the B3LYP/DZVP level of theory for Cr^+ and Mn^+ respectively.

The surfaces for the reactions of both Cr^+ and Mn^+ are similar to those we have reported in previous chapters with the first step being the formation of the $M(OH_2)^+$ ion-molecule complex. Through $TS1^+$, one hydrogen atom is passed from oxygen to the metal, leading to the HM^+OH molecule, the intermediate whose existence was surmised by experimentalists. As it was observed for V^+ , but not for Sc^+ or Ti^+ , on the low-spin surface the $TS1^+$ transition state lies above the energy of the high-spin ground state reactants.

The second hydrogen transfer from oxygen to the metal takes place through $TS2^+$. This transition state leads to the final intermediate found on the reaction path: the $(H_2)MO^+$ ion-molecule complex. In the case of $M = Cr$, this complex is bound by 0.455eV, while it is bound by 0.407eV in the case of Mn . These values are larger than the ones observed for Sc (0.270eV), Ti (0.375eV) and V (0.353eV). From this intermediate the loss of H_2 proceeds without transition state to the low-spin MO^+ and H_2 .

The first step on the high-spin surface can also be formation of the ion-molecule complex. Note, however, that the high-spin $Mn(OH_2)^+$ complex is not as stabilized as were the other species due to the complete half-filled valence shell of 7S Mn^+ . Despite numerous varied strategies for finding a transition state between this complex and the HCr^+OH molecule, none was found, as was the case for the Sc triplet and Ti quartet surfaces. This was not the case for the quintet surface for V^+ and septuplet surface for Mn^+ . A septuplet $TS1^+$ has been found on the $Mn^+ + H_2O$ surface corresponding to the migration of one hydrogen from oxygen to manganese. The high- low-spin splitting for this transition state is much greater than it was in the case of the V^+ system (0.928eV for Mn^+ vs 0.143eV for V^+).

Once the high-spin HM^+OH intermediate is formed, another intermediate, $(H_2)MO^+$, can be realized by passing through another high-lying H transfer transition state, $TS2^+$. This $TS2^+$ in the Cr^+ case lies 0.997eV higher in energy than the corresponding low-spin. From that isomer, the loss of an H_2 molecule gives one of the reaction products, high-spin MO^+ . No high-spin $TS2^+$ isomer has been encountered for the Mn^+ system.

These reaction pathways follow the same general scheme as was seen for the

Figure 4.1. *B3LYP/DZVP potential energy surface following the $Cr^+ + OH_2 \rightarrow CrO^+ + H_2$ reaction path. Energies given are in eV and are relative to the separated ground state reactants, $Cr^+({}^6S) + OH_2$.*

Figure 4.2. *B3LYP/DZVP potential energy surface following the $Mn^+ + OH_2 \rightarrow MnO^+ + H_2$ reaction path. Energies given are in eV and are relative to the separated ground state reactants, $Mn^+(^7S) + OH_2$.*

early first-row transition metals with the low- and high-spin surfaces crossing between the $M(OH_2)^+$ and HM^+OH structures. There are many specific differences between the potential energy surfaces of the $M^+ + H_2O$ $M = Sc - Mn$ series, but the same pathway to products $MO^+ + H_2$ is followed and there is a definite trend of increasing barrier heights and endothermicity as we move from left to right along the periodic table.

Equilibrium geometry parameters for the various reaction products are given in Table 4.14.

Table 4.14. *Equilibrium geometry parameters for the various $M^+ + OH_2$ reaction products at the B3LYP/DZVP and B3LYP/TZVP+G(3df,2p) levels of theory. Bond lengths are reported in Å, bond angles in degrees.*

Product	Metal	State	B3LYP/DZVP			B3LYP/TZVP+G(3df,2p)		
			M-O	M-H	Angle	M-O	M-H	Angle
MO ⁺	Cr	⁴ Π	1.586			1.572		
		⁶ Π	1.831			1.829		
	Mn	⁵ Π	1.723			1.729		
		⁷ Π	1.850			1.852		
	Fe	⁴ Φ	1.689			1.696		
		⁶ Σ	1.655			1.637		
MH ⁺	Cr	³ Σ		1.580		1.586		
		⁵ Σ		1.598		1.602		
	Mn	⁴ Σ		1.578		1.574		
		⁶ Σ		1.587		1.612		
	Fe	³ Φ		1.529		1.532		
		⁵ Δ		1.559		1.574		
HMO ⁺	Cr	³ A'	1.537	1.575	100.3	1.520	1.585	106.6
		⁵ A'	1.583	2.301	117.2	1.568	2.242	132.9
	Mn	⁴ A'	1.662	1.555	91.7	1.654	1.566	95.6
		⁶ A'	1.726	2.188	179.9	1.731	2.142	179.7
	Fe	³ A'	1.634	1.504	88.8	1.630	1.512	91.6
		⁵ A'	1.728	1.649	120.8	1.736	1.610	125.1
MOH ⁺	Cr	³ A'	1.737	0.973	140.0	1.737	0.965	138.3
		⁵ A'	1.753	0.973	137.0	1.751	0.965	135.8
	Mn	⁴ A'	1.722	0.975	140.7	1.715	0.967	137.8
		⁶ A'	1.744	0.970	146.1	1.751	0.963	140.5
	Fe	³ A'	1.725	0.975	139.1	1.718	0.968	133.9
		⁵ A'	1.712	0.972	144.2	1.715	0.965	140.1

The Iron case

Figure 4.3 shows the potential energy surface starting from the $Fe^+ + OH_2$ separated reactants and leading to the products $FeO^+ + H_2$ for the low- and high-spin states at the CCSD(T)//B3LYP level of theory. Due to the mislea-

Figure 4.3. *CCSD(T)//BSLYP* potential energy surface following the $Fe^+ + OH_2 \rightarrow FeO^+ + H_2$ reaction path. Energies given are in eV and are relative to the separated ground state reactants, $Fe^+(^6D) + OH_2$. Note that for iron we give this surface rather than usual *BSLYP/DZVP*, because the latter is qualitatively misleading.

-ding description at the B3LYP level of theory, no potential energy surface is shown for this system at that level of theory. The potential energy surface for the $Fe^+ + H_2O$ system is fairly complicated. Danovich and Shaik[129] predicted two spin crossings for this reaction - one between $Fe(OH_2)^+$ and HFe^+OH and a second between HFe^+OH and H_2FeO^+ . The first step is the formation of the $Fe(OH_2)^+$ ion-molecule complex. Through $TS1^+$, one hydrogen atom is passed from oxygen to the metal, leading to the HFe^+OH intermediate. In all results reported in the literature and in our own results this sextuplet transition state lies higher in energy than the quartet one. However, this accordance it is not obtained for the HFe^+OH intermediate. All DFT results agree in assigning a quartet ground state, but as larger basis sets are used the splitting between the two states becomes smaller. At the B3LYP/DZVP level of theory a 0.493eV value is obtained and at the B3LYP/TZVP+G(3df,2p) level the value is reduced to 0.194eV. The group in Berlin gives a 0.477eV splitting value calculated at the CASPT2 level; and the group in Jerusalem [130], reports a 0.130eV value with the B3LYP functional, 0.325eV with BP86, and 0.351eV with FT97. All these results seem to agree quite well, but the surprise comes with our CCSD(T)//B3LYP results, where the sextuplet electromer is calculated to be the ground state, however the quartet lies only 0.065eV higher in energy.

The second hydrogen transfer from oxygen to the metal takes place through $TS2^+$. Full agreement is found here and the sextuplet isomer lies higher in energy than the quartet state. This transition state leads to the final molecular hydrogen metal oxide adduct intermediate found on this reaction path: the $(H_2)FeO^+$ ion-molecule complex, whose ground state corresponds once again to a sextet state that is bound by 0.490eV at the B3LYP/DZVP level of theory, similar to the *Cr* and *Mn* values (0.455eV and 0.407eV, respectively) for their low-spin ground state $(H_2)MO^+$ moieties. From this intermediate the loss of H_2 proceeds without transition state to the high-spin MO^+ and H_2 .

The dehydrogenation process described here has not been observed experimentally. As it was pointed out in the introduction, Armentrout's group observed only the FeD^+ and $FeOD^+$ products under their conditions. The reverse reaction, however, was observed and it could follow the path described here. In the $FeO^+ + H_2 \rightarrow Fe^+ + H_2O$ reaction, Clemmer *et al.*[127] observed a very inefficient barrierless reaction (once in every 600 collisions) and a very efficient reaction with a barrier of 0.6eV. On our CCSD(T)//B3LYP surface, $TS2^+$ lies 0.547eV above the separated $FeO^+(^6\Sigma) + H_2$ reactants and thus the efficient reaction with barrier is in concurrence with our calculated sextet surface. However, the quartet $TS2$ also lies higher in energy than $FeO^+(^6\Sigma) + H_2$ (by 0.326eV), which means that a barrierless pathway, inefficient due to spin crossing, would not agree with our predictions at the CCSD(T)//B3LYP level of theory. At the B3LYP/DZVP and B3LYP/TZVP+G(3df,2p) levels of theory, the quadruplet $TS2^+$ lies only 0.061eV and 0.045eV above the $FeO^+(^6\Sigma) + H_2$ asymptote in reasonable agreement with the predictions of Filatov and Shaik[130]. In one of the experimental works, it was put forward that perhaps

small amounts of $FeO^+(^4\Phi)$ could be in the beam[127]. A later article, however, dismisses that possibility[19]. At all levels of theory used, the quartet $TS2^+$ lies below the $FeO^+(^4\Phi)+H_2$ asymptote.

Equilibrium geometry parameters for the various reaction products are given in Table 4.14.

4.4 Conclusions

The reactions of Cr^+ , Mn^+ and Fe^+ with water have been investigated in detail extending the study of the reactivity of the first row transition metals. Both the low- and high-spin potential energy surfaces have been characterized at the B3LYP/DZVP and B3LYP/TZVP+G(3df,2p) levels of theory. In addition CCSD(T)//B3LYP single-point energies were computed for many points of interest. From these data, the following conclusions are drawn:

1. Whereas the only exothermic products of the $M^+ + H_2O$ reaction for $M=Sc$ to V were $MO^+ + H_2$ with exothermicity decreasing from Sc to V , this reaction is endothermic for $M=Cr$ to Fe^+ with endothermicity increasing through the series.
2. The $Fe^+ + H_2O$ system has proven to be significantly different throughout the reaction pathway. There is less difference between the high- and low-spin structures in the case of Fe^+ . An explanation for this is that the high spin Fe^+ cation has a set of paired electrons while the Sc^+ to Mn^+ high-spin cations do not.
3. Similarly, the Mn^+ high-spin shows some minor differences because its valence shell is completely half-filled with unpaired electrons.
4. Both, high- and low-spin potential energy surfaces cross once in the entrance channel for Cr^+ and Mn^+ , but, at least, two crossings have been observed for the Fe^+ potential energy surface, at the entrance and exit channels. All these crossings occur at an energy *above* that of the ground-state reactants, as it was observed earlier in the V potential energy surface.

Chapter 5

The Late First-Row Transition Metal Cases. General Conclusions

In this chapter we conclude the study of the reaction of water with the first row transition metal ions. We report the study of the reaction of water with the late (Co^+ , Ni^+ and Cu^+) first row transition metal cations in both high- and low-spin states. In agreement with experimental observations, no exothermic products are found and the oxides are predicted to be more reactive than the metal ions. Formation of endothermic products is examined. An in-depth analysis of the reaction paths possible for these reactions is given, including various minima and several important transition states. All results have been compared with existing experimental and theoretical data, and our earlier works covering the (Sc^+ - Fe^+) + H_2O reactions in order to observe existent trends for the first row transition metal ions.

5.1 Introduction

With the results reported in this chapter we finish our works on the reactivity of first row transition metal cations with water with the aim of understanding this paradigm for the reactivity of these metal cations and their oxides. Previously, we have discussed the importance of both high- and low-spin potential energy surfaces, their particular features, and the spin-forbidden crossings that they involve. For the early (Sc, Ti and V) and middle (Cr and Mn) transition metal cations the high-spin state was the one corresponding to the ground state, while the low-spin state was the ground state for their oxides. The iron cation presented a high-spin ground state, but its oxide also has a high-spin ground-state, resulting in a very complicated two-state-specific reactivity. In the late transition metals we have in the ground states low-spin metal cations and high-spin metal oxide cations.

As we pointed out in Chapter 4, the reactivity of the transition metals was studied by Kang and Beauchamp[121, 124] in 1986. Based on the bond dissociation energies of the metal oxide cations they pointed out that the early MO^+ molecules (Sc, Ti, V) were too stable to react exothermically with alkenes as their dissociation energies are significantly larger than the ones corresponding to the Mn-Ni oxides, which are very reactive, the low dissociation energies leading to the possibility of exothermic processes. Cr was somewhat between these two different behaviours, exhibiting a balance in being reactive but selective. They also pointed out that exothermic thermochemistry does not ensure a facile reaction, but that a number of examples support the contention that barriers in exothermic reactions of transition metal oxide ions are rare[121].

Several groups have developed a large body of work around the reactivity of these transition metals showing that the behaviour of these systems is much more complicated than expected. In 1994 Schröder *et al.*[126] observed very low reactivities for the reactions of FeO^+ , CoO^+ and NiO^+ with H_2 . They surprisingly found that while CoO^+ has a binding energy close to that of FeO^+ , and NiO^+ 's binding energy is much smaller, their $MO^+ + H_2$ reaction rates are very similar, and give rise to the exclusive formation of water and M^+ .

Armentrout's group[94] also studied these reactions in both directions for the cobalt system. They observe a $0.75 \pm 0.04 eV$ activation barrier for the exothermic oxidation of D_2 by CoO^+ , probably attributable to a four-centered TS associated with addition of $D - D$ across the CoO^+ bond. They observe two products in the oxidation of Co^+ , the CoD^+ and $CoOD^+$ species, but no evidence of CoO^+ formation was observed in their study, a process that is thermochemically less endothermic than the ones giving rise to the two other products observed.

Fiedler *et al.*[128] postulate some generalities on the reactivity patterns of CoO^+ , NiO^+ and CuO^+ with the hydrogen molecule based in their detailed theoretical study of the iron system, and experimental study of the reactions of CoO^+ with hydrogen, methane, and small alkanes[135]. They highlighted a low stabilization energy potential energy surface, where the high-spin surface must

surmount a significant barrier in addition to the spin-inversion requirement, giving an explanation of the low efficiencies of these reactions in spite of the favorable thermochemistry.

As it was concluded in a review by Schröder and Schwarz[8], despite favorable thermochemistry for the reaction of middle and late metal oxide cations with hydrogen molecule, only the reaction of MnO^+ with H_2 is efficient; CrO^+ , CoO^+ , and NiO^+ hardly react and FeO^+ reaction occurs only rarely. These reactions must be controlled by reaction barriers and the ease of curve crossing from the high-spin ground-states of MO^+ to the low-spin surface.

No experimental data is available for the copper system as it seems that CuO^+ can not be generated in reasonable quantities[8], but a low efficiency is expected for the ground-state high-spin copper oxide in the reaction $CuO^+ + H_2 \rightarrow Cu^+ + H_2O$ [128].

Seeing that there exists an interest in the reactivities of the entire series of first row transition metals, we here complete our goal of providing high- and low-spin potential energy surfaces for their reactions with water. We present, as usual, the full reaction mechanism geometries and energetics for both the high and low-spin states, considering the various possible transition states, intermediates, and products.

5.2 Methods

The experience of this group (Chapters 1-4) shows that Density Functional Theory (B3LYP functional) [57, 58] with the DZVP basis sets given by Salahub *et al.*[76, 77] is a reasonable choice for optimization and frequency calculations of these systems. Recent calibration calculations on transition metal compounds affirms this choice[113]. The choice of the B3LYP functional is largely motivated by its satisfactory performance reported recently [31, 68, 73, 113, 114, 115, 116, 130] for transition metal containing systems. Reactants and products of the possible reactions have also been reoptimized at the B3LYP/TZVP+G(3df,2p) level of theory. All the calculations have been corrected with the ZPVE calculated at the corresponding theoretical level.

In order to confirm the B3LYP results, some single point CCSD(T)/TZVP+G(3df,2p) calculations have been carried out at the B3LYP/TZVP+G(3df,2p) equilibrium geometries. The 1s electrons of O and 1s to 2p electrons of the metals were frozen in the CCSD(T) calculations. Once more we have abbreviated CCSD(T)/TZVP+G(3df,2p)//B3LYP/TZVP+G(3df,2p) as CCSD(T)//B3LYP.

The triple zeta quality basis set, TZVP+G(3df,2p), used for the metals was that given by Schäfer, Hubert and Ahlrichs [78], supplemented with a diffuse *s* function (with an exponent 0.33 times that of the most diffuse *s* function on the original set), two sets of *p* functions optimized by Wachters [79] for the excited states, one set of diffuse pure angular momentum *d* function (optimized by Hay) [80], and three sets of uncontracted pure angular momentum *f* functions, including both tight and diffuse exponents, as recommended by Ragavachari

and Trucks[101]. For the oxygen and hydrogen atoms the 6-311++G(2df,2p) basis set of Pople *et al.*[81] was used.

All DFT and CCSD(T) calculations reported in this chapter have been carried out with the GAUSSIAN94/DFT [71] and GAUSSIAN98/DFT[136] suites of programs. Also NBO [106, 107] calculations have been done to give additional insight into the bonding properties of some of the structures.

5.3 Results and Discussion

5.3.1 Dissociation Energies

Dissociation energies of the $Co(OH_2)^+$, $Ni(OH_2)^+$ and $Cu(OH_2)^+$ ion-molecules calculated at the B3LYP/DZVP, B3LYP/TZVP+G(3df,2p) and CCSD(T)//B3LYP levels of theory are shown in Table 5.1. Dissociation energies were calculated as the difference between the energy of the isolated monomers and the complex, including both BSSE and ZPVE corrections.

$M(OH_2)^+$ dissociation energies predicted by various levels of theory (MCPF/[8s6p4d1f] results from Rosi and Bauschlicher [64], QCISD(T) results from Magnusson and Moriarty [65] and the recent CCSD(T)(FULL)/6-311++G**//MP2(FULL)/6-311++G** results from Trachtman *et al.* [132]) and those experimentally observed [61, 62, 117] are given also in Table 5.1. Note that the temperature is not specified in references [61] and [117].

Once more, good values are obtained with both the B3LYP and CCSD(T) methods when used in conjunction with the TZVP+G(3df,2p) basis set[100, 112, 123, 134]. The difference found between the B3LYP/DZVP and B3LYP/TZVP+G(3df,2p) results is again around 0.065eV and both are in reasonable agreement with the experimental and theoretical values that can be found in Table 5.1, especially with the more recent and precise data from Armentrout's group [62]. The CCSD(T) values are systematically lower as is usual for dissociation energies.

The values listed for the $Co(OH_2)^+$ complex correspond to the 3A_2 ground state, in accordance with Trachtman *et al.*[132] but not with Rosi and Bauschlicher[64], as they predict a 3B_2 ground state for this ion-molecule, with a geometry reasonably similar to ours. They predict that the 3A_2 excited state is only 0.030eV higher in energy, while our 3A_2 state lies 0.091eV lower in energy than the 3B_2 state at the CCSD(T)//B3LYP level of theory. In any case, these discrepancies at the various computational levels are not large and do not change the overall trend of the dissociation energies in comparison with experimental data.

In considering the results of this study of the first row transition metals, examination of the mean deviations of the obtained values with respect to the values given by Armentrout's group[62] shows a very good agreement: a deviation of 0.08eV at the B3LYP/DZVP level of theory, 0.05eV at the B3LYP/TZVP+G(3df,2p) level and 0.12eV at the CCSD(T)//B3LYP level.

Table 5.1. Total energies (E), in hartree, zero-point vibrational energy corrections ($\Delta ZPVE$), basis set superposition error corrections ($BSSE$), and dissociation energies (D_0) in eV, for the $M(OH_2)^+$ ion-molecule complexes ($M = Co, Ni, Cu$).

M	Method	E	$\Delta ZPVE$	BSSE	D_0
Co	B3LYP/DZVP	-1458.72473	0.069	0.104	1.664
	B3LYP/TZVP+G(3df,2p)	-1459.00896	0.065	0.025	1.637
	CCSD(T)//B3LYP	-1458.04010	0.065	0.079	1.514
	Exp. [62]**				1.67±0.06
	Exp. [61]*				1.610±0.13
	Exp. [117]*				1.740±0.174
	Theo. [64]MCPF/[8s6p4d1f]				1.658
	Theo. [65]QCISD(T)/[8s6p4d1f]				1.575
	Theo. [132]CCSD(T)(FULL)				
	/6-311++G(d,p)***				1.610
Ni	B3LYP/DZVP	-1584.24268	0.056	0.103	1.861
	B3LYP/TZVP+G(3df,2p)	-1584.57010	0.061	0.026	1.823
	CCSD(T)//B3LYP	-1583.56652	0.061	0.080	1.690
	Exp. [62]**				1.87±0.03
	Exp. [61]*				1.584±0.13
	Exp. [117]*				1.723±0.174
	Theo. [64]MCPF/[8s6p4d1f]				1.784
	Theo. [65]QCISD(T)/[8s6p4d1f]				1.672
	Theo. [132]CCSD(T)(FULL)				
	/6-311++G(d,p)***				1.575
Cu	B3LYP/DZVP	-1716.40775	0.061	0.126	1.784
	B3LYP/TZVP+G(3df,2p)	-1716.77247	0.065	0.040	1.653
	CCSD(T)//B3LYP	-1715.72612	0.065	0.101	1.452
	Exp. [62]**				1.63±0.08
	Exp. [61]*				1.519±0.13
	Exp. [117]*				1.424±0.174
	Theo. [64]MCPF/[8s6p4d1f]				1.619
	Theo. [65]QCISD(T)/[8s6p4d1f]				1.559
	Theo. [132]CCSD(T)(FULL)				
	/6-311++G(d,p)***				1.567

* Temperature not specified.

** Values at 0K.

*** Values at 298K.

It should be pointed out that while a tendency to overestimate has been observed at the B3LYP level, the CCSD(T) level underestimates the dissociation energies in all the cases, except for the iron case where a perfect matching was obtained. These tendencies are those expected for the methods used. The method that best fits the experimental data is the B3LYP/TZVP+G(3df,2p) level of theory, all the values calculated are almost within the experimental error bar, the greatest discrepancy coming in the iron system, 0.08eV vs. the experimental error bars of 0.06eV.

5.3.2 Excitation Energy

Let us look now to the high-/low-spin relative energies of M^+ , $M(OH_2)^+$, and MO^+ shown in Table 5.2 ($M = Co$), Table 5.3 ($M = Ni$) and Table 5.4 ($M = Cu$), and compare them with the values given for the other first row transition metal M^+ , $M(OH_2)^+$, and MO^+ moieties in previous chapters.

For the early and middle transition metal cations the calculated high-/low-spin splittings were always lower than the experimental ones, but for the late M^+ there is an inversion in the trend. Discounting the Fe^+ case, notably poorly described by the B3LYP method[67, 130, 131, 133, 134], this change can be related to the fact that for the earlier transition metals the ground state of the cation is high-spin, while the ground state of these last three is low-spin. Calculating the overall deviations from the experimental values [85] we obtain that for all the row B3LYP/TZVP+G(3df,2p) and CCSD(T)//B3LYP levels of theory perform similarly, with respective overall deviations of 0.196eV and 0.214eV, a performance slightly better than the B3LYP/DZVP method, which has a deviation of 0.286eV. We must point out the significant overestimation obtained at the CCSD(T)//B3LYP level for the $Cu^+ \ ^1S - ^3D$ splitting, and the poor B3LYP/TZVP+G(3df,2p) description of the $Fe^+ \ ^4F \rightarrow ^6D$ splitting.

For the $M(OH_2)^+$ ion-molecules low \rightarrow high spin excitation energies we observe, continuing the trend shown by the $M = Sc - Cr$ ion-molecules, that CCSD(T)//B3LYP gives smaller splittings than B3LYP. Note that an increased gap is observed for the copper ion-molecule.

Finally, we examine the metal oxide cation MO^+ molecule. While the CCSD(T)//B3LYP method predicted lower excitation energies for CrO^+ and MnO^+ than did the B3LYP method, it gives larger excitation energies for these three late metal oxide cations, in good accordance with the values obtained with the iron oxide and the early transition metal oxides. In general, the calculated gaps are smaller than the ones reported by Fiedler *et al.*. Our predictions of lowest-lying high- and low-spin states agree with those of Fiedler *et al.* except for the NiO^+ doublet ground state. We obtain a $^2\Sigma$ doublet ground state with a $^2\Delta$ state lying 0.187eV higher in energy. A $^2\Delta$ state has been assigned as the ground state in Fiedler's calculations, while they do not give a value for the $^2\Sigma$ state.

Table 5.2. Relative energies in eV for the ${}^5F(sd^7)$ state of Co^+ with respect to the ${}^3F(d^8)$ ground state (Δ_1), the 5B_2 state of $Co(OH_2)^+$ with respect to the 3A_2 ground state (Δ_2), and the ${}^3\Sigma$ state of CoO^+ with respect to the ${}^5\Delta$ ground state (Δ_3).

Method	Δ_1	Δ_2	Δ_3
B3LYP/DZVP	0.935	1.211	0.657
B3LYP/TZVP+G(3df,2p)	0.721	0.966	0.645
CCSD(T)//B3LYP	0.530	0.719	0.887
Exp. [85]	0.43		
Theo.[128]			1.0

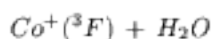
Table 5.3. Relative energies in eV for the ${}^4F(sd^8)$ state of Ni^+ with respect to the ${}^2D(d^9)$ ground state (Δ_1), the ${}^4A'$ state of $Ni(OH_2)^+$ with respect to the 2A_1 ground state (Δ_2), the ${}^2\Sigma$ state of NiO^+ with respect to the ${}^4\Sigma$ ground state (Δ_3), and the ${}^2\Delta$ state of NiO^+ with respect to the ${}^4\Sigma$ ground state (Δ_4).

Method	Δ_1	Δ_2	Δ_3	Δ_4
B3LYP/DZVP	1.377	1.783	0.391	0.558
B3LYP/TZVP+G(3df,2p)	1.210	1.572	0.411	0.538
CCSD(T)//B3LYP	1.262	1.550	0.606	0.793
Exp. [85]	1.08			
Theo.[128]				1.3

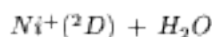
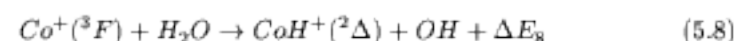
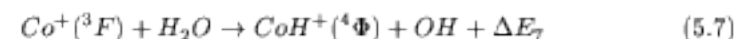
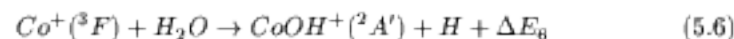
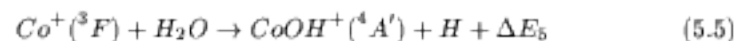
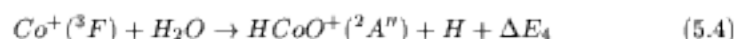
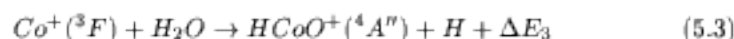
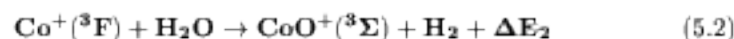
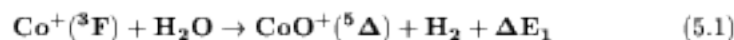
Table 5.4. Relative energies in eV for the ${}^3D(sd^9)$ state of Cu^+ with respect to the ${}^1S(d^{10})$ ground state (Δ_1), the 3B_1 state of $Cu(OH_2)^+$ with respect to the 1A_1 ground state (Δ_2), and the ${}^1\Delta$ state of CuO^+ with respect to the ${}^3\Sigma$ ground state (Δ_3).

Method	Δ_1	Δ_2	Δ_3
B3LYP/DZVP	2.998	3.243	0.583
B3LYP/TZVP+G(3df,2p)	2.911	3.123	0.562
CCSD(T)//B3LYP	3.291	3.447	0.632
Exp. [85]	2.81		
Theo.[128]			1.4

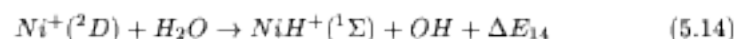
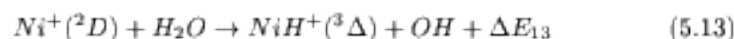
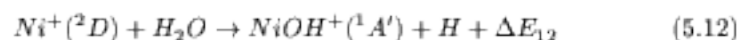
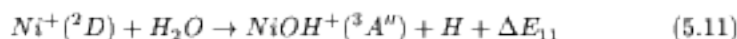
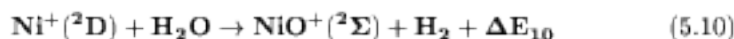
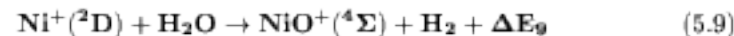
5.3.3 Reaction Energetics

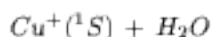


Equations (5.1)-(5.8) represent the main ionic products observed in the reaction of $Co^+(^3F)$ with H_2O . The predicted ΔE energies are listed in Table 5.5 together with values extracted from the available thermodynamical data[137] for reactions (5.1), (5.5) and (5.7).

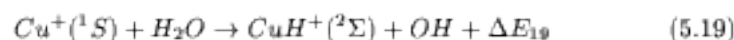
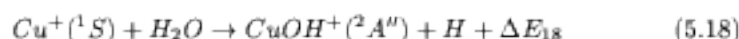
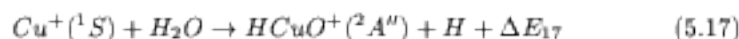
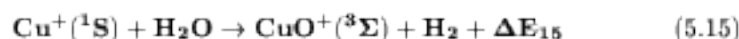


Equations (5.9)-(5.14) represent the main ionic products of the reaction of $Ni^+(^2D)$ and H_2O . Table 5.6 lists the calculated ΔE values along with the values extracted from the available thermodynamical data[137].





The corresponding equations for the main ionic products resulting in the reaction of $\text{Cu}^+(^1S)$ with H_2O are shown below. The various predicted ΔE values are listed in Table 5.7. Values extracted from the available thermodynamical data[137] are also listed for reactions (5.15) and (5.19).



5.3.4 The Stationary Points

In this section we examine the geometrical parameters calculated at the B3LYP/DZVP and B3LYP/TZVP+G(3df,2p) levels of theory for the relevant minima and transition states on the potential energy surfaces for the reaction of the late transition metal cations with water. General trends are also concluded for the entire row.

Table 5.8. Geometrical parameters of the various $M(\text{OH}_2)^+$ stationary points on the B3LYP/DZVP and B3LYP/TZVP+G(3df,2p) potential energy surfaces. Bond lengths are reported in Å, bond angles in degrees.

Metal	State	B3LYP/DZVP			B3LYP/TZVP+G(3df,2p)		
		M-O	O-H	\widehat{MOH}	M-O	O-H	\widehat{MOH}
Co	3A_2	2.005	0.971	126.0	1.999	0.965	126.0
Co	5B_2	2.088	0.975	126.1	2.066	0.969	126.0
Ni	3A_1	1.952	0.971	125.7	1.953	0.965	125.6
Ni	4A_2				2.050	0.968	125.6
Ni	$^4A'$	2.086	0.975	123.3	2.055	0.968	125.3
Cu	1A_1	1.946	0.971	125.7	1.946	0.965	125.7
Cu	3B_1	2.096	0.979	126.2	2.035	0.971	126.0

Table 5.8 shows the geometrical parameters of the $M(\text{OH}_2)^+$ ion-molecule complexes. The low-lying triplet $\text{Co}(\text{OH}_2)^+$ ion-molecule shows several excited states lying very close in energy, which makes it quite hazardous to declare which of them is the ground-state. First, Rosl & Bauschlicher assigned

a 3B_2 ground-state to this ion-molecule. Later, Tratchman and co-workers assigned a 3A_2 state as the ground-state. Our B3LYP/TZVP+G(3df,2p) and CCSD(T)//B3LYP results are in accordance with this second work, but the B3LYP/DZVP level of theory predicts otherwise. At this latter level a 3B_1 state is predicted to be the ground state with the 3A_2 state lying 0.053eV higher in energy and the 3B_2 state is higher still. No significant geometrical changes are observed between these two states. Based in our high-level calculations, and the results from Tratchman and co-workers, we have taken the 3A_2 state to be the ground state. The difference on the $Co - O$ distance between the low-spin and high-spin states is only 0.067Å.

The ground state of the $Ni(OH_2)^+$ metal cation-water complex corresponds to a well described C_{2v} 2A_1 state, with a $Ni - O$ distance of 1.953Å. However, things are not so clear at the high-lying quartet state. The lowest-lying quartet, according to the B3LYP/TZVP+G(3df,2p) level of theory, is a 4A_2 state with C_{2v} symmetry. However, no C_{2v} minimum exist on the B3LYP/DZVP surface. That level of theory predicts a C_s minimum where the Ni lies 21.2 degrees out of the HOH plane. It was also possible to characterize a C_s minimum at the B3LYP/TZVP+G(3df,2p) level of theory, but the out-of-plane angle is only 8.5 degrees and the structure lies 0.006eV higher in energy than the C_{2v} ground state.

Both high- and low-spin $Cu(OH_2)^+$ states have been found to be in accordance with all the methods and other theoretical data reported in the literature. The 1A_1 ground state has a $Cu - O$ bond length of 1.945Å, and the 3B_1 state has a 2.035Å bond length at the B3LYP/TZVP+G(3df,2p) level of theory.

In all three of these late transition metal ion complexes the bond length corresponding to the high-spin state is longer than the low-spin one, as has been true along the row. Also, the tendency of complex $M - O$ bond length shrinking continues in these late metals, as can be appreciated in Graph 5.1 which plots $M - O$ bond distances for the high- and low-spin $M(OH_2)^+$ complexes for the first row transition metals.

Graph 5.1. $M - O$ bond lengths for the $M(OH_2)^+$ ion-molecule complexes through the first-row transition metal ions (B3LYP/DZVP values).

The first hydrogen transfer from oxygen to the metal is characterized by the $TS1^+$ structures. Geometrical parameters are listed in Table 5.9. While the $M - O$ distance in the high-spin states is seen to increase in moving from left to right through the first row transition metals, a tendency to decrease this bond distance is observed for the low-spin structures.

Table 5.9. Geometrical parameters of the various $TS1^+$ transition states on the $B3LYP/DZVP$ potential energy surfaces. Bond lengths are reported in \AA , bond angles in degrees.

Metal	State	M-O	M-H(1)	O-H(1)	O-H(2)	$\widehat{M\bar{O}H}(1)$
Co	3A	1.736	1.498	1.717	0.979	51.4
Co	5A	1.867	1.723	1.591	0.984	59.1
Ni	2A	1.749	1.557	1.548	0.974	56.0
Ni	4A	1.882	1.688	1.519	0.987	58.3
Cu	3A	1.959	1.692	1.498	0.990	56.8

Table 5.10. Geometrical parameters of the various $H(1)M^+OH(2)$ stationary points on the $B3LYP/DZVP$ potential energy surfaces. Bond lengths are reported in \AA , bond angles in degrees.

Metal	State	M-H(1)	M-O	O-H(2)	$\widehat{H(1)\bar{M}O}$	$\widehat{M\bar{O}H}(2)$
Co	3A	1.468	1.694	0.981	87.5	123.1
Co	$^5A''$	1.570	1.738	0.982	145.9	134.7
Ni	$^2A''$	1.429	1.685	0.981	84.5	124.7
Ni	$^4A''$	1.498	1.897	0.989	122.0	126.2
Ni	$^4A'$	1.513	1.872	0.982	106.6	186.9
Cu	3A	1.527	1.903	0.989	118.4	125.0

Graph 5.2. $M - H$ bond lengths for the HM^+OH intermediates through the first-row transition metal ions ($B3LYP/DZVP$ values).

Table 5.10 shows the geometrical data for the HM^+OH minima, almost all of them have C_s symmetry. This intermediate has been well-characterized for all the reactions studied by our group, except for the singlet copper surface, where it has not been possible to obtain this minimum even at high levels of theory. The non-existence of a singlet HCu^+OH intermediate is reasonable, because the valence space on the Cu atom would be filled with lone pairs and $Cu - O$ bonding, leaving no opportunities for $Cu - H$ interaction. Note also that these intermediates in the high-spin Ni and Cu cases have very long $M - O$ bonds in comparison with the rest of the row. For the existent HM^+OH intermediates, the differences between the low- and high-spin $M - H$ distances are minimal in the $Fe - Ni$ metals which was not the case for the earlier metals (see Graph 5.2). The low-spin cases follow the expected trend, with the $M - H$ bond distance decreasing from Sc to Ni . In the high-spin cases this decreasing trend is only broken in the Cu moiety, but its $M - H$ bond length is only 0.029\AA larger than that of HNi^+OH .

The second oxygen to metal hydrogen transfer occurs through $TS2^+$. As it can be seen in Table 5.11, the low-spin isomers of these transition states show $H - H$ distances that are still quite long for bonds. The tendency seen earlier is continued; that is, these bond distances tend to be shorter as we go through the row.

Table 5.11. Geometrical parameters of the various $TS2^+$ transition states on the $B3LYP/DZVP$ potential energy surfaces. Bond lengths are reported in \AA , bond angles in degrees.

Metal	State	M-H(1)	M-O	O-H(2)	H(1)-H(2)	$\widehat{H(1)MO}$	$\widehat{MOH(2)}$
Co	$^3A'$	1.949	1.716	1.451	0.852	70.4	77.2
Co	$^5A''$	1.748	1.752	1.257	1.063	76.2	71.4
Ni	$^2A'$	1.825	1.762	1.553	0.833	75.6	69.8
Ni	$^2A''$	1.702	1.893	1.409	0.953	76.8	62.9
Ni	$^4A''$	1.688	1.890	1.359	0.975	75.6	64.5
Ni	$^4A'$	1.781	1.879	1.320	0.976	72.3	68.6
Cu	$^1A''$	1.763	1.882	1.380	0.931	73.6	66.2
Cu	$^3A''$	1.742	1.910	1.313	0.963	71.4	67.9

For the early transition metal cations we found that the $M - O$ distance in low-spin $TS2^+$ is closer to the HM^+OH value than that to the following $(H_2)MO^+$ species, for the middle transition metal cations these distances were similar, and for the late transition metals the $M - O$ distance at the second transition state is closer to that of the ion-molecule complex than to the previous intermediate.

For the high-spin four-centered $Sc - Cr$ transition metal $TS2^+$ transition states we observed an almost-fully formed $H - H$ bond and very long $M - H$

and $O-H$ bond distances. For the high-spin iron transition state we found a $H-H$ bond 0.199\AA longer than the respective bond in the chromium complex, and $M-H$ and $O-H$ bonds appreciably shorter than the previous ones. For iron also the $O-H$ distance was shorter than its low-spin $O-H$ distance. For the late transition metals the low-spin $M-H$ and $O-H$ distances are slightly longer than the high-spin ones, and now shorter $H-H$ bond lengths are observed in the low-spin transition states than in the high-spin ones.

The final stationary points located on our potential energy surfaces were the $(H_2)MO^+$ hydrogen molecule metal oxide adducts illustrated in Table 5.12. As we have discussed previously in Chapter 2 this minimum should be considered an ion-molecule complex. The $M-H$ bond length in these complexes is seen to shorten slightly in moving from Sc through to Cu in both the high- and low-spin cases. The only exception to this is the low-spin $(H_2)FeO^+$ case in which the $H-Fe$ bond is significantly shorter than those found in the other $(H_2)MO^+$ moieties.

Table 5.12. Geometrical parameters of the various $(H_2)MO^+$ stationary points on the B3LYP/DZVP potential energy surfaces. Bond lengths are reported in \AA , bond angles in degrees.

Metal	State	M-O	M-H(1)	M-H(2)	H-H	\widehat{HMO}
Co	$^3A''$	1.696	1.879	1.879	0.774	116.3
Co	$^5A''$	1.657	1.945	1.945	0.767	180.0
Ni	$^2A''$	1.697	1.834	1.834	0.777	115.4
Ni	$^2A'$	1.814	1.810	1.810	0.776	180.0
Ni	$^4A'$	1.781	1.841	1.841	0.773	180.0
Ni	$^4A''$	1.762	1.857	1.857	0.776	180.0
Cu	1	1.788	1.810	1.810	0.775	180.0
Cu	$^3A''$	1.814	1.798	1.798	0.776	180.0

For these three late transition metal low-spin systems also there is an interaction between the singly occupied d orbital of the metal and the σ_{H-H}^* orbital (shown in Figure 2.2). It is significantly lower than for the previous metals (5.09kcal/mol for iron vs. 2.35kcal/mol , 2.90kcal/mol and 2.22kcal/mol , respectively for cobalt, nickel and copper). The back donation from the σ_{H-H} orbital to the metal's s orbital should also be remarked upon in this three metal systems. The NBO analysis gives that donation a value of 7.91kcal/mol in the case of Co , 15.36kcal/mol in the case of Ni and 15.40kcal/mol in the case of Cu , which can be compared to the value of 11.77kcal/mol in the iron case.

5.3.5 Potential Energy Surfaces

Armentrout and co-workers in investigating the $Co^+ + H_2O$ reaction[94] did not observe any evidence of CoO^+ formation. They only found evidence of CoH^+ and $CoOH^+$ formation even though the thermodynamic threshold found for these ions is higher than for that of CoO^+ (see energetics in Table 5.5). Several other experimental works on the cobalt systems have also shown that even if the reverse reaction is clearly exothermic it is very inefficient, so detailed PES calculations have been required in order to clarify the reasons for this inefficiency[126, 135]. Such calculations are summarized in Figures 5.1-5.3, where the potential energy surfaces starting from the $M^+ + OH_2$ separated reactants and leading to the products $MO^+ + H_2$ for the high- and low-spin states at the B3LYP/DZVP level of theory for Co^+ , Ni^+ and Cu^+ are shown respectively. Graph 5.3 shows the evolution of the high-/low-spin relative energies across the row. The graphs given in this section are energies predicted at the B3LYP/DZVP level of theory except for the notoriously difficult Fe case, for which the CCSD(T)//B3LYP level of theory was used.

Graph 5.3. Evolution of the high-/low-spin $M^+ + H_2O$ relative energies with respect to the most stable $M^+ + H_2O$ system across the row. Except for Fe , where CCSD(T)//B3LYP values were used, B3LYP/DZVP predicted energies are shown.

Generally the surfaces for the reactions of Co^+ , Ni^+ and Cu^+ are similar to those we have reported in previous chapters, with the first step being the formation of the $M(OH_2)^+$ ion-molecule complex. Through $TS1^+$, one hydrogen atom is passed from oxygen to the metal, leading to the HM^+OH intermediate. Note that on the low-spin surfaces the HCo^+OH intermediate lies only 0.062eV below the associated $TS1^+$ and the HNi^+OH minimum a mere 0.014eV. As discussed earlier, no HCu^+OH intermediate exists on the singlet surface. Along the row the relative energy of this barrier on the low-spin surface has augmented in relative energy somewhat, with the exception of Cr which shows an especially large low-spin barrier. The relative energies of the high-spin $TS1^+$ stationary points, too, increase in moving from left to right along the row, as can be seen in Graph 5.4.

Figure 5.1. *B3LYP/DZVP potential energy surface following the $\text{Co}^+ + \text{H}_2\text{O} \rightarrow \text{CoO}^+ + \text{H}_2$ reaction path. Energies given are in eV and are relative to the separated ground state reactants, $\text{Co}^+(\text{}^3\text{F}) + \text{H}_2\text{O}$.*

Graph 5.4. Evolution of the high-/low-spin $TS1^+$ relative energies with respect to the most stable $M^+ + H_2O$ system across the row. Except for Fe, where $CCSD(T)//B3LYP$ values were used, $B3LYP/DZVP$ predicted energies are shown.

Armentrout and co-workers[94] note that qualitatively the first barrier corresponding to the low-spin $TS1^+$ in the $Co^+ + H_2O$ reaction should not be higher than the energy of $CoOD^+ + D$. Our results are in accordance with this since we obtain a value of 2.070eV for reaction (5.5) (see Table 5.5), and predict that $TS1^+$ represents a barrier of 0.628eV (see Figure 5.1).

The second barrier is associated with the second hydrogen transfer from oxygen to the metal, $TS2^+$. Through the early and middle transition metals, the gap between the high- and low-spin $TS2^+$ stationary points has decreased along the row significantly. We find now that for cobalt the high- and low-spin states of $TS2^+$ are almost energetically degenerate and for nickel and copper there is an inversion, with the high-spin transition states being lower in energy. Graph 5.5 plots the relative energies of these stationary points along the row.

Graph 5.5. Evolution of the high-/low-spin $TS2^+$ relative energies with respect to the most stable $M^+ + H_2O$ system across the row. Except for Fe, where $CCSD(T)//B3LYP$ values were used, $B3LYP/DZVP$ predicted energies are shown.

Figure 5.2. *B3LYP/DZVP potential energy surface following the $Ni^+ + H_2O \rightarrow NiO^+ + H_2$ reaction path. Energies given are in eV and are relative to the separated ground state reactants, $Ni^+(^2D) + H_2O$.*

It should be pointed out that the lowest barrier for the doublet $TS2^+$ in the Ni case is a $^2A'$ state, while the HNi^+OH species has a $^2A''$ ground state. We give the lower barrier because movement of the H atoms should be facile, opening the possibility of dropping into C_1 where the states can mix. The $^2A''$ state lies $0.121eV$ above the $^2A'$ $TS2^+$.

After overcoming this maximum we fall to the final intermediate found on the reaction path, the $(H_2)MO^+$ ion-molecule complex. For the low-spin cases this complex bonding becomes stronger from Co ($0.492eV$) to Cu ($0.730eV$), continuing the observed trend. For the high-spin complexes we found that there is a minimum in the bond strength at the vanadium complex, and afterwards this bond becomes stronger in moving from left to right along the row. This nice picture is broken by nickel, in which the $^4A'$ ground-state complex is bound by only $0.233eV$, $0.120eV$ weaker than the vanadium complex.

Experimental results from Armentrout and co-workers studying the reverse reaction, $CoO^+ + D_2$ [94], found a barrier to reaction of $0.75 \pm 0.04eV$. As seen in Figure 5.1, our B3LYP/DZVP level of theory predicts a barrier $0.605eV$ above the $CoO^+ + D_2$ asymptote energy.

From the $(H_2)MO^+$ intermediate, the loss of H_2 proceeds without transition state to the corresponding high- and low-spin MO^+ and H_2 molecules. The relative energies of the $MO^+ + H_2$ products with respect to the most stable $M^+ + H_2O$ system are plotted in Graph 5.6.

Graph 5.6. Evolution of the high-/low-spin $MO^+ + H_2$ relative energies with respect to the most stable $M^+ + H_2O$ system across the row. Except for Fe , where $CCSD(T)//B3LYP$ values were used, $B3LYP/DZVP$ predicted energies are shown.

For these metals clearly the surface crossings takes place near the $TS2^+$ transition state, that is, at the exit channel, while this crossing was observed at the entrance channel for the $Sc - Mn$ metals and at both sites for iron.

Equilibrium geometry parameters for the various reaction products are given in Table 5.13.

Figure 5.3. *B3LYP/DZVP potential energy surface following the $\text{Cu}^+ + \text{H}_2\text{O} \rightarrow \text{CuO}^+ + \text{H}_2$ reaction path. Energies given are in eV and are relative to the separated ground state reactants, $\text{Cu}^+(^1S) + \text{OH}_2$.*

Table 5.13. Equilibrium geometry parameters for the various $M^+ + OH_2$ reaction products at the B3LYP/DZVP and B3LYP/TZVP+G(3df,2p) levels of theory. Bond lengths are reported in Å, bond angles in degrees.

Product	Metal	State	B3LYP/DZVP			B3LYP/TZVP+G(3df,2p)		
			M-O	M-H	Angle	M-O	M-H	Angle
MO ⁺	Co	³ Σ	1.705			1.705		
		⁵ Δ	1.648			1.634		
	Ni	² Δ	1.687			1.681		
		⁴ Δ	1.643			1.638		
	Cu	¹ Δ	1.786			1.775		
³ Σ		1.807			1.797			
MH ⁺	Co	³ Δ	1.461			1.467		
		⁴ Φ	1.520			1.535		
	Ni	¹ Σ		1.414		1.415		
		³ Δ		1.474		1.485		
	Cu	² Δ		1.488		1.488		
HMO ⁺	Co	³ A*	1.615	1.451	84.7	1.599	1.455	85.7
		⁴ A*	1.601	1.475	81.9	1.585	1.485	83.4
	Cu	² A*	2.047	1.508	178.3	1.969	1.501	178.6
MOH ⁺	Co	³ A'	1.758	0.980	126.3	1.748	0.972	125.0
		⁴ A'	1.731	0.978	126.6	1.726	0.969	125.8
	Ni	¹ A'	1.697	0.979	124.2	1.688	0.972	122.4
		³ A*	1.714	0.979	129.4	1.708	0.971	127.8
	Cu	² A*	1.816	0.984	124.1	1.808	0.977	123.3

5.4 Conclusions

The reactions of Co^+ , Ni^+ and Cu^+ with water have been investigated in detail completing the study of the reactivity of the first row transition metals. Both the low- and high-spin potential energy surfaces have been characterized at the B3LYP/DZVP level of theory. Energy differences between key low- and high-spin species and total reaction energies for the possible products have been predicted at even higher levels of theory including B3LYP/TZVP+G(3df,2p) and CCSD(T)/TZVP+G(3df,2p)//B3LYP/TZVP+G(3df,2p).

From these data, the following conclusions are drawn:

1. The expected trends for the $M(OH_2)^+$ ion-molecule dissociation energies has been well described through the row. B3LYP/TZVP+G(3df, 2p) appears to be the best method fitting the experimental data.
2. Similar performance from the B3LYP/TZVP+G(3df,2p) and CCSD(T)//B3LYP levels of theory was obtained in comparison with experimental data of high-/low-spin splittings on the metal cations.
3. Whereas the only exothermic products of the $M^+ + H_2O$ reaction for $M=Sc$ to V were $MO^+ + H_2$ with exothermicity decreasing from Sc to V , said reactions were endothermic for $M=Cr$ to Cu with endothermicity increasing through the series.
4. As in the $Fe^+ + H_2O$ system, less difference between the high- and low-spin structures than in the early transition metal systems was observed for the late transition metals. The reason for this is that the high spin Fe^+ to Cu^+ cations have at least one set of paired electrons while the Sc^+ to Mn^+ high-spin cations do not.
5. Both, high- and low-spin potential energy surfaces cross once in the entrance channel for Sc^+ to Mn^+ . Two crossings were observed, at the entrance and exit channels, on the Fe^+ potential energy surfaces. Finally, the surfaces of Co^+ to Cu^+ demonstrate one crossing, near the exit channel.

Bibliography

- [1] Barton, D.H.R. *Aldrichimica Acta* **1990**, 23, 3.
- [2] Bersuker, I.B. "Electronic Structure and Properties of Transition Metal Compounds", Wiley-Interscience, **1995**.
- [3] Armentrout, P.B.; *Annu.Rev.Phys.Chem.* **1990**, 41, 313.
- [4] Shaik, S.; Danovich, D.; Fiedler, A.; Schröder, D.; Schwarz, H. *Hel.Chim.Acta*, **1995**, 78, 1393.
- [5] Armentrout, P.B.; *Science* **1991**, 251, 175.
- [6] Lopez, X. *On the Gas-Phase Chemistry of P⁺: Ionic Clusters, Dioxides and Interstellar Chemistry*, **1995**, Thesis, University of the Basque Country, 30.
- [7] Eller, H.; Schwarz, H. *Chem.Rev.* **1991**, 91, 1121.
- [8] Schröder, D.; Schwarz, H. *Angew.Chem.Int.Ed.Engl.* **1995**, 34, 1973.
- [9] Freiser, B.S. *J.Mass.Spec.* **1996**, 31, 703.
- [10] Armentrout, P.B.; Beauchamp, J.L. *Acc.Chem.Res.* **1989**, 22, 315.
- [11] Armentrout, P.B.; *Gas Phase Inorganic Chemistry 1989*; Ed. Russell, D.H.; Plenum Press, New York, 1.
- [12] Bauschlicher, C.W.; Maitre, P. *Theo.Chim.Acta* **1995**, 90, 189.
- [13] Armentrout, P.B.; Kickel, B.L. *Organometallic Ion Chemistry*, Freiser B.S. (Ed.), Kluwer, Dordrecht, **1996**, 1.
- [14] For example: a) Bauschlicher, C.W.; Langhoff, S.R.; Partridge, H.; Barnes, L.A. *J.Chem.Phys.* **1989**, 91, 2399. b) Barnes, L.A.; Rosi, M.; Bauschlicher, C.W. *J.Chem.Phys.* **1990**, 93, 609. c) Rosi, M.; Bauschlicher, C.W.; Langhoff, S.R.; Partridge, H. *J.Phys.Chem.* **1990**, 94, 8656. d) Sodupe, M.; Bauschlicher, C.W. *J.Phys.Chem.* **1991**, 95, 8640. e) Langhoff, S.R.; Bauschlicher, C.W.; Partridge, H.; Sodupe,

- M. *J.Phys.Chem.* **1991**, *95*, 10677. f) Sodupe, M.; Bauschlicher, C.W.; Langhoff, S.R.; Partridge, H. *J.Phys.Chem.* **1992**, *96*, 2118. g) Bauschlicher, C.W.; Partridge, H.; Langhoff, S.R. *J.Phys.Chem.* **1992**, *96*, 3273. h) Bauschlicher, C.W.; Partridge, H.; Sheehy, J.A.; Langhoff, S.R.; Rosi, M. *J.Phys.Chem.* **1992**, *96*, 6969. i) Bauschlicher, C.W.; Partridge, H.; Scuseria, G.E. *J.Chem.Phys.* **1992**, *97*, 7471. j) Thomas, J.L.C.; Bauschlicher, C.W.; Hall, M.B. *J.Phys.Chem.* **1997**, *101*, 8530.
- [15] Armentrout, P.B. *Acc.Chem.Res.* **1995**, *28*, 430.
- [16] For example: a) Ricca, A.; Bauschlicher, C.W. *J.Phys.Chem.* **1997**, *101*, 8949. b) Maitre, P.; Bauschlicher, C.W. *J.Phys.Chem.* **1995**, *99*, 6836. c) Bauschlicher, C.W.; Maitre, P. *J.Phys.Chem.* **1995**, *99*, 3444. d) Rosi, M.; Bauschlicher, C.W.; *J.Chem.Phys.* **1989**, *90*, 7264. e) Rosi, M.; Bauschlicher, C.W.; *J.Chem.Phys.* **1990**, *92*, 1876.
- [17] For example: Jiao, C.Q.; Ranatunga, D.R.A.; Freiser, B.S. *J.Phys.Chem.* **1996**, *100*, 4755.
- [18] For example: a) Guo, B.C.; Kerns, K.P.; Castleman, A.W. *Science* **1992**, *255*, 1411. b) Wei, S.; Guo, B.C.; Purnell, J.; Buzza, S.; Castleman, A.W. *Science* **1992**, *256*, 818. c) Bowers, M.T. *Acc.Chem.Res.* **1994**, *27*, 324.
- [19] Schröder, D.; Schwarz, H.; Clemmer, D.E.; Chen, Y.-M.; Armentrout, P.B.; Baranov, V.I.; Bohme, D.K. *Int.J.Mass.Spec.Ion.Proc.* **1997**, *161*, 175.
- [20] a) Eller, K.; Schwarz, H. *Int.J.Mass.Spec.Ion.Proc.* **1989**, *93*, 243. b) Eller, K.; Zummack, W.; Schwarz, H. *J.Am.Chem.Soc* **1990**, *112*, 621. c) Marshall, A.G.; Grosshans, P.B. *Anal.Chem.* **1991**, *63*, 215A.
- [21] a) Ervin, K.M.; Armentrout, P.B. *J.Chem.Phys.* **1985**, *83*, 166. b) Schultz, R.H.; Armentrout, P.B. *Int.J.Mass.Spec.Ion.Proc.* **1991**, *107*, 29.
- [22] a) Mackay, G.I.; Vlachos, G.D.; Bohme, D.K.; Schiff, H. *Int.J.Mass Spec.Ion.Phys.* **1980**, *36*, 259. b) Raksit, A.B.; Bohme, D.K. *Int.J.Mass.Spec.Ion.Proc.Int.J.Mass.Spec.Ion.Proc.* **1983**, *55*, 69.
- [23] Cooks, R.G. (Ed.) *Collision Spectroscopy*, Plenum Press, New York, **1978**.
- [24] Mabud, M.A.; DeKrey, M.J.; Cooks, R.G. *Int.J.Mass.Spec.Ion.Proc.* **1985**, *67*, 285.
- [25] a) Bowers, M.T. (Ed.) *Gas Phase Ion Chemistry*, 3, Academic Press, New York, **1984**. b) Hettich, R.C.; Jackson, T.C.; Stanko, E.M.; Freiser, B.S. *J.Am.Chem.Soc.* **1986**, *108*, 5086. c) Ranasinghe, Y.A.; Surjasmita, I.B.; Freiser, B.S. *Organometallic Ion Chemistry*; Freiser, B.S. (Ed.); **7**,

- Kluwer, Dordrecht, **1996**. d) Willey, K.F.; Yeh, C.S.; Robbins, D.L.; Duncan, M.A. *Chem.Phys.Lett.* **1992**, 192, 179.
- [26] Huang, Y.; Freiser, B.S. *J.Am.Chem.Soc.* **1993**, 115, 737.
- [27] Cody, R.B.; Freiser, B.S. *Anal.Chem.* **1987**, 59, 1056.
- [28] Siegbahn, P.E.M. *J.Chem.Phys.* **1980**, 72, 1647.
- [29] Roos, B.O.; *Lecture Notes in Quantum Chemistry*, **1992**, 58, 177.
- [30] Siegbahn, P.E.M. *Lecture Notes in Quantum Chemistry*, **1992**, 58, 255.
- [31] Siegbahn, P.E.M.; "Electronic structure calculations for molecules containing transition metals", *Advances in Chemical Physics*, Vol. XCIII, **1996**.
- [32] Sadlej, A.J. *Lecture Notes in Quantum Chemistry*, **1992**, 58, 203.
- [33] Levine, N.I. *Quantum Chemistry*, 4th edition, Ed: Prentice-Hall, Inc., **1991**.
- [34] Szabo, A.; Ostlund, N.S.; *Modern Quantum Chemistry*, Revised 1st edition. Ed: McGraw-Hill, **1982**.
- [35] Szabo, A.; Ostlund, N.S.; *Modern Quantum Chemistry*, Revised 1st edition. Ed: McGraw-Hill, **1982**, 43.
- [36] Levine, N.I. ; *Quantum Chemistry*, 4th edition, Ed: Prentice-Hall, Inc., **1991**, 189.
- [37] Eriksson, L.A. *Computational Quantum Chemistry: Applications to Radical Cations, Polymerisation Reactions, Polymers an Charge Transfer Systems.*, Thesis, Uppsala University, **1992**, 22.
- [38] Szabo, A.; Ostlund, N.S.; *Modern Quantum Chemistry*, Revised 1st edition. Ed: McGraw-Hill, **1982**, 108.
- [39] Löwdin, P.O. *Int.J.Quan.Chem.* **1995**, 55, 77.
- [40] Levine, N.I. ; *Quantum Chemistry*, 4th edition, Ed: Prentice-Hall, Inc., **1991**, 221.
- [41] Levine, N.I. ; *Quantum Chemistry*, 4th edition, Ed: Prentice-Hall, Inc., **1991**, 511.
- [42] Szabo, A.; Ostlund, N.S.; *Modern Quantum Chemistry*, Revised 1st edition. Ed: McGraw-Hill, **1982**. 322, 350.
- [43] Szabo, A.; Ostlund, N.S.; *Modern Quantum Chemistry*, Revised 1st edition. Ed: McGraw-Hill, **1982**. Chapter 4.

- [44] Wolinski, K.; Pulay, J. *J. Chem. Phys.* **1989**, *90*, 3647.
- [45] Levine, N.I. ; *Quantum Chemistry*, 4th edition, Ed: Prentice-Hall, Inc., **1991**, 509.
- [46] Davidson, E.R.; Silver, W. *Chem. Phys. Lett.* **1977**, *52*, 403.
- [47] Bartlett, R.J. *J.Phys.Chem.* **1989**, *93*, 1697.
- [48] Noga, J.; Bartlett, R.J. *J.Chem.Phys.* **1987**, *86*, 7041.
- [49] a) Shepard, R.; "The Multiconfiguration Self-Consistent Method" in *Ab Initio Methods in Quantum Chemistry-II*, Edited by K.P. Lawley, Ed: John Wiley Sons Ltd, **1987**, 63. b) Roos, B.O.; "The Complete Active Space Self-Consistent Field Method and Its Applications in Electronic Structure Calculations" in *Ab Initio Methods in Quantum Chemistry-II*, Edited by K.P. Lawley, Ed: John Wiley Sons Ltd, **1987**, 399. c) S.J. Fermosinho *et al. Theoretical and Computational Models for Organic Chemistry*, Kluwer Academic Publishers, **1991**, 253.
- [50] Levine, N.I. ; *Quantum Chemistry*, 4th edition, Ed: Prentice-Hall, Inc., **1991**, 420.
- [51] Andersson, K.; Malmqvist, P.-Å.; Roos, B.O.; Sadlej, A.J.; Wolinski, K.; *J.Phys.Chem.* **1990**, *94*, 5483.
- [52] Andersson, K.; Malmqvist, P.-Å.; Roos, B.O.; *J.Chem.Phys.* **1992**, *96*, 1218.
- [53] Parr, R.G.; Yang, W.; "Density Functional Theory of Atoms and Molecules"; Clarendon Press: Oxford **1989**, 278.
- [54] Kryachko, E.S.; Ludeña, E.V.; *Energy Density Functional Theory of Many-Electron Systems*, Ed: Kluwer Academic Publishers, London **1990**.
- [55] Vosko, S.H.; Wilk, L.; Nusair, M. *Can. J. Phys.* **1980**, *58*, 1200.
- [56] Slater, J.C. *Quantum Theory of Molecules and Solids. Vol. 4. The Self-Consistent Field for Molecules and Solids*, (McGraw-Hill, New York, **1974**).
- [57] Becke, A.D. *Phys. Rev. A* **1988**, *38*, 3098.
- [58] Lee, C.; Yang, W.; Parr, R.G. *Phys. Rev. B* **1980**, *37*, 785.
- [59] Becke, A.D. *J. Chem. Phys.* **1993**, *98*, 5648.
- [60] Ziegler, T. *Chem. Rev.* **1991**, *91*, 651; and references therein.
- [61] Magnera, T.F.; David, D.E.; Michl, J. *J.Am.Chem.Soc.* **1989**, *111*, 4100.

- [62] Dalleska, N.F.; Honma, K.; Sunderlin, L.S. Armentrout, P.B. *J.Am.Chem.Soc.* **1994**, *116*, 3519.
- [63] Armentrout, P.B., Personal communication.
- [64] Rosl, M.; Bauschlicher, C.W. *J.Chem.Phys.* **1989**, *90* (12), 7264. *ibid.* **1990**, *92*, 1876.
- [65] Magnusson, E.; Moriarty, N.W. *J.Comp.Chem.* **1993**, *14* (8), 961.
- [66] (a) Perdew, J.P.; and Wang, Y. *Phys.Rev.B* **1986**, *33*, 8800; (b) Perdew, J.P.; *ibid.* **1986**, *33*, 8822; **1986**, *34*, 7406; (c) Perdew, J.P.; and Wang, Y. *ibid.* **1992**, *45*, 13244; Perdew, J.P. in *Electronic Structure of Solids*, edited by P. Ziesche and H. Eischering (Akademie, Berlin, 1991); Perdew., J.P.; Chevary, J.A.; Vosko, S.H.; Jackson, K.A.; Pederson, M.R.; Singh, D.J.; and Fiolhais, C. *Phys.Rev.B* **1992**, *46*, 6671; (d) Lee, C.; Yang, W.; and Parr, R.G. *ibid.* **1988**, *37*, 785.
- [67] Ricca, A.; Bauschlicher, C.W. *J.Phys.Chem.* **1995**, *99*, 9003.
- [68] Ricca, A.; Bauschlicher, C.W. *J.Phys.Chem.* **1994**, *98*, 12899.
- [69] Eriksson, Leif A.; Petterson, L.G.M.; Siegbahn, P.E.M.; Wahlgren, U. *J.Phys.Chem.* **1995**, *102*, 2.
- [70] Boys, S.F. and Bernardi, F. *Mol Phys.* **1970**, *19*, 553; Schwenke, D.W. and Truhlar, D.B. *J.Chem.Phys.* **1985**, *82*, 2418.
- [71] Frish, M. J.; Trucks, G. W.; Schlegel, H. B.; Gill, P. M. W.; Johnson, B. G.; Robb, M. A.; Cheeseman, J. R.; Keith, T. A.; Petersson, G. A.; Montgomery, J. A.; Raghavachari, K.; Al-Laham, M. A.; Zakrzewski, V. G.; Ortiz, J. V.; Foresman, J. B.; Cioslowski, J.; Stefanov, B. B.; Nanayakkara, A.; Challacombe, M.; Peng, C. Y.; Ayala, P. Y.; Chen, W.; Wong, M. W.; Andres, J. L.; Replogle, E. S.; Gomperts, R.; Martin, R. L.; Fox, D. J.; Binkley, J. S.; Defrees, D. J.; Baker, J.; Stewart, J. P.; Head-Gordon, M.; Gonzalez, C.; Pople, J. A. Gaussian 94 (Revision C.3), Gaussian, Inc., Pittsburgh PA, **1995**.
- [72] a) Dupuis, M.; Spangler, D.; Wendoloski, J.J. NRCC Software Catalog, University of California: Berkeley, CA **1980**, Program QG01. b) Schmidt, M.W.; Baldrige, K.K.; Boatz, J.A.; Jensen, J.H.; Koseki, S.; Gordon, M.S.; Nguyen, K.A.; Windus, T.L.; Elbert, S.T. QCPE Bulletin, **1990**, *10*, 42-54.
- [73] Bauschlicher, C.W.; Maitre, P. *J.Phys.Chem.* **1995**, *99*, 3444.
- [74] Russo, T.V.; Martin, R.L.; Hay, P.J. *J.Chem.Phys.* **1994**, *101*, 7729.

- [75] Dunning, T.H. and Hay, P.J. in *Methods of Electronic Structure Theory*, Vol. 3, Edited by: Schaefer III, H.F. (Plenum Press, Inc., New York, **1977**), 1.
- [76] Sim, F.; Salahub, D.R.; Chim, S. and Dupuis, M. *J.Chem.Phys.* **1991**, *95*, 4317.
- [77] Godbout, N.; Salahub, D.R.; Andzelm, J. and Wimmer, E. *Can.J.Chem.* **1992**, *70*, 560.
- [78] Schäfer, A.; Hurbert, C. and Ahlrichs, R. *J.Chem.Phys.* **1994**, *100*, 5829.
- [79] Wachters, A.J. *J.Chem.Phys.* **1970**, *52*, 1033.
- [80] Hay, P.J. *J.Chem.Phys.* **1971**, *66*, 4377.
- [81] Krishnan, J.S.; Binkley, J.S.; Seeger, P.v.R.; Pople, J.A. *J.Chem.Phys.* **1980**, *72*, 650.
- [82] Stevens, W.J.; Krauss, M.; Basch, H.; Jasien, P.G. *Can.J.Chem.* **1992**, *70*, 612.
- [83] Botch, B.H.; Dunning, T.H.; Harrison, J.F. *J.Chem.Phys.* **1981**, *75* (7), 3466.
- [84] Jones, R.O.; Gunnarson, O. *Rev.Mod.Phys.* **1989**, *61*, 689.
- [85] Moore, C.E. *Atomic Energy Levels* (National Bureau of Standards, Washington, D.C.. **1952**; Natl.Bur.Stand.Circular **1959**, *2*, *3*, 467.
- [86] Raghavachari, K.; Trucks, G.W. *J.Chem.Phys.* **1989**, *91*, 2457.
- [87] Jonas, V.; Thiel, W. *J.Chem.Phys.* **1995**, *102*, 8474.
- [88] Belbere, J.; Person, W.B.; and Szczepaniak, K. *J.Phys.Chem.* **1995**, *99*, 10705.
- [89] Ruiz, E.; Salahub, D.; and Vela, A. *J.Am.Chem.Soc.* **1995**, *117*, 1141.
- [90] Guo, B.C.; Kerns, K.P.; Castleman, A.W., Jr. *J.Phys.Chem.* **1992**, *96*, 4879.
- [91] Gordons, M.S.; Cundari, T.R.; *Coordination Chemistry Reviews* **1996** *147*, 87.
- [92] Martinho-Simoes, J.A.; Beauchamp, J.L.; *Chem.Rev.* **1990** *90*, 629.
- [93] Clemmer, D.E.; Chen Y.-M., Aristov, N.; Armentrout, P.B.; *J.Phys.Chem.* **1994**, *98*, 7538.
- [94] Chen Y.-M., Clemmer, D.E.; Armentrout, P.B.; *J.Am.Chem.Soc.* **1994**, *116*, 7815.

- [95] Clemmer, D.E.; Sunderlin, L.S.; Armentrout, P.B.; *J.Phys.Chem.* **1990**, *94*, 3008.
- [96] Kickel, B.L.; Armentrout, P.B.; *J.Am.Chem.Soc.* **1994**, *116*, 10742.
- [97] Clemmer, D.E.; Aristov, N.; Armentrout, P.B.; *J.Phys.Chem.* **1993**, *97*, 544.
- [98] Tilson, J.L.; Harrison, J.F.; *J.Phys.Chem.* **1991**, *95*, 5097.
- [99] Chen, Y.M.; Clemmer, D.E.; Armentrout, P.B.; *J.Phys.Chem.* **1994**, *98*, 11490.
- [100] Irigoras, A.; Ugalde, J.M.; Lopez, X.; Sarasola, C.; *Can.J.Chem.* **1996**, *74*, 1824.
- [101] Raghavachari, K.; Trucks, G. W.; *J. Chem. Phys.* **1989**, *91*, 1062.
- [102] Blomberg, M.R.A.; Siegbahn, P.E.M.; Svensson, M.; *J.Chem.Phys.* **1996**, *104*, 9546.
- [103] Huzinaga, S.; *J.Chem.Phys.* **1965**, *42*, 1293.
- [104] Musaev, D.G.; Morokuma, K.; *J.Phys.Chem.* **1996**, *100*, 11600.
- [105] Andersson, K.; Fscher, M.P.; Karlstrm, G.; Lindh, R.; Malmqvist, P.-.; Olsen, J.; Roos, B.O.; Sadlej, A.J.; Blomberg, M.R.A.; Siegbahn, P.E.M.; Kell, V.; Noga, J.; Urban, M.; and Widmark, P.-O. MOLCAS Version 3. Dept. of Theor. Chem., Chem. Center, Univ. Of Lund, P.O.B. 124, S-221 00 Lund, Sweden, **1994**.
- [106] Reed, A. E.; Curtiss, L. A.; Weinhold, F.; *Chem. Rev.* **1988**, *88*, 899.
- [107] NBO Version 3.1, Glendening, A. E.; Reed, A. E. ; Carpenter, J, E. y F. Weinhold.
- [108] MOLDEN, a visualization program of molecular and electronic structure. <http://www.caos.kun.nl/~schaft/molden/molden.html>
- [109] Irikura, K.K.; Beauchamp, J.L.; *J.Am.Chem.Soc.* **1989**, *111*, 75.
- [110] Elkind, J.L.; Armentrout, P.B.; *J.Phys.Chem.* **1987**, *91*, 2037.
- [111] Ye, S.; *Theochem* **1997**, *417*, 157.
- [112] Irigoras, A.; Fowler, J.E.; Ugalde, J.M.; *J.Phys.Chem.A* **1998**, *102*, 293. *ibid.* **1998**, *102*, 2252.
- [113] Bauschlicher, C.W., Jr.; Ricca, A.; Partridge, H.; Langhoff, S.R.; *Recent Advances in Density Functional Theory*; Chong, D.P., Ed.; World Scientific Publishing Co.: Singapore **1997**, Part II.

- [114] Sodupe, M.; Branchadell, V.; Rosi, M.; Bauschlicher, C.W., Jr.; *J.Phys.Chem. A* **1997**, 101, 7854.
- [115] Hartmann, M.; Clark, T.; Eldik, R.van; *J.Am.Chem.Soc.* **1997**, 119, 7843.
- [116] Pavlov, M.; Siegbahn, P.E.M.; Sandström, M.; *J.Phys.Chem.A* **1998**, 102, 219.
- [117] Marinelli, P.J.; Squires, R.R. *J.Am.Chem.Soc.* **1989**, 111, 4101.
- [118] Dyke, J.M.; Gravenor, B.W.J.; Hastings, M.P.; Morris, A.; *J.Phys.Chem.* **1985**, 89, 4613.
- [119] CRC *Handbook of Chemistry and Physics*, 63rd ed.; Weast, R.C., Ed.; CRC Press: Boca Raton, FL, 1982.
- [120] Murad, E.J. *J.Geophys.Res.* **1978**, 83, 5525.
- [121] Kang, H.; Beauchamp, J.L. *J.Am.Chem.Soc.* **1986**, 108, 5663.
- [122] Aristov, N.; Armentrout, P.B. *J.Am.Chem.Soc.* **1984**, 106, 4065.
- [123] Irigoras, A.; Fowler, J.E.; Ugalde, J.M.; *J.Am.Chem.Soc.* **1999**, 121, 574.
- [124] Kang, H.; Beauchamp, J.L. *J.Am.Chem.Soc.* **1986**, 108, 7502.
- [125] Ryan, M.F.; Fiedler, A.; Schröder, D.; Schwarz, H. *J.Am.Chem.Soc.* **1995**, 117, 2033.
- [126] Schröder, D.; Fiedler, A.; Ryan, M.F.; Schwarz, H. *J.Phys.Chem.* **1994**, 98, 68.
- [127] Clemmer, D.E.; Chen, Y.-M.; Khan, F.A.; Armentrout, P.B. *J.Phys.Chem.* **1994**, 98, 6522.
- [128] Fiedler, A.; Schröder, D.; Shaik, S.; Schwarz, H. *J.Am.Chem.Soc.* **1994**, 116, 10734.
- [129] Danovich, D.; Shaik, S. *J.Am.Chem.Soc.* **1997**, 119, 1773.
- [130] Filatov, M.; Shaik, S. *J.Phys.Chem.A* **1998**, 102, 3835.
- [131] Ricca, A.; Bauschlicher, C.W.; *Theor.Chim.Acta* **1995**, 92, 123.
- [132] Trachtman, M.; Markham, G.D.; Glusker, J.P.; George, P.; Bock, C.W. *Inorg.Chem.* **1998**, 37, 4421.
- [133] Holthausen, M.C.; Fiedler, A.; Schwarz, H.; Koch, W. *J.Phys.Chem.* **1996**, 100, 6236.
- [134] Irigoras, A.; Fowler, J.E.; Ugalde, J.M.; *J.Am.Chem.Soc.* Accepted.

- [135] Ryan, M.F.; Fiedler, A.; Schröder, D.; Schwarz, H. *Organometallics* **1994**, *13*, 4072.
- [136] Frisch, M. J.; Trucks, G. W.; Schlegel, H. B.; Scuseria, G. E.; Robb, M. A.; Cheeseman, J. R.; Zakrzewski, V. G.; Montgomery, J. A.; Stratmann, R. E.; Burant, J. C.; Dapprich, S.; Millam, J. M.; Daniels, A. D.; Kudin, K. N.; Strain, M. C.; Farkas, O.; Tomasi, J.; Barone, V.; Cossi, M.; Cammi, R.; Mennucci, B.; Pomelli, C.; Adamo, C.; Clifford, S.; Ochterski, J.; Petersson, G. A.; Ayala, P. Y.; Cui, Q.; Morokuma, K.; Malick, D. K.; Rabuck, A. D.; Raghavachari, K.; Foresman, J. B.; Cioslowski, J.; Ortiz, J. V.; Stefanov, B. B.; Liu, G.; Liashenko, A.; Piskorz, P.; Komaromi, I.; Gomperts, R.; Martin, R. L.; Fox, D. J.; Keith, T.; Al-Laham, M. A.; Peng, C. Y.; Nanayakkara, A.; Gonzalez, C.; Challacombe, M.; Gill, P. M. W.; Johnson, B. G.; Chen, W.; Wong, M. W.; Andres, J. L.; Head-Gordon, M.; Replogle, E. S.; Pople, J. A. Gaussian 98 (Revision A.5), Gaussian, Inc., Pittsburgh PA, **1998**.
- [137] (a) Chase, M.W.; Davies, C.A.; Downey, J.R.; Frurip, D.J.; McDonald, R.A.; Syvonen, A.N. *J.Phys.Chem.Ref.Data.* **1985**, *14*, Suppl. N 1 (JANAF Tables).
- (b) Gurvich, L.V.; Veyts, I.V.; Alcock, C.B. "Thermodynamic Properties of Individual Substances", 4th ed.; Hemisphere: New York, **1989**; Vol. 1 Part 2.
- (c) Armentrout, P.B.; *Gas Phase Inorganic Chemistry* **1989**; Ed. Russell, D.H.; Plenum Press, New York, 1.
- (d) Armentrout, P.B.; Kicket, B.L. *Organometallic Ion Chemistry*, Freiser B.S. (Ed.), Kluwer, Dordrecht, **1996**, 1.

List of Publications

1. AB INITIO STUDY OF THE P^+L_n ION MOLECULE COMPLEXES OF THE FIRST AND SECOND ROW HYDRIDES
X. LOPEZ, A. IRIGORAS, J.M. UGALDE AND F.P. COSSIO
JOURNAL OF THE AMERICAN CHEMICAL SOCIETY. **116**, 10670 (1994).
 2. AB INITIO CHARACTERIZATION OF GASEOUS $(H_n, P <^O > C)^+$ SPECIES
A. IRIGORAS, F.P. COSSIO, C. SARASOLA, J.M. UGALDE
JOURNAL OF PHYSICAL CHEMISTRY. **100**, 8758 (1996).
 3. ON THE DISSOCIATION ENERGY OF $Ti(OH_2)^+$. AN MCSCF, CCSD(T) AND DFT STUDY
A. IRIGORAS, X. LOPEZ, J.M. UGALDE
CANADIAN JOURNAL OF CHEMISTRY. **74**, 1824 (1996).
 4. ELECTRONIC STRUCTURE: PREDICTION AND APPLICATIONS.
EDITORS: A. IRIGORAS AND J.M. UGALDE
EUSKO IKASKUNTZA
CUADERNOS DE CC. FISICO QUIMICAS Y MATEMATICAS.
Formula. **4**, 1-150 (1997).
ISSN: 1137-4411.
 5. ON THE REACTIVITY OF $Ti^+(^4F, ^2F)$. REACTION OF Ti^+ WITH OH_2 .
A. IRIGORAS, J.E. FOWLER, J.M. UGALDE
JOURNAL OF PHYSICAL CHEMISTRY A. **102**, 293 (1998). JOURNAL OF PHYSICAL CHEMISTRY A. **102**, 2252 (1998).
-

-
6. ON THE REACTIVITY OF $Sc^+(^3D, ^1D)$ and $V^+(^5D, ^3F)$. REACTION OF Sc^+ AND V^+ WITH WATER.

A.IRIGORAS, J.E.FOWLER, J.M.UGALDE

JOURNAL OF THE AMERICAN CHEMICAL SOCIETY. **121(3)**, 574 (1999).

-
7. ON THE REACTIVITY OF $Cr^+(^6S, ^4D)$, $Mn^+(^7S, ^5S)$ and $Fe^+(^6D, ^4F)$: REACTION OF Cr^+ , Mn^+ AND Fe^+ WITH WATER.

A.IRIGORAS, J.E.FOWLER, J.M.UGALDE

JOURNAL OF THE AMERICAN CHEMICAL SOCIETY. In Press.

-
8. ON THE REACTIVITY OF $Co^+(^3F, ^5F)$, $Ni^+(^2D, ^4F)$ and $Cu^+(^1S, ^3D)$: REACTION OF Co^+ , Ni^+ AND Cu^+ WITH WATER.

A.IRIGORAS, O.ELIZALDE, I.SILANES, J.E.FOWLER, J.M.UGALDE

JOURNAL OF THE AMERICAN CHEMICAL SOCIETY. Accepted.

-
9. THE PRIMARY REACTION OF THE TITANIUM-CATALYZED OLIGOMERIZATION OF PHOSPHORUS IN THE GAS PHASE.

A.IRIGORAS, J.E.FOWLER, J.M.UGALDE

JOURNAL OF THE AMERICAN CHEMICAL SOCIETY. Submitted.
